Universitat Politècnica de Catalunya

Master Thesis

Report

Study of stability control systems applied to a racing car

Author:
Albert Inglés Navarrete

Supervisor:
Dr. David Gonzàlez

A thesis submitted in fulfillment of the requirements
for Màster Universitari en Enginyeria Aernàutica (MUEA)

in the

Escola Superior d'Enginyeries Industrial, Aeroespacial i Audiovisual de Terrassa

January 13^{th}, 2021

Declaration of Authorship

I, Albert Inglés Navarrete, declare that this thesis titled, 'Study of stability control systems applied to a racing car' and the work presented in it is my own. I confirm that this work submitted for assessment is my own and is expressed in my own words. Any uses made within it of the works of other authors in any form (e.g., ideas, equations, figures, text, tables, programs) are properly acknowledged at any point of their use. A list of the references employed is included.

Signed: _____

Date: _____

"Thirty-five years later, I can Look back on an eventful,fruitful career – one spent designing cars and asking myself the same series of simple questions. How can we increase performance? How can we improve efficiency? How can we do this differently?
How can I do this better ? *"*

Adrian Newey

Abstract

Recently, a trend in the development of the electric vehicles has arrived to the motorsport and hyper-cars industries. Thus, causing a increase on the interest of developing new technologies that will introduce the electric vehicle as a sport car in the popular mindset.

This study tackles the state-of-the-art technologies of different Torque Vectoring strategies and implements, tune, and simulates a new algorithm that combines the typical yaw rate controllers with a anti-slip control using an optimization methodology.

To do so, a self-made Simulink model has been developed and validated using real test data of a Formula Student vehicle. This simulation testing environment has permitted the comparison of the developed algorithm against without any controller and without the optimization assembly methodology achieving promising results.

Acknowledgements

This project was conducted as a final master thesis on Escola Superior d'Enginyeries Industrial, Aeroespacial i Audiovisual de Terrassa (Universitat Politècnica de Catalunya).

I am very grateful to my Master thesis director Dr. David Gonzàlez for the received support.

Finally, I would like to thank my friends for accepting nothing less than excellence from me. Last but not the least, I would like to thank my family: my parents, my brother and my girlfriend for supporting me spiritually throughout writing this thesis and my life in general.

Albert Inglés Navarrete

Contents

List of Figures

List of Tables

Abbreviations

CoG	**C**enter **o**f **G**ravity
WB	**W**heel **B**ase
TR	**TR**ack
SA	**S**lip **A**ngle
SR	**S**lip **R**atio
IA	**I**nclination **A**ngle
PI$_i$	**P**ressure **I**nternal @ wheel$_i$
AoA	**A**ngle **o**f **A**ttack
ARB	**A**nti **R**oll **B**ar
MR	**M**otion **R**atio
GR	**G**ear **R**atio
@	at

Physical Constants

Gravity acceleration	g	=	$9.81\ \mathrm{ms}^{-2}$
Air Density	ρ	=	$1.225\ \mathrm{kgm}^{-3}$

Symbols

a	Front Axis distance from the CoG	m
b	Rear Axis distance from the CoG	m
h	Height of the CoG	m
k_i	Spring Rate	Nm^{-1}
k_{ARB}	Anti Roll Bar stiffness	Nm^{-1}
TR_f	Front Track	m
TR_r	Rear Track	m
P	Power	W (Js^{-1})
P_r	Real Power	W (Js^{-1})
PI_i	Internal Pressure @ wheel$_i$	Pa
V	Velocity @ CoG	ms^{-1}
r	Yaw velocity @ CoG	rads^{-1}
dr/dt	Yaw acceleration @ CoG (Principal inertia axis Frame)	rads^{-2}
N_i	Normal Force @ wheel$_i$	N
F_{x_i}	Longitudinal Force @ wheel$_i$	N
F_{y_i}	Lateral Force @ wheel$_i$	N
F_{z_i}	Vertical Force @ wheel$_i$	N
M_{x_i}	Rolling Moment @ wheel$_i$	Nm
M_{y_i}	Pitching Moment @ wheel$_i$	Nm
M_{z_i}	Yawing Moment @ wheel$_i$	Nm
a_x	Longitudinal Acceleration @ CoG (Body Frame)	ms^{-2}
a_y	Lateral Acceleration @ CoG (Body Frame)	ms^{-2}
a_z	Vertical Acceleration @ CoG (Body Frame)	ms^{-2}
L	Lift/Downforce	N
D	Drag	N

Q	Aerodynamic Lateral Force	N
m	Mass	kg
C_m	Aerodynamic Pitching Moment Coefficient	[-]
C_n	Aerodynamic Yawing Moment Coefficient	[-]
C_l	Aerodynamic Rolling Moment Coefficient	[-]
PM	Aerodynamic Pitching Moment	Nm
YM	Aerodynamic Yawing Moment	Nm
RM	Aerodynamic Rolling Moment	Nm
MR	Motion Ratio: Sprig deflection VS Wheel movement	[-]
GR	Gear Ratio: Motor shaft angular velocity VS Hub angular velocity	[-]

β	Vehicle Slip angle @ the CoG	rad
α_i	Slip angle @ wheel$_i$	rad
α_{di}	Dynamic Slip angle @ wheel$_i$	rad
ϕ	Pitch angle	rad
θ	Roll angle	rad
γ_i	Angle between velocity and xassis frame @ wheel$_i$	rad
δ_i	Steering angle @ wheel$_i$	rad
δ	Steering angle	rad
ω	Rolling velocity	rads^{-1}

For/Dedicated to/To my family...

Chapter 1

Introduction

In this chapter, a description of this thesis objectives and scope will be described as well as the current technologies on this field. Finally, a proposal will be summarized.

1.1 Aim of the study

The main objectives of developing this study are, on one hand, developing new control algorithms capable to improve the drivability and performance of electric vehicle not only in normal driving conditions but also at limit handling conditions. On the other hand, describe the improvements in control and performance of the electric vehicles in the motorsport industry making possible the association of electric vehicle as a sport vehicle.

1.2 Need identification

On one hand, the climate change awareness is a key factor on the development of electric vehicles and its technologies, concretely during the last decades huge improvements in batteries, motors and motor controllers have been developed by universities and private companies with the objective to improve the electric technologies, reducing the CO_2 emissions.

On the other hand, the need of improving the mobility at the crowded cities and the road safety are key factors of developing autonomous and semi-autonomous systems, such as Advanced driver-assistance systems (ADAS), autopilots, etc.; that may not only improve the comfort during normal driving, but also increasing the safety such as avoiding pedestrians accidents, extreme lane changing manoeuvres, low friction surface braking, etc.

The torque vectoring is a system capable to combine the best part of both objectives, as it is easily applied in independent electric motors vehicles. It can contribute in improving the performance of the vehicle in different aspects:

- It improves the driving comfort and safety during normal and extreme manoeuvres.
  - It will increase the vehicle stability and control by preserving other critical safety limits such as the roll over stability.
  - It reduce the vehicle time reaction when avoiding obstacles, increasing the safety.
  - It increases the manoeuvrability making the vehicle feel more sportive.
- It increases the efficiency by reducing the tire sliding, and hence increasing the longitudinal acceleration.
- It can combine mechanical and regenerative braking capabilities, increasing the efficiency by recovering some energy when braking.

1.3 Contributions

The principal contributions of this thesis are:

- The development of a high fidelity vehicle model that includes:
  - A detailed description of the vehicle, including the suspension and steering systems, the aerodynamics, and the low level controllers of the electric motors.
  - Also, it includes a high fidelity transient tire model, that will introduce some delays in the control actions.
  - In addition, the sensors will be modelled including some delays (Figures 1.1 and 1.2) caused by the communications times, the data filtering (Optical sensor delays), or the physical sensor principle (GPS velocity delay).

- Development of 5 independent classical control algorithms (the yaw rate controller and the 4 wheels anti-slip system) that will be connected by solving a optimization problem.
- Development of a automatic calibration algorithm based on an optimization of a cost function defined by the user, connecting the Simulink model to MATLAB.

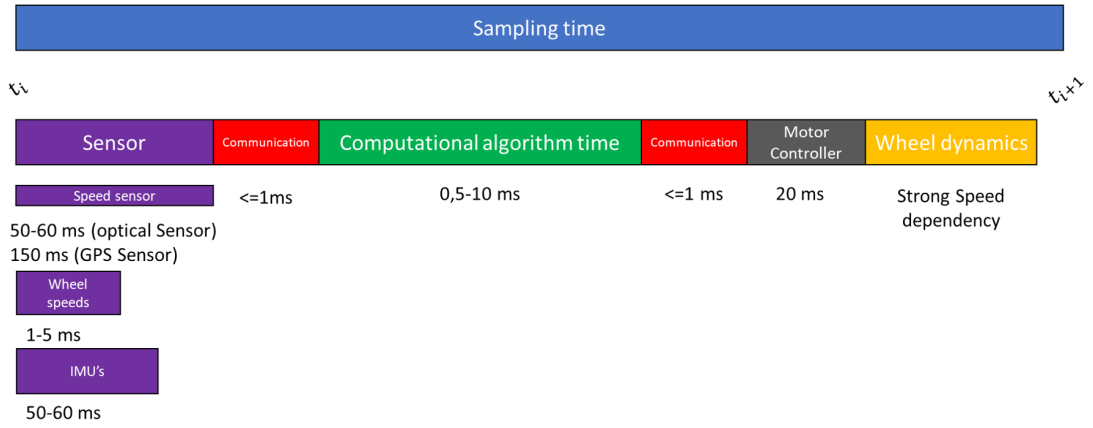

FIGURE 1.1: Sensor delays causes and magnitudes.

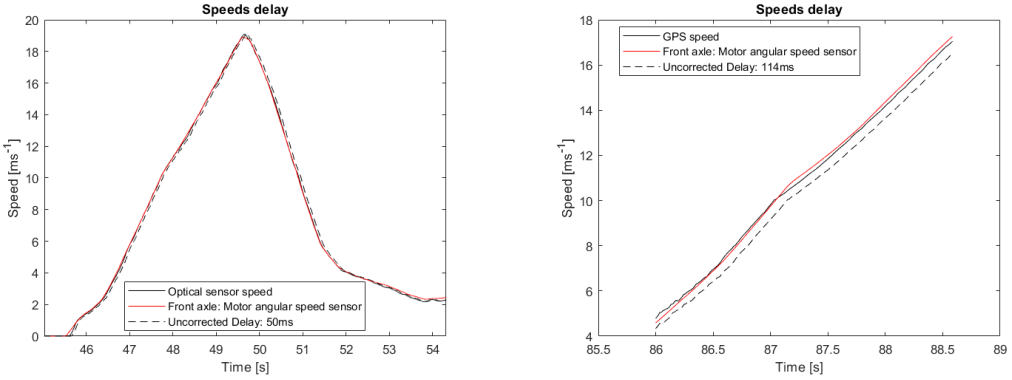

FIGURE 1.2: Speed sensors delays. Left: Optical sensor delay test, Kistler Correvit S-350: 2-Axis Optical Sensors. Right: GPS speed sensor delay test, XSENS MTI-710-G-NGSS.

1.4 Requirements

In this section the requirements of the control algorithm will be described:

- Estimation of the vehicle dynamics in transient manoeuvres.
- Estimation of the tire non-linear behaviour using semi-empirical equations extracted from the literature.
- Estimation of the sensors' errors, variances, delays, and other non-linear features that may affect the control algorithm performance.

The requirements to properly develop this virtual testing environment has been extracted from the recommendations from the reference [20]:

- The user should be a competent vehicle dynamist with the ability to perform mental connections between measured (or simulated data) and the physical data.
- Make a cross-check on magnitudes and sign conventions of the model of all input data items.
- Use a self-developed tire modelling due to the importance of understanding how the raw data have been processed, as it has a huge impact on stability and control of the vehicle.
- It must never be forgotten that the purpose of these model is designing a control algorithm suitable for an electric race car. It is because of this, that the model needs to be so detailed.

1.5 Scope

The scope of this study is to:

- Develop a non-linear vehicle model using Simulink that will represent the most important dynamic features of the real-world vehicle.
- Introduce hardware modelling making possible the study of real-world problems.
- Develop a control strategy capable to perform an improvement of the baseline vehicle by using a combination of state-of-the-art control strategies.
- There will be a study of different combinations of controllers and a comparison of their performance and computational costs.

There will be some analysis out of the scope:

- There will not be a study of the vehicle parameters that will be used.
- There will not be a real-world test of the new developed algorithm.

The engineering process that will be followed is:

1. First, an understanding of the vehicle dynamics and a description of the motion will be described
2. Then, an analysis of the state-of-the-art controllers will be done.
3. Finally, the model will be generated using SIMULINK ©, and the different controller's combination will be tested.

1.6 State-of-the-art

At this section, a detail explanation of the current technologies related with vehicle modelling and control strategies will be done, comparing the advantages and disadvantages of each solution.

1.6.1 Tire models

There exist different types of tire models and they are used in the literature based on different objectives. There exist quite simple models that can predict the normal driving conditions of a passenger car, others that are more complex and are able to estimate the limit handling conditions of the vehicle. Finally, there exists extremely complex models that are used to determine accurately the tire behaviour in a huge range of different conditions, including its transient behaviour.

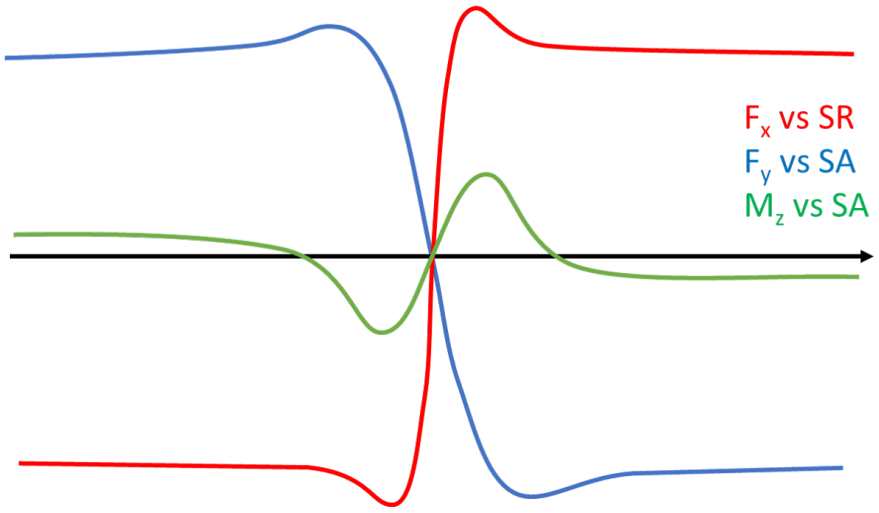

FIGURE 1.3: Parametric representation of the forces generated by the tire.

1.6.1.1 Linear model

It is widely used due to its simplicity, normally its combined by a simplified bicycle model (Ref capitol bicycle model) to achieve a fully linear model, permitting low computational cost solutions with a moderate error. Due to its simplicity is commonly used as a predictive model not as simulation model [4, 19, 29].

The main advantages of this tire model are:

- Independency of longitudinal and lateral forces.
- Longitudinal forces considered as instantaneous.
- Linearity.
- Complex vehicle dynamic approximation.

The main disadvantages are:

- It does not consider saturation.
- It does not consider combined forces.
- It does not consider other effects such as:
  - Inflation pressure.
  - Temperature.
  - Camber (inclination Angle).
  - Tire Moments.
  - Normal force sensitivity.
  - ...

1.6.1.2 Piece-wise linear model

It is based on a linear fitting of the model using piece-wise defined functions used in [11, 31]. This kind of models are used to reduce the computational cost during estates predictions by using a linear evolution of the vehicle depending on the tire working region.

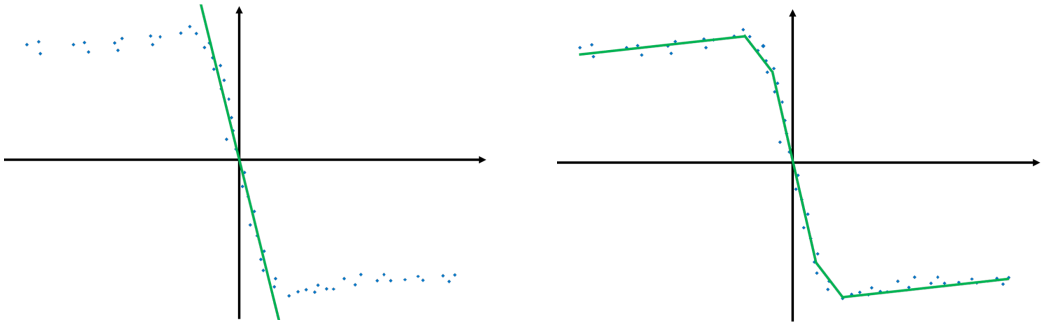

FIGURE 1.4: Linear tire models. Left: linear model. Right: Piece-wise linear model.

Its main advantages are:

- The linearity of the equations.
- The saturation modelling.

The main disadvantages are:

- It has discontinuities in the derivative.
- It does not consider combined forces.
- It does not consider other effects such as:
  - Inflation pressure.
  - Temperature.
  - Camber (inclination Angle).
  - Tire Moments.
  - Normal force sensitivity.
  - ...

1.6.1.3 Burckhardt model

It is based on experimental fitting of a simple tire model based on an exponential function and a linear function, that combined can predict the tire performance during enough range to be used in simple models or controllers [4].

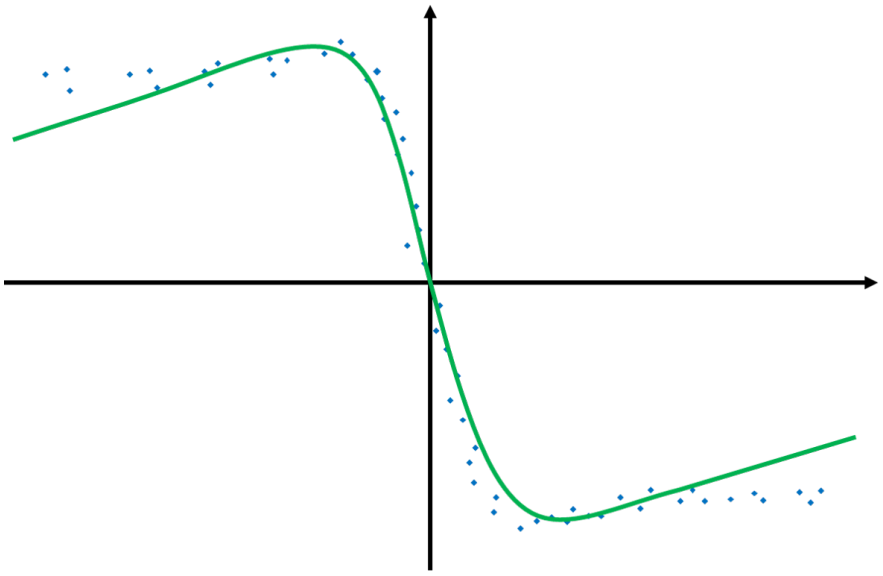

FIGURE 1.5: Linear tire model

Its main advantage is the simplicity of the equation. But it has some disadvantages:

- Do not consider combined forces.
- Do not consider other effects such as:
  - Inflation pressure.
  - Temperature.
  - Camber (inclination Angle).
  - Tire Moments.
  - Normal force sensitivity.
  - ...

1.6.1.4 Brush model

It is based on a physical modelling of the tire, assuming certain pressure distribution at the contact patch and some distributed stiffness properties as well as grip factors. Obtaining a piecewise function defined by a polynomial like equation between the saturation points and a constant value after these saturation points [14, 21].

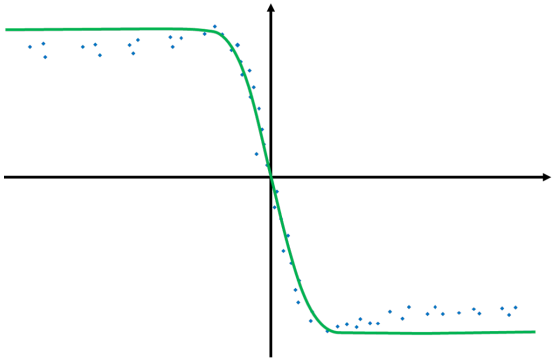

FIGURE 1.6: Brush tire model

Its main advantages are:

- It can consider the saturation.
- It is derivable.
- It can consider combined forces.
- It is based just three parameters.
- It predicts the M_z tire moment.
- It may predict under certain restrictions the Inclination Angle effect (Camber).

Its main disadvantages are:

- It cannot predict the Ackermann behaviour of the tire.
- Its combined behaviour is circular not elliptical. It assumes equal longitudinal and lateral grip factors.
- It does not consider other effects such as:
  - Inflation pressure, temperature, ...

1.6.1.5 Pacejka 2002

It is a semi-empirical tire model based in trigonometric functions that describe the general behaviour of a tire and those coefficients are obtained by empirical data [21].

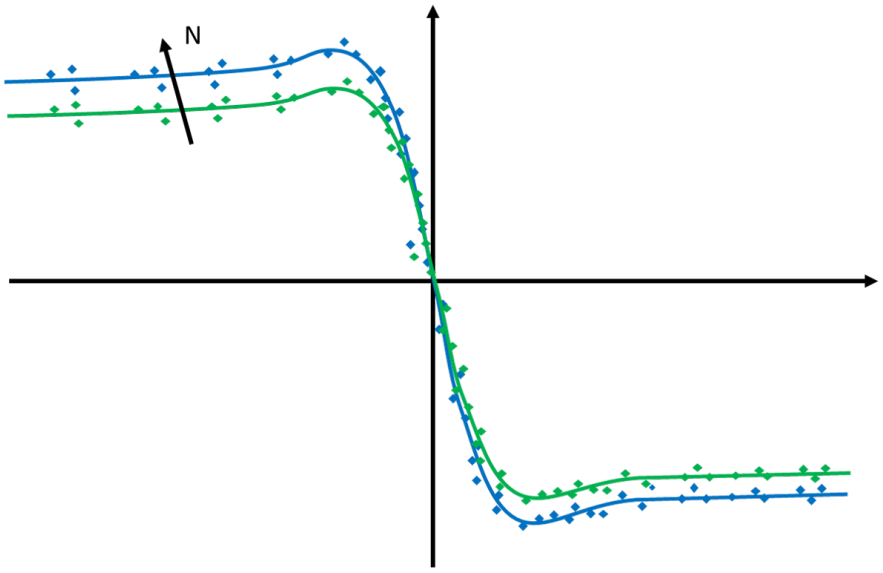

FIGURE 1.7: Pacejka tire semi-empirical tire model.

Its main advantages are:

- It can consider the saturation.
- It is derivable.
- It is continuous.
- It can predict the Ackermann behaviour of the tire.
- It can consider combined forces.
- It predicts the tire moments.
- It may predict other effects such as:
  - Inflation pressure.
  - Camber.
  - Normal force sensitivity.

Its main disadvantages are:

- It is a complex model that need, empirical testing to obtain reliable data.
- It has a huge number of parameters that must be obtained.
- It has higher computational cost than the above models.

1.6.1.6 Magic formula 6.1

It is a semi-empirical tire model based in trigonometric functions that describe the general behaviour of a tire and those coefficients are obtained by empirical data [21]. Concretely is an extension of the previous explained model 1.6.1.5 with increased number of parameters that models better the tire at different conditions.

Its main advantages are:

- It can consider the saturation.
- It is derivable.
- It is continuous.
- It can predict the Ackermann behaviour of the tire.
- It can consider combined forces.
- It predicts the tire moments.
- It may predict other effects such as:
  - Inflation pressure.
  - Camber.
  - Normal force sensitivity.
- It can be implemented in transient using, first order simplification or higher order non-linear approximation.
- It is a precise lumped model.

Its main disadvantages are:

- It is a complex model that need, empirical testing to obtain reliable data.
- It has a huge number of parameters that must be obtained.
- It has higher computational cost than the above models.

1.6.2 Vehicle models

There are different types of vehicle models that are used in the literature to model a car, their choice is based on the main objective of the model. On one hand, there are simplified models that are used to predict the vehicle states in the control loop, those models must have lower computational cost making possible the real-time computation. On the other hand, there are extremely accurate models that are used to estimate accurately the vehicle behaviour during different manoeuvres, making possible a good correlation with the reality.

1.6.2.1 Bicycle model

The bicycle model is the simplest vehicle model that can be used. Its main advantage is the ease of separating the longitudinal dynamics from the lateral-directional dynamics, by assuming that the longitudinal speed changes smoothly and slowly compared with the lateral-directional forces and moments generation. It is because of its simplicity that is mainly used to estimate the vehicle behaviour in the model-based controllers [4, 11, 17, 19, 29].

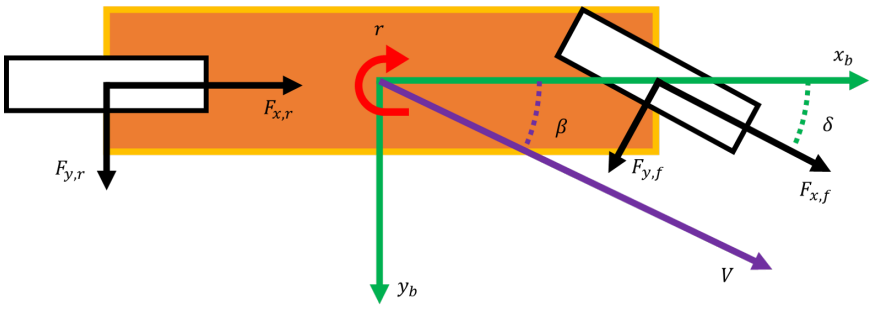

FIGURE 1.8: Bicycle vehicle model.

The main advantages of this model are:

- If it only considers lateral-directional equations, it can be easily linearized:
  - Obtaining a system with simplified planar dynamics.
  - It uses linear tire model.
  - Small angles assumption.
- It has low computational costs.

- It can be described in matrix form, permitting linear algebra operations.
- It may consider longitudinal weight transfer during acceleration/braking manoeuvres.

The main disadvantages of this model are:

- It does not consider lateral load transfer.
- It does not consider tire deflections due to suspension movement.
- It considers instant torque response neglecting tire rotation dynamics.
- Tire moments are neglected.
- It does not consider transient tire dynamics. It needs a inverse longitudinal traction function.

1.6.2.2 Two-track model

The two-track model is the direct evolution of the previous vehicle model, it is used in the literature when combined forces and tire non-linearities need to be considered [ref]. This model can be used not only as a predictive model for the control algorithm but also as a mid to high fidelity level for simulation, depending on the interactions and tire models that are used [4, 11, 12, 17, 19, 22].

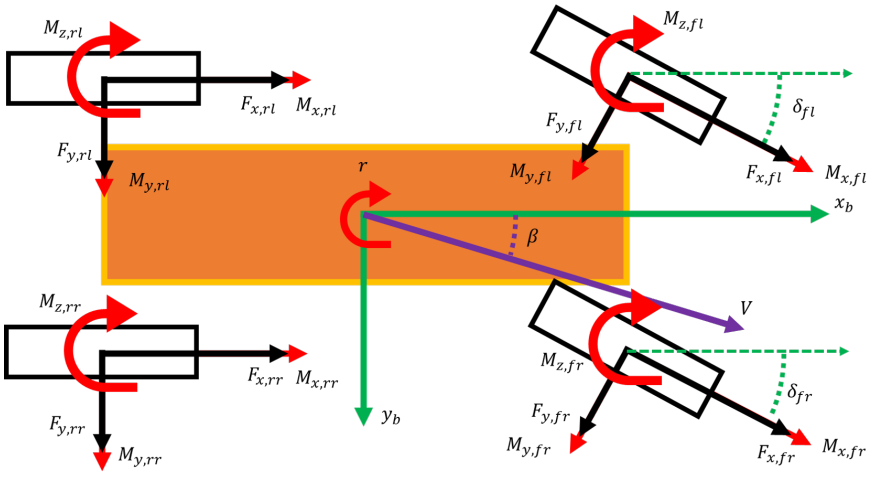

FIGURE 1.9: Two track model description.

The main advantages of this model are:

- There are four independent wheels.
  - It considers longitudinal forces distribution.
  - It considers each wheel lateral forces.
  - Small angles assumption.
- It can be linearized:
  - It may consider planar dynamics, assuming smooth longitudinal dynamics.
  - Small angles hypothesis.
  - Tire linearization.
  - Steady-state tire forces.
- It may consider tire moments.
- It may consider the tire rotational dynamics, or it may have instant torque response.
- It may consider the tire lateral dynamics.

The main disadvantages of this model are:

- It does not consider tire deflections due to suspension movement or it assumes polynomial regression as function of body acceleration.
- The load transfer precision is limited due to the suspension modelling.
  - The load transfer is assumed to be instantaneous, assuming steady state conditions and not considering the damping forces.
  - Road surface must be considered smooth.
- It has higher computational costs.
- Detailed information about the vehicle is needed.

1.6.2.3 Multi-body model

It is the most complex and accurate model that can be used. It is only used as simulation model.

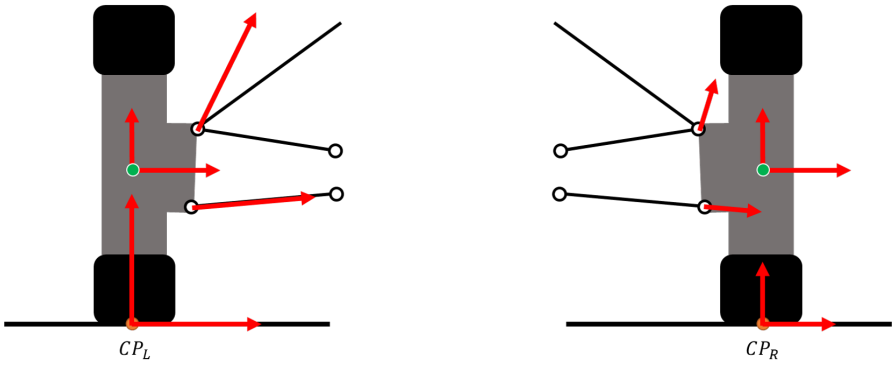

FIGURE 1.10: Multi-body dynamic model description.

The main advantages of this model are:

- It is a high-fidelity model.
- It may consider any or few assumptions.
- It can model the full vehicle dynamics including each moving element independently.
- It can consider bumpy road surfaces.
- Parametrizable aerodynamics based on body motion.

The main disadvantages of this model are:

- It has high computational costs.
- Extremely detailed information about the car is needed.

1.6.3 Control algorithms

In this section, a review of the current algorithm used in the torque vectoring systems will be done.

1.6.3.1 Feed-forward controllers

These types of controllers are used as a first approximation of the optimal control action for Yaw Rate control algorithm at [29].

FIGURE 1.11: Feed-forward controler scheme.

The main advantages of this controller are:

- Its simplicity.
- Its rapid response.
- The ability to counteract external disturbances.
- It does not need any sensors or measurements of the systems states.

The main disadvantages are:

- Its inaccuracy, as they do not know the real state of the system.
- Its dependency on the system model precision and accuracy.

To solve these disadvantages, these controllers are commonly combined with feed-back controllers, that introduce the real state of the system increasing the accuracy and decreasing the long-term deviation, maintaining the rapid response and the possibility of tracking desired outputs path by rejecting disturbances.

1.6.3.2 Feed-back controllers

The feed-back controllers are based on the error information between the desired output and the current output. Its main objective is minimizing this difference by using the feedback information to obtain an improved input.

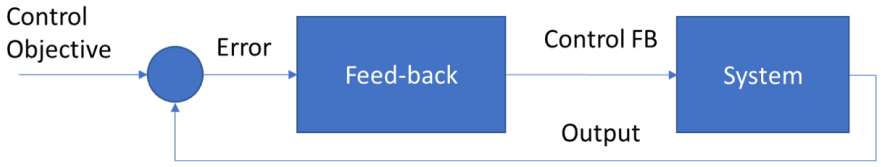

FIGURE 1.12: Feed-back controller scheme.

PID:
It is one of the most used control systems in the industry for controlling simple plants, because of this it is very used as a first approach as a control algorithm for the Torque Vectoring [4, 30].

The main advantages of this controller are:

- Its simplicity.
- The integral component can reduce the long-term tracking error to zero.

The main disadvantages are:

- It is based in SISO systems
- It is only useful for linear or quasi-linear systems.
- It does not use any information of the system, making the response less robust.
- It has slow response.
- It may need anti-windup strategies for the integral part tracking error.
- It cannot deal with physically constrained inputs.

Linear quadratic regulator:
The Linear Quadratic Regulator (LQR) is a proportional feedback controller that is used because of the easy tuning capability based on response objectives. It is used to improve the PI controllers' capabilities, as it can control not only the yaw rate but also the slip angle of the vehicle increasing the stability and thus the safety [4, 29].

The main advantages of this controller are:

- Its ease of implementation as it is based on the multiplication of error vectors and gain matrix.
- The ability to control MIMO systems.
- It uses information of the system by obtaining the optimal K matrix coefficients.

The main disadvantages are:

- It is only useful for linear or quasi-linear systems.
- It may have long-term tracking error as it does not use error integration.
- It cannot deal with physically constrained inputs.

And improvement of the simples proportional LQR system is based on adding some error integration and converting the LQR to a kind of LQR-I controller as proposed by [J. Antunes].

Model predictive control:
The Model Predictive Controllers (MPC) are useful for controlling systems that can be easily modelled. Depending on the complexity of those models there are different approach.

Linear MPC:
The Linear-MPC is used when the plant can be modelled as a linear system, and the system dynamics need to be controlled accurately and the inputs and/or outputs are physically constrained [11, 17, 19].

The main advantages of this controller are:

- It is based on an optimization problem, obtaining an optimal or sub-optimal response of the system.
- The ability to control MIMO systems.
- It uses information of the system.
- It can deal with constrained outputs and inputs.

The main disadvantages are:

- It is only useful for linear or quasi-linear systems.
- Its implementation is complex.
- An accurate model guarantees an optimal response.
- It might have high computational costs and times.

Non-linear MPC

It is the generalization of the previous controller. There exist several strategies to deal with the non-linearity of the system, [16, 19, 25]:

- Some authors propose a linearization of the system at each step by using ACADO Toolkit obtaining a sequential quadratic programming problem [19, 25]. Concretely, [19] uses the RTI scheme to solve the sequential linear quadratic problem.
- Some authors propose a linearization of the system at each step by using PDIP obtaining a sequential quadratic programming problem [25].

The main advantages of this controller are:

- It is based on an optimization problem, obtaining an optimal or sub-optimal response of the system.
- The ability to control MIMO systems.
- It uses information of the system.
- It can deal with constrained outputs and inputs.
- It can deal with non-linear systems

The main disadvantages are:

- Its implementation is complex.
- Its calibration and tuning are complex
- An accurate model guarantees an optimal response.
- It has high computational costs and times.

Neural-Network
It is based on the learning capabilities of the neural network to obtain a non-linear model [12, 22].

The main advantages of this controller are:

- It is based on an optimization problem, obtaining an optimal or sub-optimal response of the system.
- The ability to control MIMO systems.
- It uses information of the system.
- It can deal with constrained outputs and inputs.
- It can deal with non-linear systems.
- It has less computational costs than the NL-MPC.

The main disadvantages are:

- Its implementation is complex.
- It needs training time and data to fit a non-linear model
- Its calibration and tuning are complex.
- An accurate model guarantees an optimal response.

1.7 Proposal

Once a study of the current technologies used in modelling and controlling the vehicle, it is possible to compare them with the requirements and the scope of this study.

On one hand, one of the main features that this model might include is the transient description of complex manoeuvres, including non-linearities, and delays. On the other hand, the model might be simple enough to develop it within 300h using the knowledge of an Aerospace engineer and to run in almost real time in a laptop. The main objective of developing this model is achieving a better understanding of the vehicle dynamics and control engineering field. Finally, it must be described by independent blocks that might be improved in the future.

Considering the previous knowledge and the objective of introducing into non-linear systems control, the main controllers that will be tested and programmed are the PID controller and the LQR controller, both combined with a linear feed-forward controller (see figures 1.13 and 1.14). Finally a novel combination of the traction control and yaw rate control will be studied and tested.

The vehicle model will be a two-track model with a linear suspension model. At the same time the aerodynamic forces will be modeled and considered. In addition,a complete description of the tire dynamics will be done using the Magic Formula 6.1 adding a linear and first order transient behaviour as described in [5]. Finally, the sensors delays and non-linearities will be considered in the model.

TABLE 1.1: Tire model comparison.

Tire Model	**Derivable**	**Saturation**	**Combined**	**Transient**	**Moments**	**Other sensitivities**
Linear	Yes	No	No	No	No	No
Piece-wise linear	No	Yes	No	No	No	No
Buckhardt	Yes	Yes	Circular	No	No	No
Brush	Yes	Yes	Circular	No	Mz	IA (limited) and Normal
Pacejka 2002	Yes	Yes	Yes	Yes	No	IA, Normal and Pressure
Magic Formula 6.1	Yes	Yes	Yes	Yes	Yes	IA, Normal, Pressure, Velocity, Temperature, ...

TABLE 1.2: Vehicle model comparison.

Vehicle Model	**Linearizable**	**Normal force Saturation**	**Combined**	**Moments**	**Transient body motion**	**Tire deflection**
Bicycle	Yes	No	No	No	No	No
2-Track	Yes	Approximation	Yes	Yes	Approximation	Approximation
Multi-body	Not useful	Yes	Yes	Yes	Exact	Exact

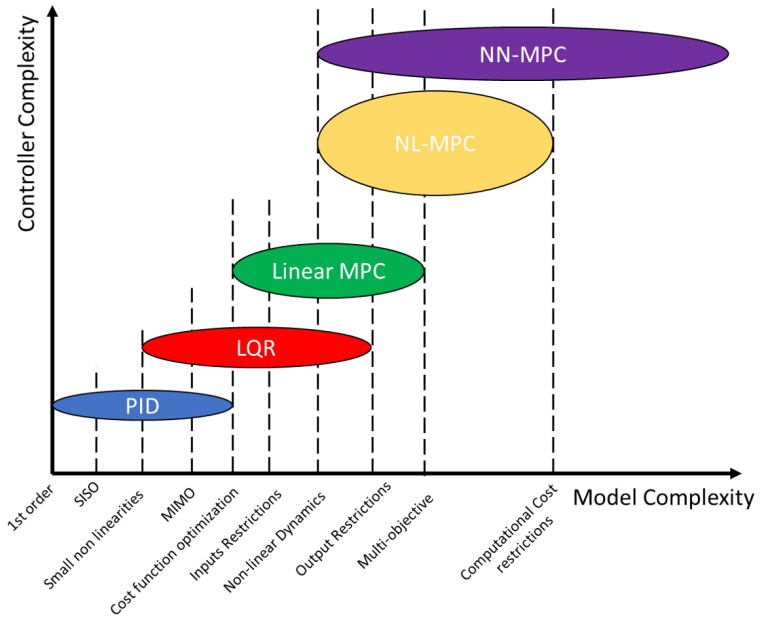

FIGURE 1.13: Control algorithms versus system complexity. Qualitative approach.

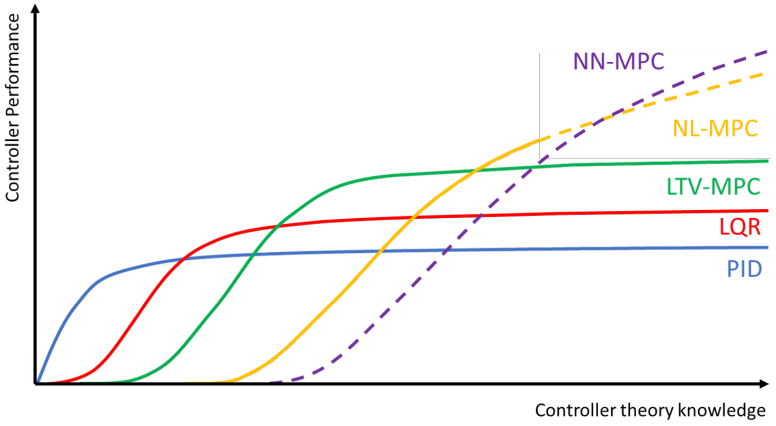

FIGURE 1.14: Control algorithms versus control theory knowledge. Qualitative approach.

Chapter 2

Theoretical development

In this chapter, a detailed explanation of the theoretical basis on this study is based will be done. In particular, different science field will be treated. Starting with reference systems moving to vehicle dynamics, after Suspension modeling, electric powertrain units, sensors modelling, and finally control theory.

2.1 Reference systems

In this section, a definition of the most suitable axis systems will be explained (Source: [2, 5, 20]). The starting point will be the earth reference system and it ends up in each subsystem reference system.

2.1.1 Inertial reference system

The most inertial reference system that could be used is one attach to the Earth, Centered at its center and with the z_I pointing at the rotation axis direction and northward, x_I contained at the Equator plane and pointing to the Aries point γ and y_I using the trihedral theorem anti-clockwise. This reference system would be highly accurate for any object subjected to the earth gravitational field. But it will be more complex to describe the trajectories of the systems and it will not be easy to extract conclusions.

2.1.2 Rotating geocentric reference system

It is the same system but attach to the Earth rotation, with the same center but with x_g axis pointing at all moments to the Greenwich Meridian. As in the previous, reference

system it will introduce some complexity that will not improve the precision significantly if applied to to a road vehicle system.

2.1.3 Earth axis system

then, the reference system that will be considered inertial is the earth axis system. This is possible after assuming, non-rotating and planar earth. Which is almost true for low speeds systems, including airplanes and road transport systems.

The origin is any point at the Earth surface defined by the longitude τ_e and the latitude λ_e and z_e pointing to the Earth center, x_e pointing, normally, to the north and y_e using the trihedral theorem anti-clockwise.

2.1.4 Body axis system

The body axis system is a references system attached to a body that is maintaining the orientation and position respect to that object at any moment. Concretely, it is centered to the CoG and x_b is contained at the symmetry plane of the vehicle and pointing forward, the z_b is contained at the symmetry plane and pointing downward and y_b using the trihedral theorem anti-clockwise, so pointing to the right side of the vehicle. The main use of this type of axis, that has its origins in aircraft usage, is that it is fixed in the vehicle and the inertia properties relative to it are taken as constant.

The body axis system will be used on two of the main bodies of the vehicle. The SAE axis will be used as a reference system at each tire as shown in figure 2.1. And, it will be used on the suspended mass as is described in the figure 2.2.

There exist a especial type of body axis system, the **Principal Inertia System**, that is defined by the principal directions of the inertia tensor of the body, this system main advantage is that the inertia tensor is diagonalised, simplifying some of the calculations.

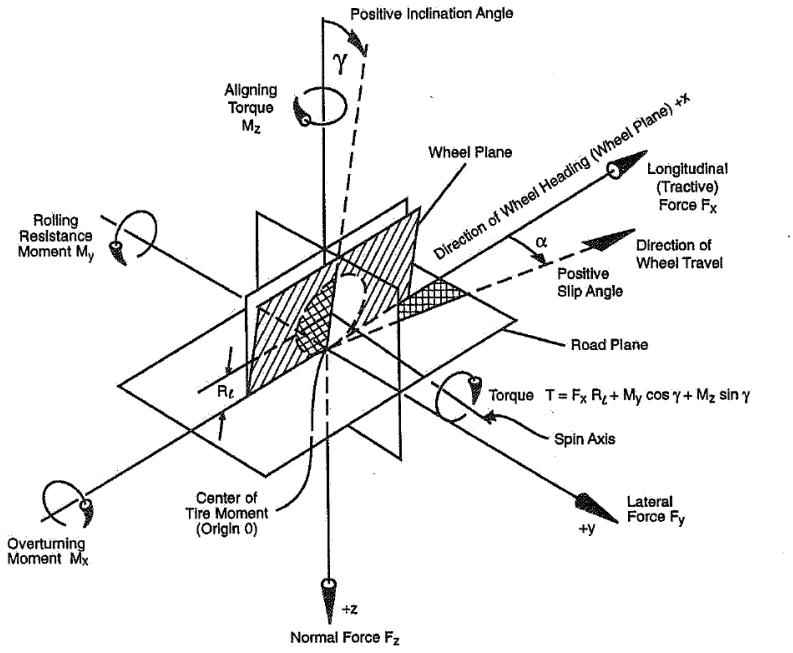

FIGURE 2.1: Wheel SAE axis. Source: [20] (p.: 62)

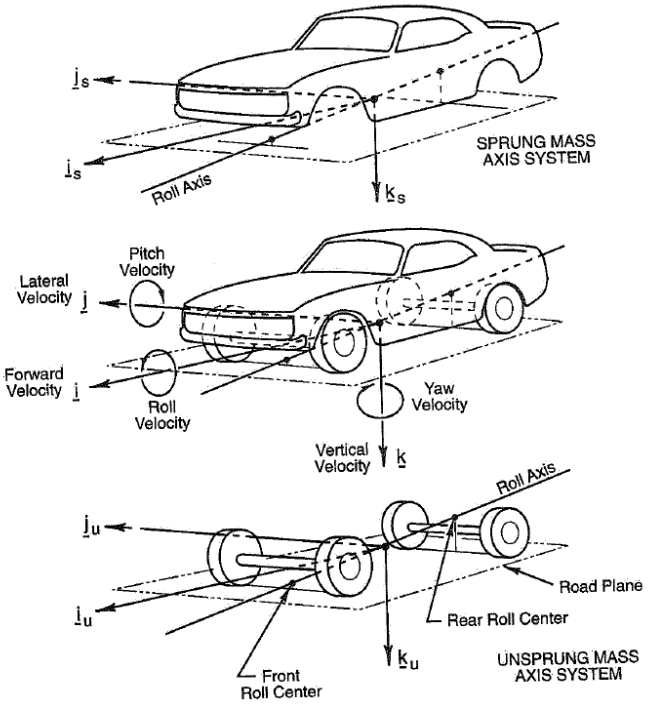

FIGURE 2.2: Sprung Mass axis and unsprung Mass axis. Source: [20] (p.: 103)

2.1.5 Intrinsic axis system

It is a reference system attach to a point and its trajectory. Concretely, it is centered to the CoG and the x_v is pointing forward in the velocity direction, the z_v is pointing vertical and the y_v using the trihedral theorem anti-clockwise.

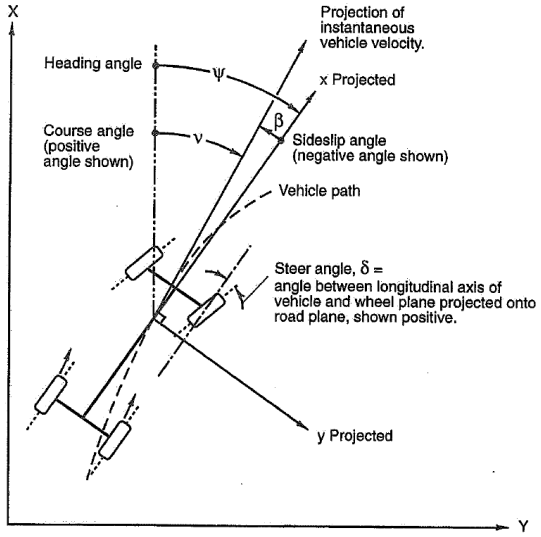

FIGURE 2.3: Intrinsic reference system vs body axis and inertial reference system. Source: [20] (p.: 105)

2.2 Vehicle dynamics

The overall technical objective in racing is the achievement of a vehicle configuration that fulfill the rules and exhibits an acceptable performance when operated manually by a driver [20, 24].

In road vehicle dynamics the causes of the movement are the wheels, because of this fact, all the design must be focused on improving the performance of the sum of the four wheel. Then, the first concepts that may be explained are the ones related to the wheel:

- **Slip Angle**: It is the main cause of generating lateral forces. It is defined as the angle between the wheel heading and the instantaneous velocity direction at the contact point in the symmetry plane. This angle appear due to the fact that a real wheel deforms when a force is applied or vice-versa, a force appear when a deformation is induced.

- **Slip Ratio**: It is the main cause of generating longitudinal forces. It is defined as the difference between the free shaft angular speed –the speed projected in the wheel plane and dived by the effective radius– and the angular velocity of the shaft and normalized by the free shaft angular speed.
- **Inclination Angle**: It is the angle between tilted wheel plane and the vertical plane.
- **Normal Force**: All tire forces and moments are function of the vertical load and near the tire limit is is one of the most important parameters.
- Other variables: That may affect to the force, such as tire temperature, pressure and longitudinal speed.

In racing the main objective is controlling the previous variables, obtaining the desired value at each moment in order to maximize the **longitudinal** and **lateral** forces and/or the **yaw moment**. To do so, it is important to understand the suspension geometry and the load transfer that occurs when accelerating and/or turning:

- **Instant axis (IA)**: It is the line where the wheel instantaneously turns from at a given time.
- **Instant Center (IC)**: It comes from the 2D kinematics study of the suspension geometry. In suspension design is convenient to break down the 3D problem into two 2D problems. Two planes have to be set, one parallel to the centre-line of the vehicle and the other perpendicular both crossing at wheel center. After this the suspension geometry is going to be projected and analyzed separately, the idea is to intersect the instant axis in both planes and find a point (IC) in each.
- **Roll Center (RC)**: It the point where the chassis turn when a rolling Moment is applied, it can be estimated by projecting the line from the center of the tire-ground contact patch through the front view IC and this is repeated for each side of the car. Where both line cross is the position of the Roll Center (for more detail go to figure 2.4)
- **Pitch Center (PC)**: It is the same as the roll center but in the pitching direction.
- **Swing Arm**: It is the distance between the IC and the wheel center and it is used to estimate the IA changing due to a given roll.
- **Center of gravity (CoG)**: It is the place where the mass forces are applied, its position is the main cause of load transfer and its a key parameter to improve the dynamics of a vehicle.

- **Sprung and Unsprung Mass**: the Sprung Mass is the one that is contained after the springs and dampers whereas the Unsprung Mass is the one is in contact with the ground and before the springs and dampers.

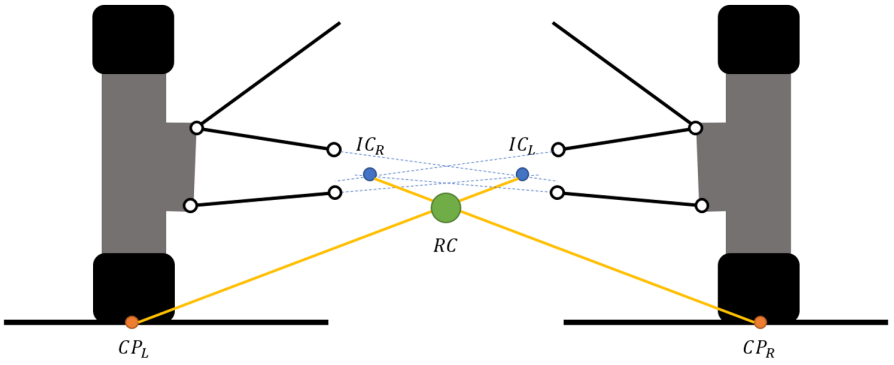

FIGURE 2.4: Lateral suspension parameters calculation: RC and IC.

All this parameters are keys when talking about load transfer, and as it has been said before, vertical load when the tire is near the limit – in Racing conditions – is one of the most important parameters, and also, all these parameters rule the variation of the roll and pitch angles as well as the Inclination Angle at each wheel that will change the tire and the aerodynamics forces contribution.

2.3 Vehicle models model

There are different types of vehicle models that are used in the literature to model a car, their choice is based on the main objective of the model. On one hand, there are simplified models that are used to predict the vehicle states in the control loop, those models must have lower computational cost making possible the real-time computation. On the other hand, there are extremely accurate models that are used to estimate accurately the vehicle behaviour during different manoeuvres, making possible a good correlation with the reality.

2.3.1 Bicycle model

The bicycle model is a simplified vehicle dynamic model that assumes that there is only on tire per axle and it is placed at the symmetry plane of the vehicle. With this simplification, the computational costs and the equations complexity is extremely reduced, obtaining a model that can predict the vehicle behaviour during different manoeuvres. In general, this model may be non-linear with longitudinal and lateral-directional dynamics coupled:

$$\ddot{x} = \frac{\sum F_{x_i} + D_x}{m} + \dot{x}sin(\beta) \cdot \dot{\phi} \tag{2.1}$$

$$\dot{\beta} = \frac{\sum F_{y_i} + Q_y}{m \cdot \dot{x}cos(\beta)} - \frac{\ddot{x}}{\dot{x}}\tan(\beta) - \dot{\phi}$$

$$\ddot{\phi} = \frac{\sum M_{z_i} + M_{z_aero}}{I_{zz}}$$

The main causes of non-linearity are the angles calculations and the tire model:

$$[F_{x_i}, F_{y_i}] = TireModel(N_i, \alpha_i, SR_i, etc) \tag{2.2}$$

Where:

$$\alpha_f = \text{atan}\left(\frac{\dot{x}\sin(\beta) + a\dot{\phi}}{\dot{x}\cos(\beta)}\right) - \delta; \qquad \alpha_f = \text{atan}\left(\frac{\dot{x}\sin(\beta) - b\dot{\phi}}{\dot{x}\cos(\beta)}\right) \tag{2.3}$$

This model is extensively used in its linearized form due to its simplicity, using other assumptions such as:

- Small angles simplification.
- Linear tire model: $F_y = C_y\alpha$
- Steady state tire dynamics.
- Considering planar dynamics. Longitudinal dynamics slower than lateral dynamics.

Then, the obtained system is [4, 17, 19, 20]:

$$\begin{bmatrix} \dot{\beta} \\ \ddot{\phi} \end{bmatrix} = \begin{bmatrix} \frac{C_{y,f}+C_{y,r}}{m\cdot V} & \frac{aC_{y,f}-bC_{y,r}}{m\cdot V^2} - 1 \\ \frac{C_{y,f}-C_{y,r}}{I_z z} & \frac{a^2C_{y,f}+b^2C_{y,r}}{I_z z\cdot V} \end{bmatrix} \begin{bmatrix} \beta \\ \dot{\phi} \end{bmatrix} + \begin{bmatrix} 0 & \frac{C_{y,f}}{m\cdot V} \\ \frac{1}{I_z z} & \frac{aC_{y,f}}{I_z z} \end{bmatrix} \begin{bmatrix} M_z \\ \delta \end{bmatrix} \tag{2.4}$$

2.3.2 Two-track model

The two-track model is the direct evolution of the previous vehicle model. On one hand, this model can consider the vertical load at each wheel independently, evaluating the lateral load transfer through considering the roll stiffness distribution effect, the aerodynamic forces, and the tire moments, permitting an exhaustive analysis on handling and stability. On the other hand, this type of model has special interest in the torque vectoring development as it is the simplest model with four independent wheels, permitting the study of the motor torque distribution on the vehicle dynamics and it can accurately predict the tire longitudinal dynamics.

Moreover, it is possible to modify this model to consider the suspension movements and the steering system non-linearities by assuming a polynomial regression of the tire movements as function of the body acceleration and steering input.

The equations of motion of this model are:

$$\ddot{x} = \frac{\sum F_{x_i} + D_x}{m} + \dot{x}\sin(\beta)\cdot\dot{\phi} \tag{2.5}$$

$$\dot{\beta} = \frac{\sum F_{y_i} + Q_y}{m\cdot\dot{x}cos(\beta)} - \frac{\ddot{x}}{\dot{x}}\tan(\beta) - \dot{\phi}$$

$$\ddot{\phi} = \frac{\sum M_{z_i} + M_{z_aero}}{I_{zz}}$$

$$\dot{\omega_i} = \frac{F_{x_i}R_{L_i} - T_i}{J_i}$$

Where the forces and moments are evaluated by using:

$$[F_{x_i}, F_{y_i}, M_{z_i}, M_{x_i}, M_{y_i}] = \text{TireModel}(N_i, \alpha_i, SR_i, etc.) \tag{2.6}$$

Where:

$$SR_i = \frac{\omega_i R_{L_i} - v_{x_i}}{v_{x_i}} \tag{2.7}$$

$$\alpha_i = \tan\left(\frac{v_{y_i}}{v_{x_i}}\right) - \delta_i \tag{2.8}$$

And:

$$v_{x_1} = \dot{x}\cos(\beta) + \frac{TR_f}{2}\dot{\phi}; \qquad v_{y_1} = \dot{x}\sin(\beta) + a\dot{\phi} \tag{2.9}$$

$$v_{x_2} = \dot{x}\cos(\beta) - \frac{TR_f}{2}\dot{\phi}; \qquad v_{y_2} = \dot{x}\sin(\beta) + a\dot{\phi}$$

$$v_{x_3} = \dot{x}\cos(\beta) + \frac{TR_r}{2}\dot{\phi}; \qquad v_{y_3} = \dot{x}\sin(\beta) - b\dot{\phi}$$

$$v_{x_4} = \dot{x}\cos(\beta) - \frac{TR_r}{2}\dot{\phi}; \qquad v_{y_4} = \dot{x}\sin(\beta) - b\dot{\phi}$$

Finally, it is possible to add transient behaviour of the tire lateral and longitudinal dynamics by using:

$$\dot{\alpha_i} = f(\alpha_i, N_i, P_i, v_{x_i}, etc); \qquad \dot{SR_i} = g(SR_i, N_i, P_i, v_{x_i}, etc) \tag{2.10}$$

It is possible to simplify this model by assuming fast tire longitudinal dynamics, but then an inverse longitudinal tire must exist:

$$[SR_i] = \text{TireModel}^{-1}(N_i, \alpha_i, F_{x_i}, etc.) \tag{2.11}$$

2.3.3 Multi-body model

It is the most complex and accurate model that can be used. It may describe the dynamics of all the moving elements that are interconnected to form the vehicle, including the suspension control arms, steering, suspended mass, unsuspended mass, etc. This model may be simplified by adding some hypothesis:

- Steady state load transfer and suspension movements.
- Linearized suspension analysis.
- Small angles simplification.
- Smooth road surface.
- Parametrizable aerodynamics based on body motion.

2.4 Suspension model

The suspension controls the body movement of the vehicle during external forces excitation. To do so, it must distribute the forces and moments though the body and the suspension elements until reaching the contact patch which are the only restrictions. As it has been explained there exist different types of models that can be classified by the number of degrees of freedom that are modelled.

On one hand, there exists the simplest 3 degrees of freedom model that are the suspended mass movements in height, roll and pitch. Also, there exists a model with 8 degrees of freedom that model the unsuspended mass vertical movement and the contact patch displacements due to road irregularities. Finally, there exist the multi body description that characterize the movement of each element of the suspension independently combining dynamic equations and kinematic restrictions with the stiffness of the flexible parts.

On the other hand, those models can be modelled using linear relations assuming small displacements, or non-linear functions that must be solve iteratively.

Finally, it is possible to model the vehicle using quasi-static formulation assuming that the suspension movements are fast enough to consider them instantaneous or assuming that they are dynamic with some damping elements and inertia and mass distribution.

2.5 Powertrain model

The powertrain will be considered in two different stages of the model, on one hand it will be considered as a torque limiter at each wheel when obtaining the anti-slip parameters. This may be done by obtaining a maximum and a minimum available torque as function of the angular speed:

- The simplest way is assuming a constant maximum and minimum torque.
- A more complex but useful way may be considering the motor as an ideal electric machine with a maximum and minimum torque, power, and angular speed as described in figure:

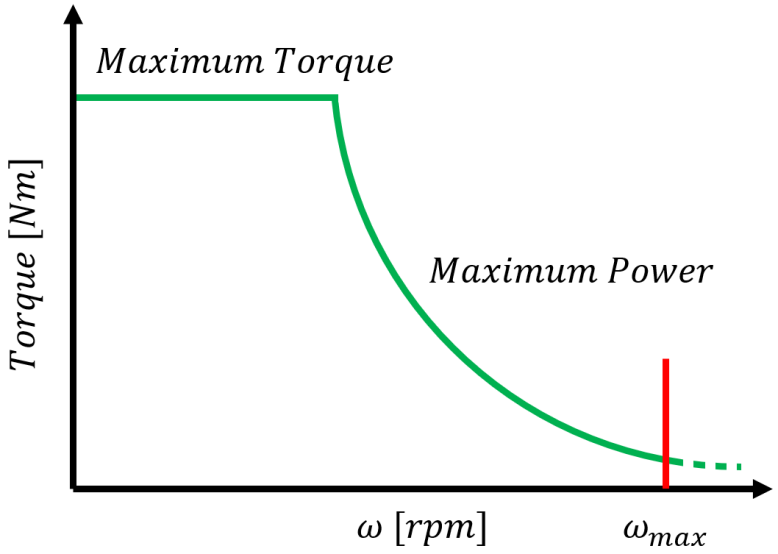

FIGURE 2.5: Powertrain model envelope.

- Finally, a look up table can be used to obtain the maximum and minimum value based on experimental tests.

For the sake of simplicity, in this thesis the first option has been chosen. Being the other option a slight modification of the developed model. On the other hand, the powertrain will affect the dynamics of the system by introducing a delay between the desired torque and the real one. This effect is caused by the low-level controller inside each motor controller unit and the electric inertia of the motor. To solve this problem, a linear one degree of freedom model will be used:

$$T(s) = \frac{T_{obj}}{(1 + \tau s)} \tag{2.12}$$

2.6 Control algorithms

In this sections the theory of the control algorithms that will be implemented are described. For the sake of simplicity, only classical control algorithms will be implemented in this thesis.

2.6.1 Feed-forward controllers

They are based in a prescribed desired path of certain control variables that may be followed by the system. Its objective is obtaining the inputs that will follow this response. To do so, a simplified model of the system is "inverted" or "pseudo-inverted" to obtain the inputs that will satisfy the desired outputs.

2.6.2 Feed-back controllers

Those controllers are based on a feed-back loop that informs the controller about the difference between the desired output and the current output.

2.6.2.1 PID

It is one of the most used control systems in the industry, the desired input that will improve the output is based on the sum of proportional feed-back error, the integration of the that error and its time derivative.

2.6.2.2 LQR

The linear quadratic regulator (LQR) is based on the feed-back of all the measurable states error of the system that will be multiply by a predefined K matrix obtaining the desired inputs. The main characteristic of this system is the way to calculate the K matrix, it is obtained by optimizing its coefficients in order to minimize cost function that is based in the error integral ($\epsilon^T Q \epsilon$), the inputs costs ($u^T R u$) and, in some cases, the crossed costs ($2C\epsilon^T N u$):

$$J = \int_0^\infty \left(\epsilon^T Q \epsilon + u^T R u + 2C\epsilon^T N u\right) dt \tag{2.13}$$

Where:

$$u = -K\epsilon \tag{2.14}$$

Chapter 3

Model development

The simulation model will be full self-developed in Simulink. On one hand, the vehicle model will be a high-fidelity model with a complete description of the vehicle taking an accurate attention on the tire modelling and behaviour. On the other hand, the control system will be based in different described control algorithm, including a model of hardware in the loop limitations, such as sensors time delays, noise, and uncertainties.

3.1 Vehicle simulation model

As it has been explained, a high detail model will be used to approximate the real-world phenomena. Using a complex and highly computational cost model.

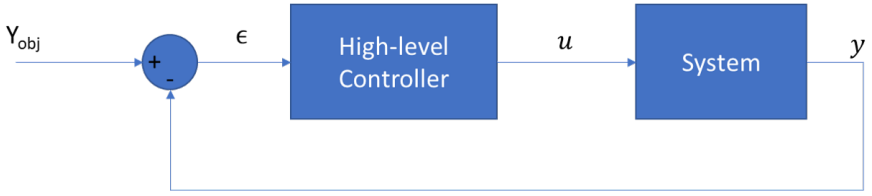

FIGURE 3.1: Developed model general scheme.

3.1.1 Tire model

The proposed tire model is the Magic Formula (MF 6.1) using linear transient behaviour for the SA calculation ([5]). This model considers several physical effects on the tire behaviour by combining, the normal force (N), tire equivalent slip angle (α), tire slip ratio (SR), tire inclination angle (IA), tire inflation pressure (P_i) and tire speed (V_x), permitting the evaluation of longitudinal (F_x) and lateral forces (F_y), overturning moment (M_x), rolling resistance (M_y) and self-aligning moment (M_z):

$$[F_x, F_y, M_x, M_y, M_z] = \text{MF6.1}(N, \alpha_d, SR, IA, P_i, V_x) \tag{3.1}$$

Where α_d is the dynamic slip angle, and it is obtained by using a first order model:

$$\dot{\alpha_d} = \frac{v_x}{\sigma_y}(\alpha - \alpha_d) \tag{3.2}$$

This tire model is based on over 100 parameters and over 50 scaling factors that must be fitted from real data. Concretely, in this study the tire data has been extracted from the Tire Test Consortium (TTC) and the fitting program that has been used is the OptimumTire.

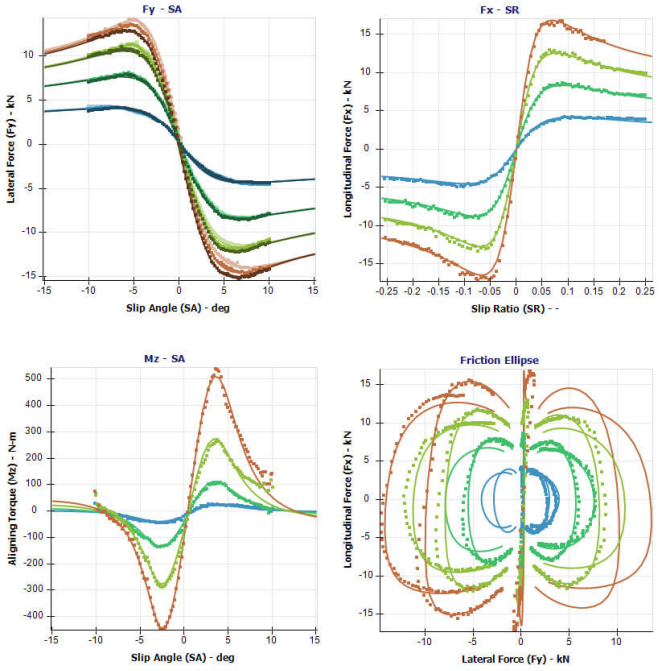

FIGURE 3.2: Optimumtire software used for tire Magic Formula 6.1 fitting. (Source: https://optimumg.com/wp-content/uploads/2019/08/tire_1-1.jpg).

3.1.2 Aerodynamic model

The aerodynamic forces and moments are defined in the intrinsic aerodynamic reference frame, supposing that there is not wind this reference system coincide with the intrinsic reference system of the vehicle. The forces are in x_v direction the drag force (D), in the y_v direction the lateral aerodynamic force (Q) and in z_v direction the Lift/Downforce (L). Similarly, the moments are in x_v direction the roll moment (RM), in the y_v direction the pitch moment (PM) and in z_v direction the yaw moment (YM). Those forces and moments can be adimensionalized obtaining the following dimensionless parameters that can be supposed constant:

$$
\begin{aligned}
D &= \frac{1}{2} C_D \rho S_{front} V^2 \\
Q &= \frac{1}{2} C_Q \rho S_{front} V^2 \\
L &= \frac{1}{2} C_L \rho S_{front} V^2 \\
RM &= \frac{1}{2} C_{M_x} \rho S_{front} L_{ref} V^2 \\
PM &= \frac{1}{2} C_{M_y} \rho S_{front} L_{ref} V^2 \\
YM &= \frac{1}{2} C_{M_z} \rho S_{front} L_{ref} V^2
\end{aligned}
\tag{3.3}
$$

However, this simplified model can be improved by adding some linear relationships between the coefficients and the suspended mass movements.

$$
\begin{aligned}
C_D &= C_{D_0} + C_{D_h} h + C_{D_\psi} \psi + C_{D_\beta} \beta \\
C_Q &= C_{Q_0} + C_{Q_h} h + C_{Q_\psi} \psi + C_{Q_\beta} \beta \\
C_L &= C_{L_0} + C_{L_h} h + C_{L_\psi} \psi + C_{L_\beta} \beta \\
C_{M_x} &= C_{M_x,0} + C_{M_x,h} h + C_{M_x,\psi} \psi + C_{M_x,\beta} \beta \\
C_{M_y} &= C_{M_y,0} + C_{M_y,h} h + C_{M_y,\psi} \psi + C_{M_y,\beta} \beta \\
C_{M_z} &= C_{M_z,0} + C_{M_z,h} h + C_{M_z,\psi} \psi + C_{M_z,\beta} \beta
\end{aligned}
\tag{3.4}
$$

3.1.3 Suspension model

During this thesis this block will be modelled as a simple linear 3 degrees of freedom suspension described by the following equations extracted form the bibliography ([20] page 682), this model cannot consider road irregularities and dynamic movements of the suspension but it may be accurate enough for modelling quite wide range of manoeuvres of a race vehicle, considering that normally in the circuits there are not big irregularities and their suspension stiffness is high enough for considering instantaneous movement.

Lateral load transfer: The main assumptions of this method are:

- A horizontal lateral load applied anywhere along the neutral roll axis produces no roll of the sprung mass.
- The front and rear roll rates are measured independently.
- Tire deflection rates are included in the front and rear roll rates values.
- Solid axles roll relative to the ground will not enter into calculations.
- The vehicle centre of gravity and toll centres are located on the centre-line of the car.
- There is not a contribution in the load transfer caused by the overturning moment (M_x).

$$\Delta W_{f,l} = -\Delta W_{f,r} = a_y \left(\frac{W_s}{TR_f} \left(\frac{h_2 K_f}{K_f + K_r - W_s h_2} \right) + \frac{b_s}{WB} z_{R,f} + \frac{W_{u,f}}{TR_f} z_{w,f} \right) \tag{3.5}$$

$$\Delta W_{r,l} = -\Delta W_{r,r} = a_y \left(\frac{W_s}{TR_r} \left(\frac{h_2 K_f}{K_f + K_r - W_s h_2} \right) + \frac{a_s}{WB} z_{R,r} + \frac{W_{u,r}}{TR_r} z_{w,r} \right)$$

Longitudinal load transfer: The main assumptions of this method is that, the vehicle is symmetric even under lateral acceleration conditions. Obtaining a symmetric distribution of the longitudinal load transfer.

$$\Delta W_f = -a_x \frac{W_t}{WB}; \qquad \Delta W_r = a_x \frac{W_t}{WB} \tag{3.6}$$

Static loads and aerodynamic forces: Finally, the static load and the aerodynamics contributions must be summed to the previous calculations. Supposing that the vehicle is symmetric and the aerodynamic coefficients and distributions are previously known:

$$W_f = \frac{W_t b}{WB} + L_f; \qquad W_r = \frac{W_t a}{WB} + L_r \tag{3.7}$$

Where:

- K_i: Axle roll stiffness.
- W_s: Sprung mass.
- W_t: Total weight of the vehicle. Including suspended and non-suspended mass.
- h_2: Distance between roll axis and centre of gravity.
- $z_{R,i}$: Axle roll centre height.
- $z_{w,i}$: Axle unsprung mass center of gravity height.
- b_s: Suspended mass front weight distribution multiplied by the wheelbase.
- a_s: Suspended mass rear weight distribution multiplied by the wheelbase.
- a: It is the total mass rear weight distribution multiplied by the wheelbase.
- b: It is the total mass front weight distribution multiplied by the wheelbase.
- L_i: Lift/downforce contribution in a specific axle.
- WB: Wheelbase.
- TR_i: Axle track.

This model can predict the steady-state load transfer of a race-car with sufficient precision.

3.1.4 Vehicle assembly

The vehicle model will be based on the assembly of 4 tires that will be described independently based on their coefficients and scaling factors as well as their own inputs. Those tires will generate lateral and longitudinal force, and the 3 moments components, all these forces will be transmitted to the vehicle body by using the suspension model. Finally, the aerodynamic forces will be added to the previous ones obtaining the accelerations of the full vehicle.

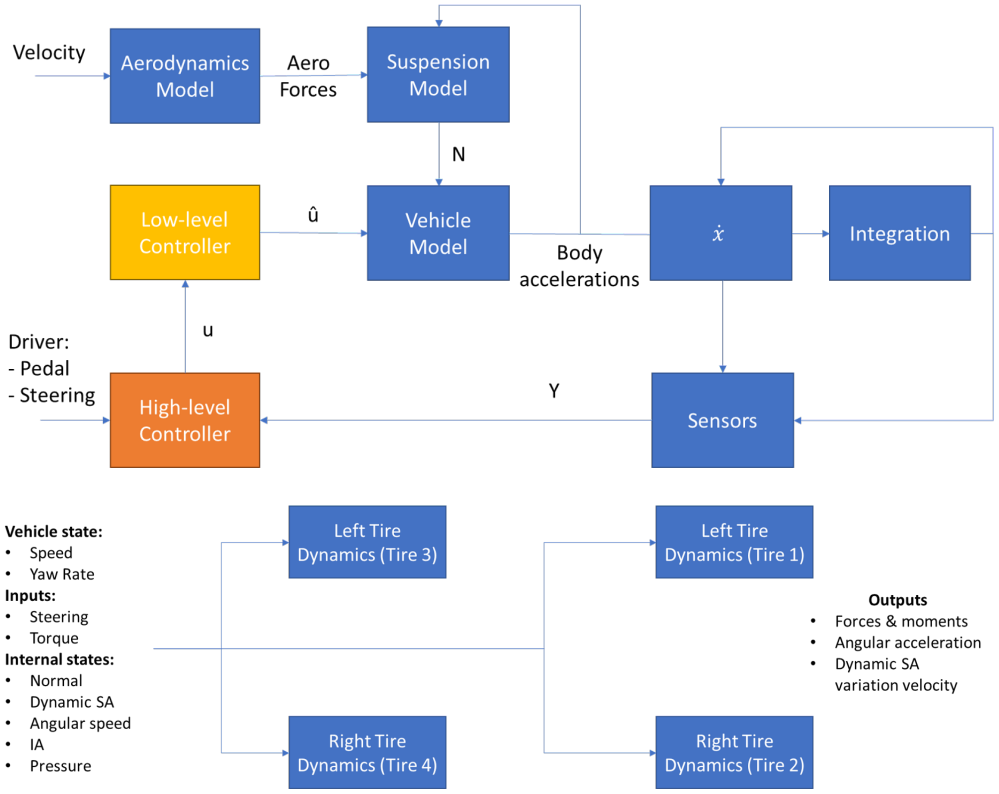

FIGURE 3.3: Mathematical modelling.
Top: General overview of the whole model and integration. Blue: physical vehicle model. Yellow: Motor and Motor-controller dynamics and control algorithms. Orange: self-developed control algorithms.
Bottom: Detailed overview of the two track model.

Summarizing, the vehicle model will be:

- A two-track model, using 4 independent wheels.
- The tire will be described using a transient tire model that will predict the tire forces and moments, accurately.
- A simplified aerodynamic model, considering linear aerodynamics around the set-up points.

- A simplified suspension model will be used to distribute the normal forces at each wheel, using a quasi-static approach. Solving iteratively the tire forces and vehicle accelerations until convergence.
- During the first approach there will not be considered the suspension movements obtaining constant inclination angles.
- Polynomial steering approximation.

Obtaining a 14 degrees of freedom dynamic model, with quasi-static normal force at each wheel calculation by using an iterative solver.

3.2 Control models

In this section, the proposed multi-functional controller will be explained. First, the global schematic of the controller will be shown and then a detailed overview of this section will be done.

The first step is obtaining an objective value of certain parameters, to do so the chosen variable that will be controlled are the yaw rate and the slip ratios of each wheel. Once they have been chosen it is necessary to compute those values as function of the driver inputs. Concretely, the yaw rate objective is obtained by assuming that the driver steering wheel input is related with the quasi-static cornering condition that he wants to follow in the near future, then it is possible to compute the reference steady-state yaw rate as:

$$r = \frac{V\delta}{(a+b)(1+K_u V^2)} \tag{3.8}$$

Where K_u is the understeer gradient that defines the desired stability under certain conditions (this parameter may be a design parameter depending on the final objective of the controller, for the sake of simplicity this parameter will be assumed constant).

This equation assumes that the vehicle motion is linear and thus it does not have any grip limitation. Then, this must be done by assuming a maximum level of lateral grip:

$$a_{y,\max} = \mu_g m g - \mu_L L \tag{3.9}$$

Where, L is the lift at the current speed. Then:

$$r_{lim} = \frac{a_{y,\max}}{V} \rightarrow r = \min\left(\mid r \mid, r_{lim}\right) \cdot \operatorname{sgn}(\delta) \tag{3.10}$$

Finally, as it will be explained in the following section, it is necessary to describe the reference yaw rate dynamically, to do so a simple linear first order approach is done:

$$r_d = \frac{r}{1 + \tau s} \tag{3.11}$$

In the case of the traction controller, the maximum and minimum permitted slip ratio values will be assumed as a function of the wheel normal force and wheel slip angle:

$$SR_{\max,i} = f(N_i, \alpha_i); \qquad SR_{\min,i} = g(N_i, \alpha_i); \tag{3.12}$$

In this case the controller will not be following a desired path, but it will be limiting the maximum available torque at each wheel.

Once defined the objective functions it is possible to describe the control algorithms that will be implemented. In both controllers, the yaw rate control (r) and in the traction control, the proposed control algorithm is based on the combination of feed-forward controllers and feed-back controllers. The feed-forward controllers' objective is obtaining a fast tracking of the desired control curves, whereas the feed-back controllers will increase the accuracy and robustness of the control algorithm. The scheme will be:

Obtaining the following control equation, where u_{fb} is the output of the feed-back controller and u_{ff} is the output of the feed-forward controller.

$$u = u_{fb} + u_{ff} \tag{3.13}$$

3.2.1 Yaw rate control

The feed-forward controller will be based in a simplified bicycle model of the vehicle. The first approach would be using a linear bicycle model without lateral-longitudinal tire coupling and only considering the lateral-directional dynamics of the vehicle, with this approach the system can be described by:

$$\dot{x} = Ax + Bu \tag{3.14}$$

$$y = Cx + Du$$

As the desired state and the desired state evolution is predefined it is possible to obtain the inputs of the system by using:

$$u_{ff} = B^{-1}(\dot{x} - Ax) \tag{3.15}$$

The feed-back controller will be comparing the current state and the objective state, obtaining a response based on the control algorithm:

3.2.2 PID

Two different control algorithms will be implemented on one hand a simple PID will be implemented. It will be a digital, discrete controller, with limited outputs. To control the over integration an anti-wind-up clamping scheme will be used in the integral part. Concretely, the final equations will be the following outputs:

$$\hat{u} = \left(k_p + \frac{k_i T_s}{z-1} + \frac{k_d}{T_f + \frac{T_s}{z-1}} \right) \varepsilon \tag{3.16}$$

$$u_{fb} = \min\left(\mid \hat{u} \mid, u_{lim}\right) \cdot \operatorname{sgn}(\hat{u_r})$$

3.2.3 LQR

The second controller will be a combination of the previous PID controller of the yaw rate (r) with a slip angle (β) controller, obtaining a fully feedback controller. The main difference between the slip angle control and the yaw rate control is that the first does not have to be perfectly controlled. Instead it has to be bounded near to zero to achieve stability. Because of this, there will not be an integral part but only proportional and derivative that will control any rapid undesired change in this variable.

This controller will increase the robustness of the yaw rate control when the grip state is reduced. This will be done by increasing the stability of the system when the driver introduce non-feasible objective (rain or snow conditions).

The final form of the controller is:

$$\hat{u_r} = \left(k_{p,r} + \frac{k_{i,r} T_s}{z-1} + \frac{k_{d,r}}{T_f + \frac{T_s}{z-1}} \right) \varepsilon_r \tag{3.17}$$

$$u_r = \min\left(\mid \hat{u_r} \mid, u_{r,lim}\right) \cdot \operatorname{sgn}(\hat{u_r})$$

$$\hat{u_\beta} = \left(k_{p,\beta} + \frac{k_{d,\beta}}{T_f + \frac{T_s}{z-1}} \right) \varepsilon_\beta \tag{3.18}$$

$$u_\beta = \min\left(\mid \hat{u_\beta} \mid, u_{\beta,lim}\right) \cdot \operatorname{sgn}(\hat{u_\beta})$$

$$u_{fb} = u_r + u_\beta \tag{3.19}$$

3.2.4 Traction control

The traction control is based on a feed-forward using previously known grip factor ad the current normal force and slip angle. And a correction of this value using a PD controller. Obtaining both a maximum permitted torque and a minimum regenerative braking torque:

$$T_{\max,i} = f(N_i, \alpha_i); \qquad T_{\min,i} = g(N_i, \alpha_i) \tag{3.20}$$

Concretely, the simplest function that can be used is:

$$T_{\max,i} = \mu N_i; \qquad T_{\min,i} = -\mu N_i \tag{3.21}$$

Then, the feed-back controller is:

$$\hat{T_{\max,i}} = \left(k_{p,SR} + \frac{k_{d,SR}}{T_f + \frac{T_s}{z-1}} \right) \varepsilon_{SR,\max}; \; \hat{T_{\min,i}} = \left(k_{p,SR} + \frac{k_{d,SR}}{T_f + \frac{T_s}{z-1}} \right) \varepsilon_{SR,\min} \tag{3.22}$$

Obtaining the torque limits as:

$$T_{\min,i} \leqslant T_i \leqslant T_{\max,i} \tag{3.23}$$

3.2.5 Torque assembly

Once the maximum and minimum longitudinal force are obtained for each wheel it is time to distribute the force between them, to do so an optimization algorithm is proposed:

$$\min \left(J = f(T,C)^2 + k_1 g(T,\pi)^2 + \sum_{i=1}^{4} h(T_i)_i^2 \right) \tag{3.24}$$

Where:

- The yaw moment control cost function is:

$$f(T,C) = ((T_1 - T_2) + (T_3 - T_4)) - C \tag{3.25}$$

- The total longitudinal force cost function is:

$$g(T,C) = ((T_1 + T_2) + (T_3 + T_4)) - \pi \tag{3.26}$$

- Minimizing each torque term for minimum effort solutions:

$$h(T_i)_i = \sqrt{k_{2,i}} T_i \tag{3.27}$$

And a set of restrictions:

$$LB_i \leqslant T_i \leqslant UB_i \tag{3.28}$$

As it can be seen, the cost functions are squared linear functions then it is possible to obtain the exact and unique solution by solving the gradient problem:

$$\nabla J = \begin{bmatrix} (k_1 + k_{2,1} + 1)T_1 + (k_1 - 1)T_2 + (k_1 + 1)T_3 + (k_1 - 1)T_4 - C - \pi k_1 \\ (k_1 - 1)T_1 + (k_1 + k_{2,2} + 1)T_2 + (k_1 - 1)T_3 + (k_1 + 1)T_4 + C - \pi k_1 \\ (k_1 + 1)T_1 + (k_1 - 1)T_2 + (k_1 + k_{2,3} + 1)T_3 + (k_1 - 1)T_4 - C - \pi k_1 \\ (k_1 - 1)T_1 + (k_1 + 1)T_2 + (k_1 + 1)T_3 + (k_1 + k_{2,4} + 1)T_4 + C - \pi k_1 \end{bmatrix} = 0 \tag{3.29}$$

Concretely, this problem is a set of linear equations that can be written in matrix form as:

$$AT = B \tag{3.30}$$

Where:

$$A = \begin{bmatrix} k_1 + k_{2,1} + 1 & k_1 - 1 & k_1 + 1 & k_1 - 1 \\ k_1 - 1 & k_1 + k_{2,2} + 1 & k_1 - 1 & k_1 + 1 \\ k_1 + 1 & k_1 - 1 & k_1 + k_{2,3} + 1 & k_1 - 1 \\ k_1 - 1 & k_1 + 1 & k_1 + 1 & k_1 + k_{2,4} + 1 \end{bmatrix} \tag{3.31}$$

$$B = \begin{bmatrix} -C - \pi k_1 \\ +C - \pi k_1 \\ -C - \pi k_1 \\ +C - \pi k_1 \end{bmatrix} = 0$$

Once the solution is obtained it is time to verify the conditions, as it can be seen each torque can be described as three states:

0 - Unknown solution: totally free and previously unknown solution.

1 - Lower bounded: Minimum permitted torque considering the traction ellipse, the physical motor limits, other limits as the maximum regenerative braking power. Known solution.

2 - Upper bounded: Minimum permitted torque considering the traction ellipse, the physical motor limits, other limits as the maximum power. Known solution.

With this in mind, it is possible to determine that 81 different solutions must be tested, concretely:

- The optimal solution: 1 solution (equation 3.30)
- One fixed torque: 8 Combinations
- Two fixed torques: 24 Combinations
- Three Fixed torques: 32 Combinations
- Four fixed torques: 16 Combinations

And from all this set of solutions the minimum value that satisfy the conditions must be chosen:

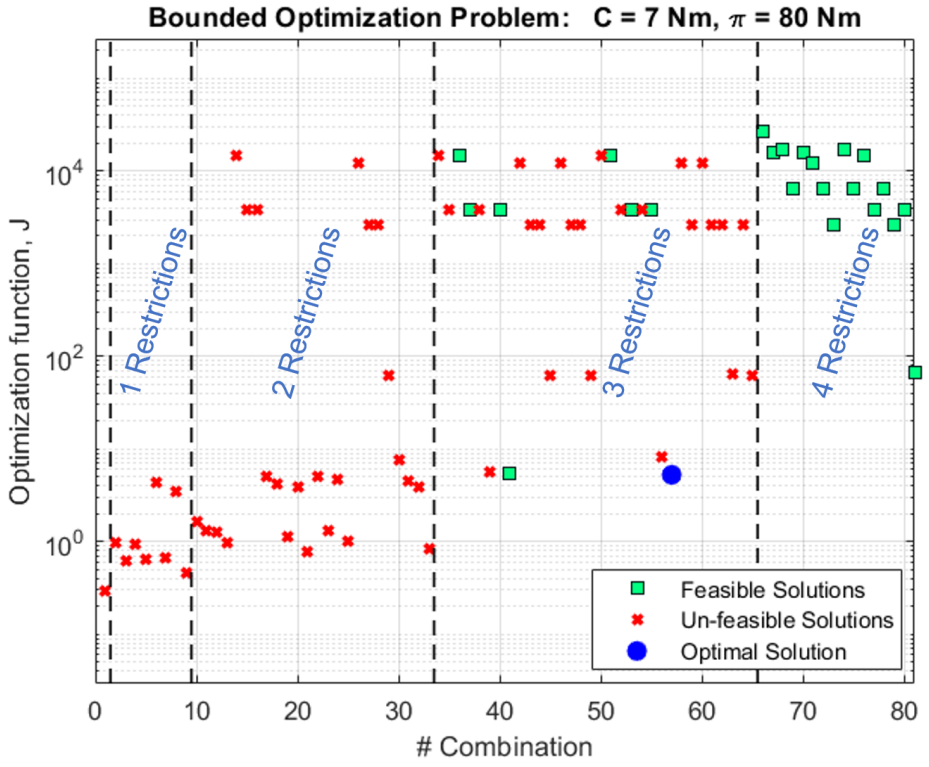

FIGURE 3.4: Optimization function of the different combinations of restrictions.Starting at the left: first solution: Non-restricted. Second set of solutions: single restriction either upper or lower. Third set of solutions: Two restrictions applied. Fourth set of solutions: Three restrictions applied. Last set of solution: Fully restricted solutions.

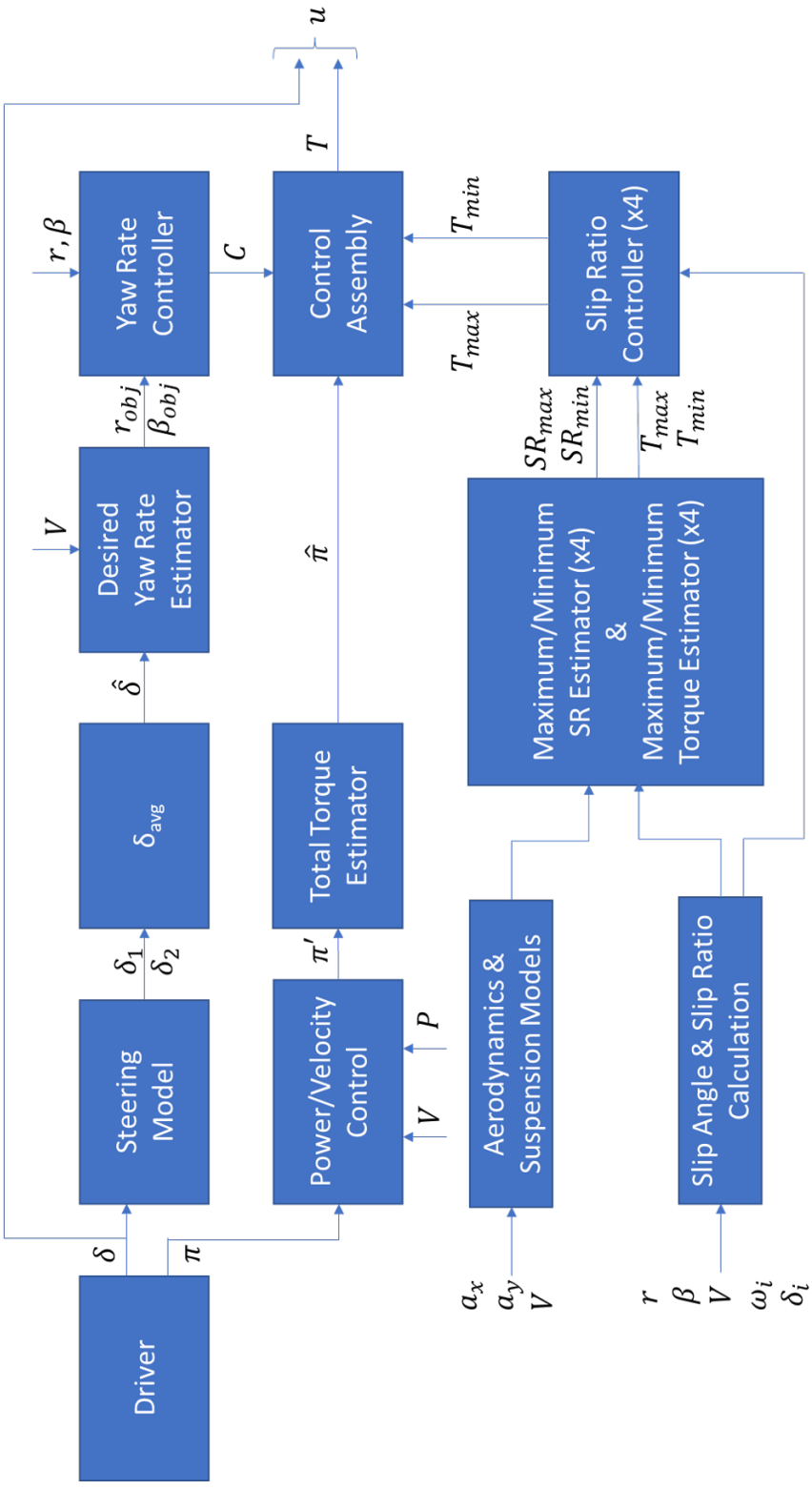

FIGURE 3.5: Controller schematics.

Chapter 4

Results

In this chapter, the obtained results and its discussion will be made. It is divided in different sections, the first section will explain the verification of the model. The second section will show the numerical results of the Torque Vectoring calibration. Finally, different test scenarios will be shown. At the end of this chapter a review of the budged of developing this study will be done as well as an environmental study.

4.1 Model verification

Once the model has been finished, the first step was to verify its accuracy, to do so a combination of longitudinal and lateral movements have been performed. Concretely, the ecoRX19 Formula Student Germany Skidpad event has been simulated and compared with the real data, obtaining figure 4.1.

The results are quite accurate, in both conditions the pure longitudinal acceleration, the pure lateral acceleration and the combination of both.

The main error occurs in the body slip angle prediction (figure 4.2), this may be caused by different factors:

- Not a completely perfect tire model and its dynamics.
- Track irregularities.
- Transient movements of the sprung mass.
- Small deviations between the theoretical sensor position and the actual.

However, the results are quite good predicting the zone were the vehicle will be working at its dynamics.

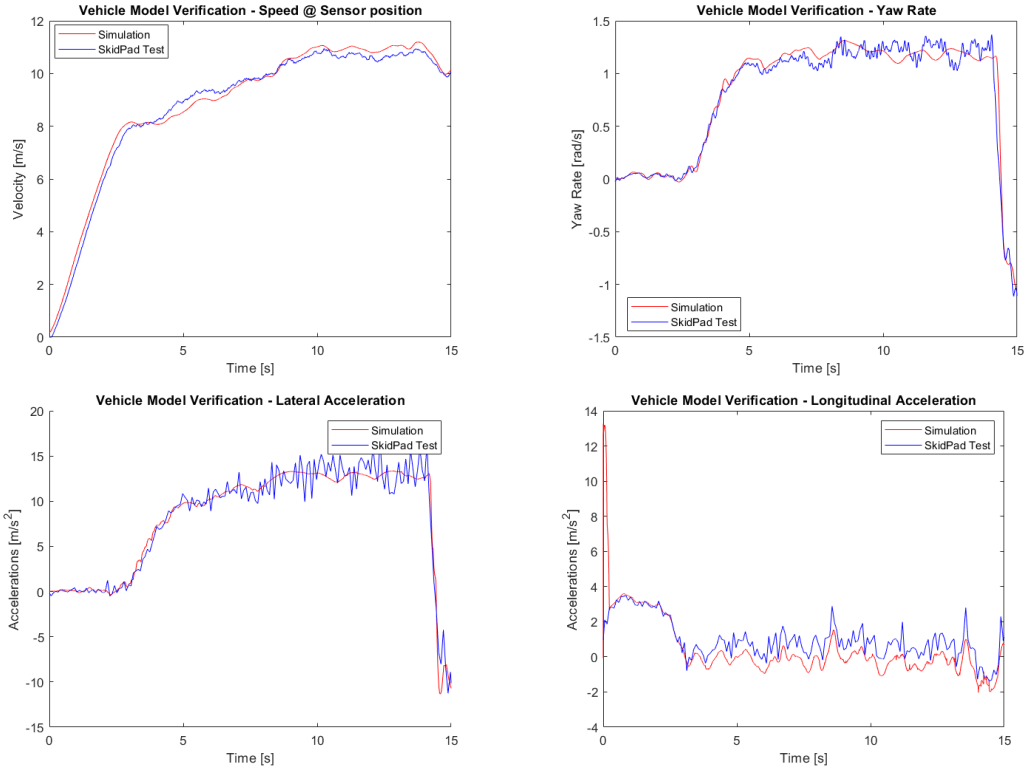

FIGURE 4.1: Model verification using real data from FSG 19 skidpad dynamic event. Top left: Linear velocity. Top right: Angular velocity in yaw. Bottom left: Lateral acceleration in body axis. Bottom right: Longitudinal acceleration in body axis.

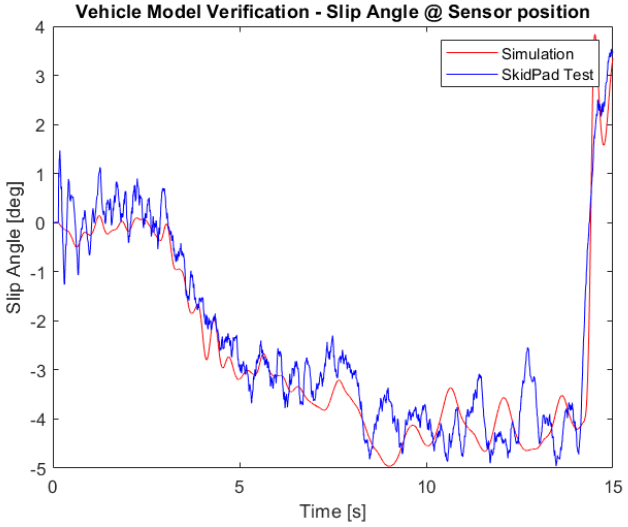

FIGURE 4.2: Model verification using real data from FSG 19 skidpad dynamic event. Vehicle slip angle at the centre of gravity.

4.2 Calibration

The calibration procedure that has been followed is based on the minimization of certain cost function that will change depending on the calibration manoeuvre:

- Step steer at different velocities and steering angles:

$$J = \int_0^{t_f} (k_\epsilon (r - r_d)^2 + k_u u^2) dt + k_{LT} \int_{t_i}^{t_f} (r - r_d)^2 dt + k_{OS} OS \tag{4.1}$$

  The first integral is related with the tracking error and the control effort that has been used, the second integral is related with the damping after a certain time t_i, and finally the last term (OS) is related with the overshoot, it introduces an extra cost only when the $(r - r_d) > r_d \cdot 105\%$.

- The procedure to tune the anti-slip controller is similar but using acceleration and braking cases minimizing the slip ratio error only when overshoot occurs by optimizing the controller parameters.

The algorithm used to solve these optimization problems is using the fmincon function of the Matlab optimization toolbox [18].

4.2.1 Yaw rate controllers calibration

The parameters of the PID and feed-forward controllers are principally dependent on the velocity and the steering angle, concretely the ratio between the maximum grip steering angle and the angle has been used to optimize the performance of the controller:

$$\hat{\delta} = \frac{\delta}{\delta_{\max a_y}} \tag{4.2}$$

Concretely, the maximum lateral acceleration steering angle has been computed using:

$$\delta_{\max a_y} = \frac{WB\left(\mu_{y,g} \cdot g \cdot m_t + \mu_{y,aero} \cdot L\right)}{m_t V^2} \tag{4.3}$$

The obtained optimal parameters can be find in the table 4.1.

TABLE 4.1: Optimization PID and feed-forward constants for step steer case.

Speed V	**Steering** δ	k_p	k_i	k_d	PID_{lim}	C_f	C_r
7	7.92	177.46	206.42	5.64	10.19	-14341	-16118
7	15.84	148.80	219.62	8.88	7.20	-10014	-17899
7	24.00	265.31	200.60	7.87	8.00	-7800	-18000
7	31.93	300.00	150.00	5.64	15.58	-10556	-17037
10	4.03	149.91	69.54	6.21	5.32	-13280	-17974
10	8.06	111.38	83.67	4.67	8.23	-14591	-19164
10	12.22	64.00	117.70	0.42	9.90	-13280	-17974
10	16.25	33.64	106.00	0.13	5.57	-18253	-22083
15	1.96	125.34	75.33	5.16	2.81	-17442	-20596
15	3.91	120.00	109.00	5.52	3.06	-12757	-15241
15	5.92	145.36	110.22	4.40	4.03	-11963	-15200
15	7.88	118.00	116.89	3.61	4.01	-9330	-14250
20	1.23	127.00	114.00	5.00	1.00	-17704	-20654
20	2.46	118.46	115.63	5.05	1.99	-16200	-19950
20	3.72	122.24	123.89	4.15	3.20	-14881	-18875
20	4.96	149.68	214.76	5.89	3.20	-12825	-18750

It is possible to obtain a fitting that approximate the ideal values obtained above. In this thesis a polynomial fitting will be used using the following expressions:

$$k_p, k_i, k_d = p_{00} + p_{10}\hat{\delta} + p_{01}V + p_{11}\hat{\delta}\cdot V + p_{20}\hat{\delta}^2 + p_{02}V^2 \tag{4.4}$$

$$+p_{21}\hat{\delta}^2\cdot V + p_{12}\hat{\delta}\cdot V^2 + p_{30}\hat{\delta}^4 + p_{31}\hat{\delta}^3\cdot V + p_{40}\hat{\delta}^4 + p_{22}\hat{\delta}^2\cdot V^2$$

$$PID_{lim} = p_{00} + p_{10}\hat{\delta} + p_{01}V + p_{11}\hat{\delta}\cdot V + p_{20}\hat{\delta}^2 + p_{02}V^2 \tag{4.5}$$

$$\frac{C_f}{1000\cdot N_f}, \frac{C_r}{1000\cdot N_r} = \hat{C_f}, \hat{C_r} = p_{00} + p_{10}\hat{\delta} + p_{01}V + p_{11}\hat{\delta}\cdot V + p_{20}\hat{\delta}^2 + p_{02}V^2 \tag{4.6}$$

Concretely, as the steering behaviour must be symmetric the even order steering parameters must be zero:

$$p_{10}, p_{11}, p_{12}, p_{30}, p_{31} = 0 \tag{4.7}$$

Then, the obtained coefficients are:

TABLE 4.2: Polynomial fitting of the PID and feed-forward control parameters for step steer case.

Param.	p_{00}	p_{01}	p_{20}	p_{02}	p_{21}	p_{40}	p_{22}
K_p	169	-1.96	365	-0.02	-60.3	7.16	2.14
K_i	558	-66.3	-95.6	0.02	14.87	-10.4	-0.32
K_d	10.2	-0.48	5.0	-0.01	-1.30	0.11	0.05
PID_{lim}	19.76	-1.834	1.43	0.05	-	-	-
$\hat{C_f}$	-0.013	-1.4e-3	2.7e-3	0	-	-	-
$\hat{C_r}$	-0.032	8.52e-4	8.78e-4	0	-	-	-

4.2.2 Traction controller calibration

On one hand, for the pure acceleration case the calibration has been performed using as initial velocity $V_0 = 1$m/s, considering this velocity as a near standstill condition. On the other hand, the pure braking case calibration has been performed at 3 different initial velocities, $V_0 = 30, 20$ and 10 m/s. The obtained parameters of this controller are summarized in the table 4.3:

TABLE 4.3: Optimization of the traction control parameters.

Case and initial velocity	k_p	k_d	PD_{lim}	μ_x
Acceleration from $V_0 = 1$ m/s	153	1.44	3.73	2.36
Braking from $V_0 = 30$ m/s	162	1.44	3.73	2.24
Braking from $V_0 = 20$ m/s	158	1.44	3.73	2.24
Braking from $V_0 = 10$ m/s	158	1.44	3.73	2.24

Observing this data it can be seen that for the negative slip ratio controller (the Anti-lock Braking System) is almost independent on the velocity, so, the final parameters will be supposed as:

TABLE 4.4: Optimization of the traction control parameters.

Case and initial velocity	k_p	k_d	PD_{lim}	μ_x
Acceleration	153	1.44	3.73	2.36
Braking	159	1.44	3.73	2.24

4.3 Case studies

The performance of the algorithm will be studied under certain conditions, starting with independent lateral and longitudinal dynamics and finally a case of combined dynamics:

- Step steer:
  - At the limit at different constant speeds:
    - Velocity: $V = 7$ m/s and steering $\delta = 24.00^o$.
    - Velocity: $V = 10$ m/s and steering $\delta = 12.22^o$.
    - Velocity: $V = 15$ m/s and steering $\delta = 5.92^o$.
    - Velocity: $V = 20$ m/s and steering $\delta = 3.72^o$.
  - Steering vs lateral acceleration at constant speed of 10 m/s.
- Pure acceleration starting near zero speed.
- Pure electric braking starting at different speeds:
  - Velocity: $V = 30$ m/s during $t = 2$s.
  - Velocity: $V = 20$ m/s during $t = 1.2$s.
  - Velocity: $V = 10$ m/s during $t = 0.75$s.
- Double lane change at constant speed using the norm ISO-3888-1-2011. With a supposed maximum acceleration of about 1.35g.
- Combined case: A step steer followed by a 85% throttle and by reducing the steering wheel to achieve the maximum lateral acceleraition at each speed.

4.3.1 Step steer at constant speed

During this simulation cases, the polynomial fitting of the optimal controller parameters have been used.

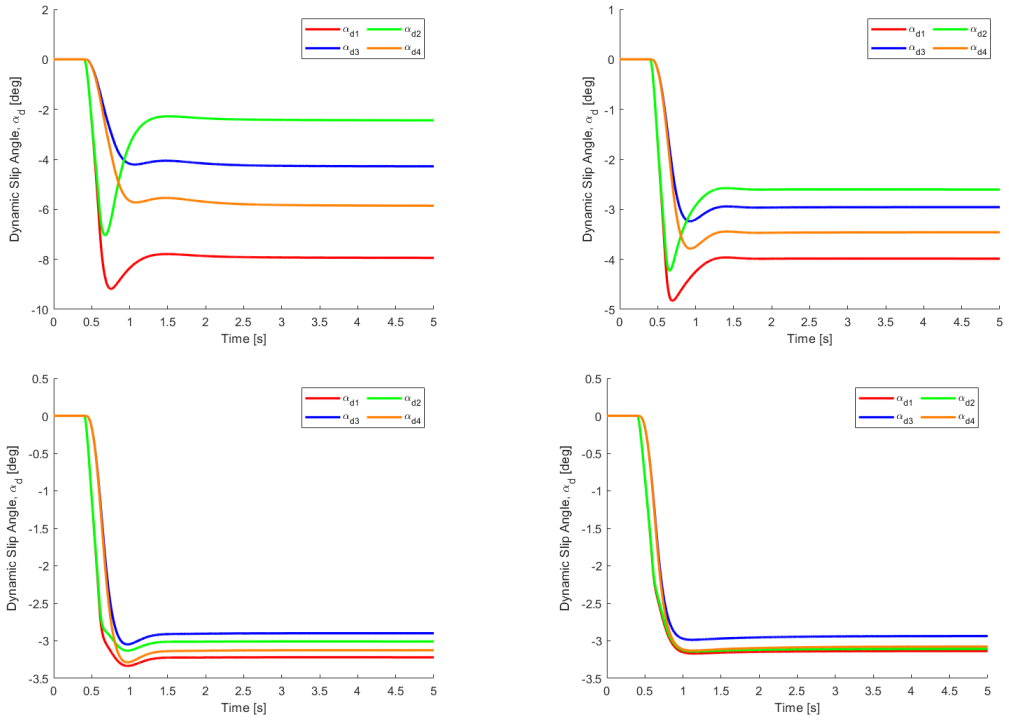

FIGURE 4.3: Step steer simulation case, dynamic slip angles at each wheel. Top left: speed of 7 m/s. Top right: speed of 10 m/s. Bottom left: speed of 15 m/s. Bottom right: speed of 20 m/s.

As it can be seen in the previous figure 4.3, the controller maintain the slip angles constant and damped, with a small overshoot at the front axle at low speeds.

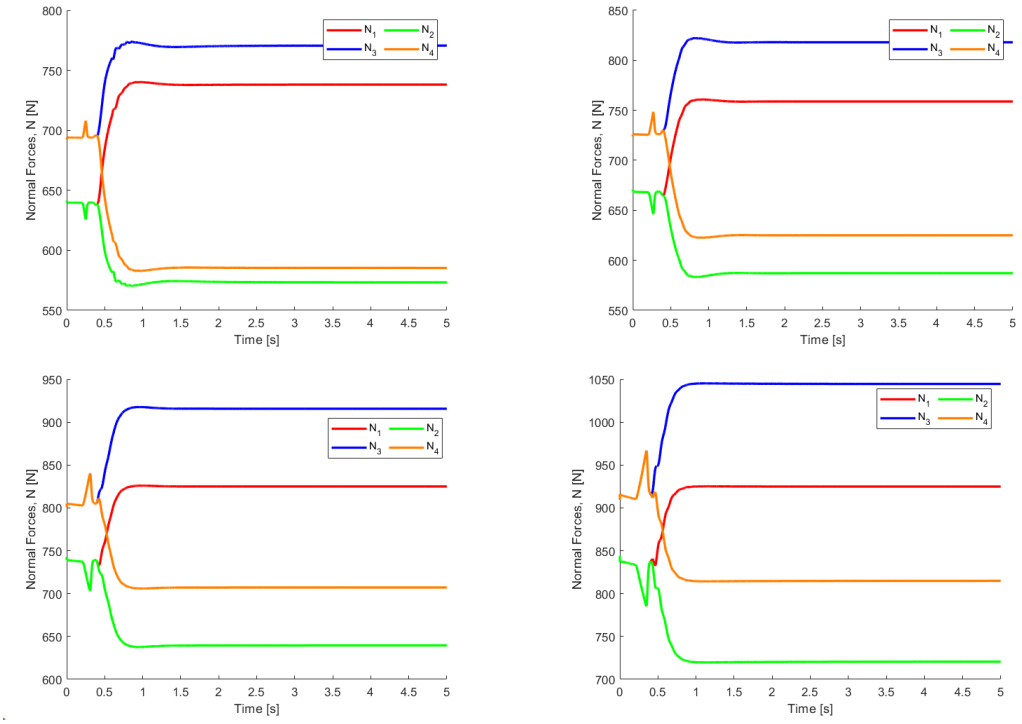

FIGURE 4.4: Step steer simulation case, normal forces at each wheel. Top left: speed of 7 m/s. Top right: speed of 10 m/s. Bottom left: speed of 15 m/s. Bottom right: speed of 20 m/s.

In these graphs, it can be seen that a peak at rear axle and a valley at the front at the very beginning of the simulation, this effect is due to the longitudinal acceleration and thus the load transfer, when the speed controller is activated. Just a few seconds after this the steering wheel is turned to the right obtaining lateral acceleration that generates a load transfer form right to left side. In addition, it can be seen when increasing the speed the total normal force is increased and the rear load distribution is also increased due to the aerodynamic forces and its distribution.

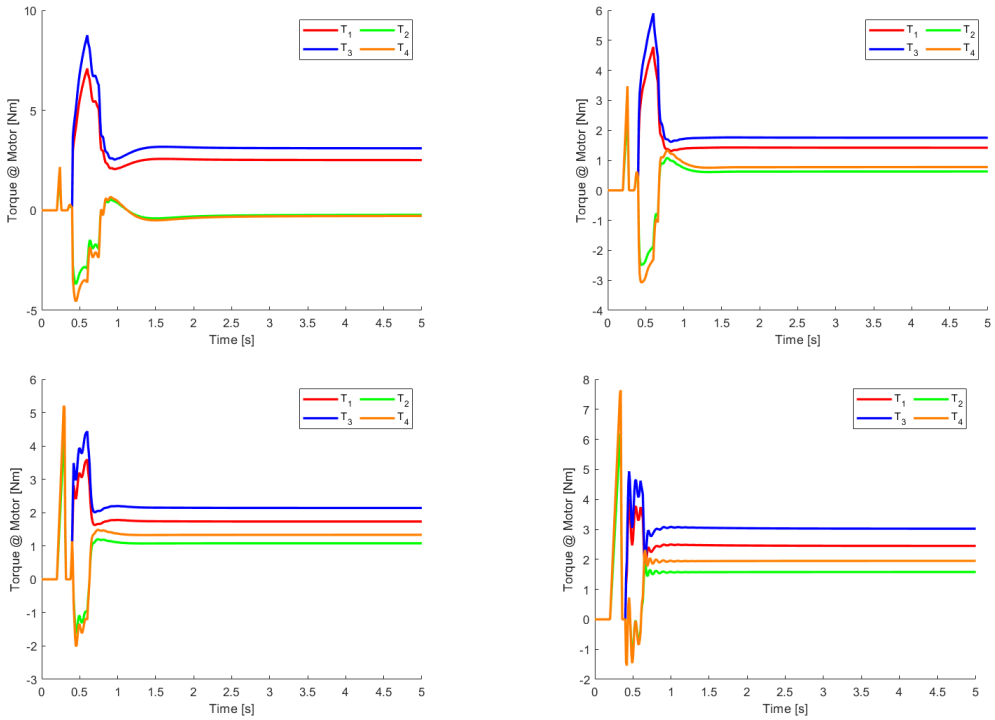

FIGURE 4.5: Step steer simulation case, motor torques at each wheel. Top left: speed of 7 m/s. Top right: speed of 10 m/s. Bottom left: speed of 15 m/s. Bottom right: speed of 20 m/s.

The first peak of torque is caused by the speed controller when is armed. Then, the step steer manoeuvre is started obtaining a huge difference between the inner and outer wheels, that, after a while, is reduced to damp the yaw velocity and, then, it is increased up to the steady-state control output. Also, it can be seen that the rear wheels have a higher torque than the front ones, this is controlled by the assembly function parameters $k_{2,3} = k_{2,3} < k_{2,1} = k_{2,2}$ from the section 3.2.5.

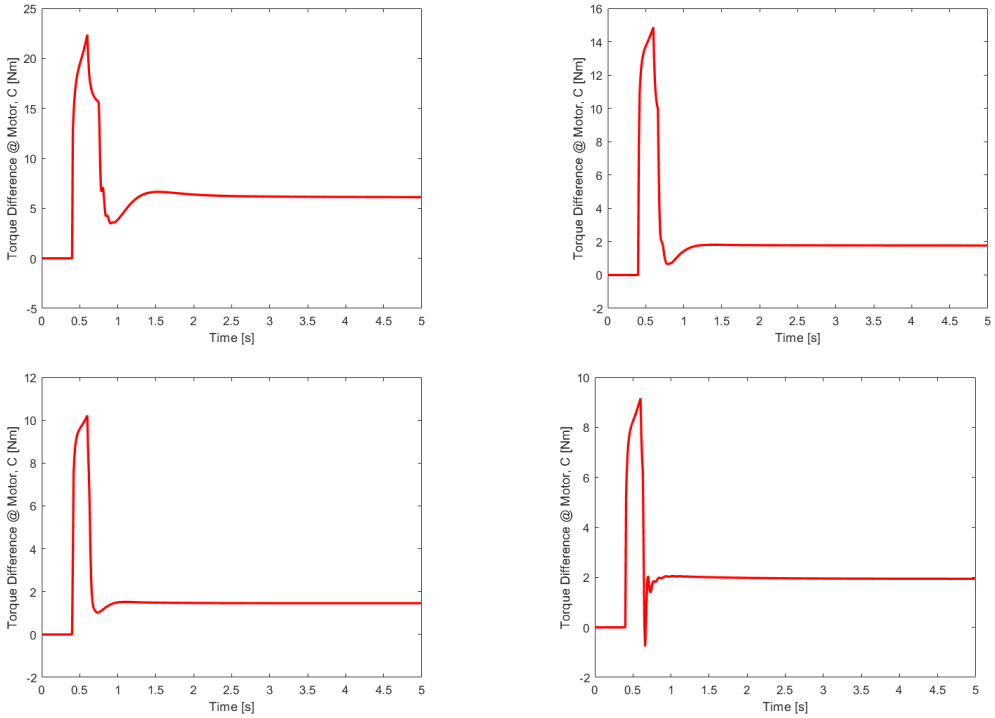

FIGURE 4.6: Step steer simulation case, yaw rate control output. Top left: speed of 7 m/s. Top right: speed of 10 m/s. Bottom left: speed of 15 m/s. Bottom right: speed of 20 m/s.

A detailed view of the previously explained at figure 4.5, just after the step steer input the controller increase its value until reaching a peak, then it is rapidly reduce to control the overshoot of the yaw rate velocity, and finally it is softly adapted to its steady-state value.

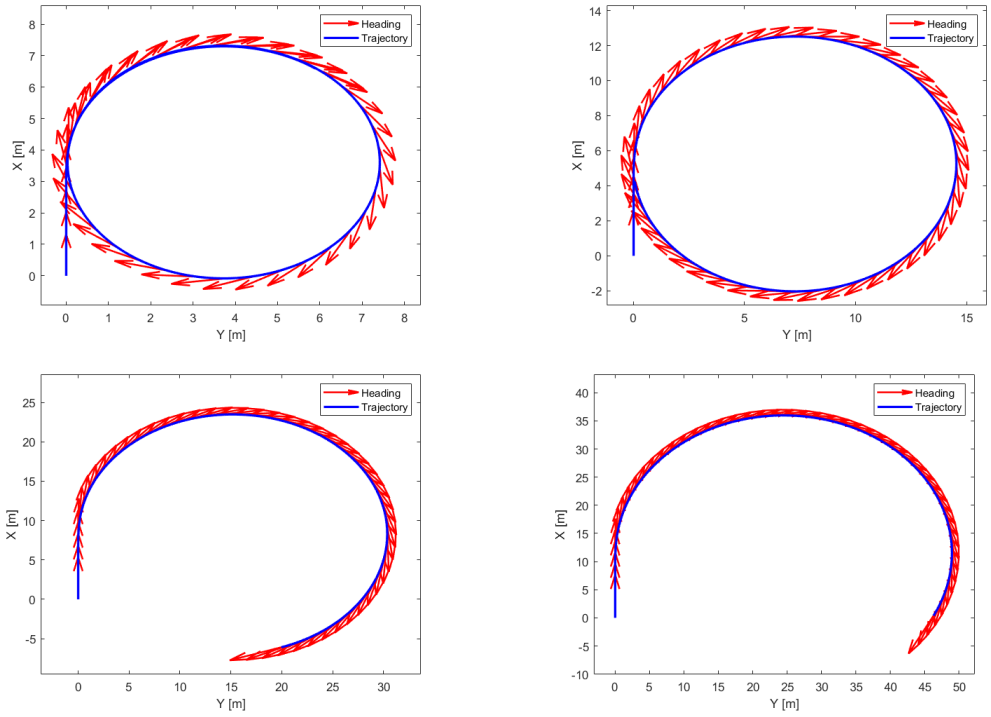

FIGURE 4.7: Step steer simulation case, trajectories. Top left: speed of 7 m/s. Top right: speed of 10 m/s. Bottom left: speed of 15 m/s. Bottom right: speed of 20 m/s.

As it is expected, when increasing the speed the radius of the trajectory is increased and thus the time to perform a complete lap. Concretely, all these are the trajectory of just 5 seconds of simulation. As it can be seen, there is a straight start and then a rapid transition to a almost perfect circular trajectory. With this graphs it is possible to conclude that the vehicle is stable and extremely agile as the transition between the completely straight and the circular trajectories is almost inappreciable. Finally, it can be seen that as the velocity increase the heading is more tangent to the trajectory, this is caused by a reduction of the centre of gravity slip angle (β).

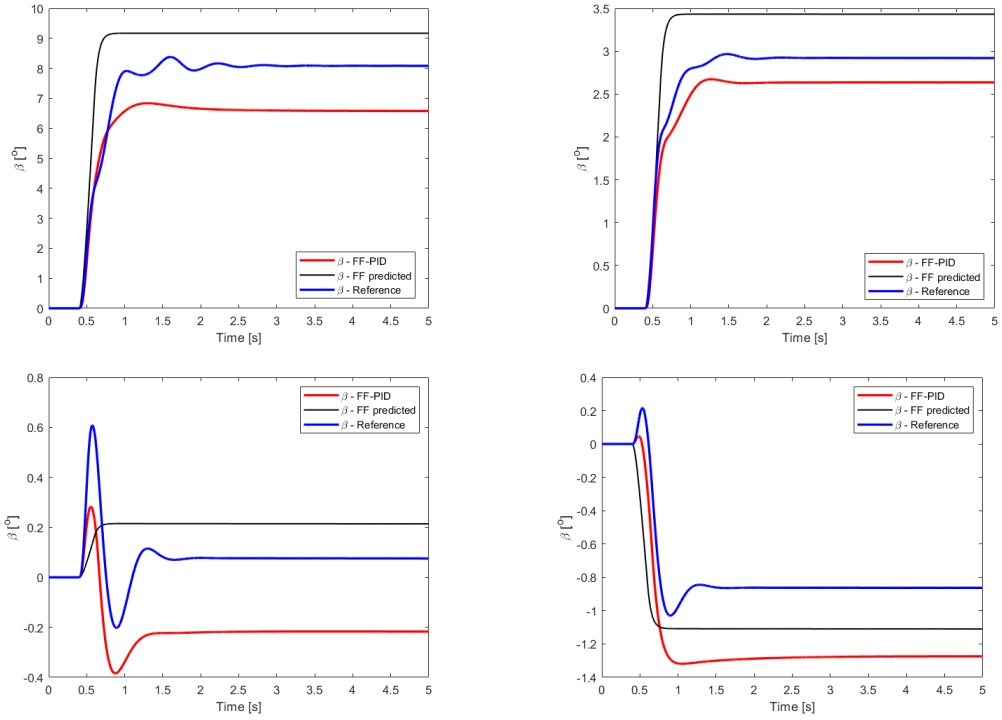

FIGURE 4.8: Step steer simulation case, centre of gravity slip angle. Top left: speed of 7 m/s. Top right: speed of 10 m/s. Bottom left: speed of 15 m/s. Bottom right: speed of 20 m/s.

As it can be seen the slip angle is decreased when the velocity is increased, this effect is due to a reduction in the slip angle at each wheel generated by the yaw rate which is related to the cornering radius, that as it is know at higher speeds the cornering radius is increased. Also, it can be seen that the linear bicycle model used in the feed-forward prediction is accurate enough to predict these tendencies. In addition, there is a clear difference in the behaviour of the slip angle when the yaw rate is controlled (β - FF-PID) and when it is not (β - reference), lower body slip angles are achieved with less wavy behaviour. Finally, as it was explained in section 3.2.3, the slip angle can be used as a robustness increase of the model, but is is not important to achieve the exact value predicted by the feed-forward as it is just a general estimation of the behaviour of the vehicle.

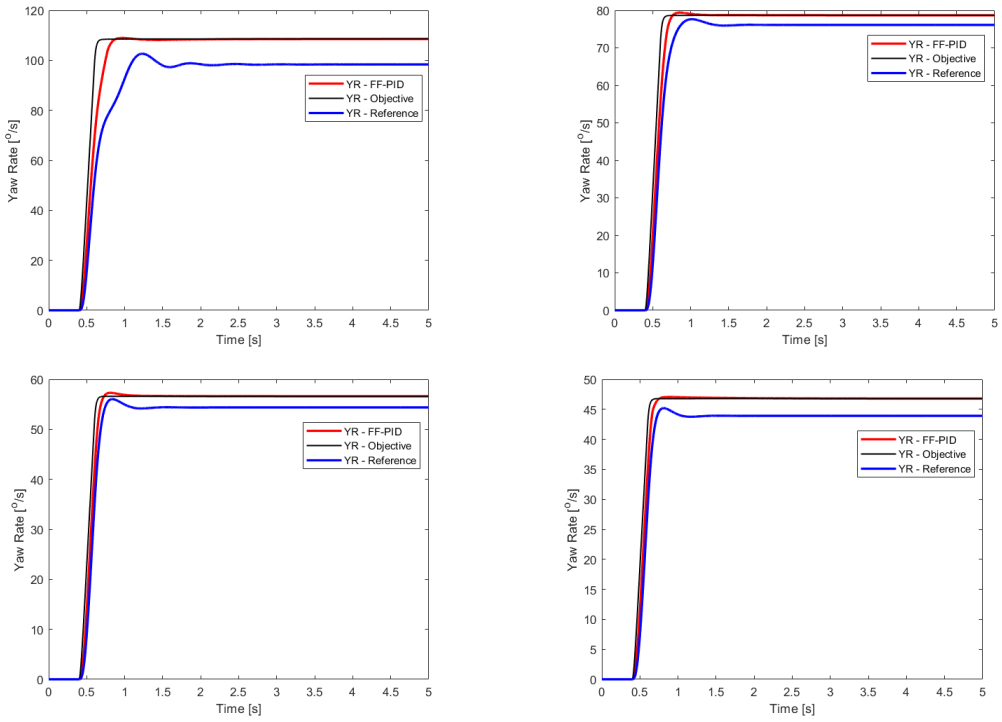

FIGURE 4.9: Step steer simulation case, yaw rate. Top left: speed of 7 m/s. Top right: speed of 10 m/s. Bottom left: speed of 15 m/s. Bottom right: speed of 20 m/s.

In these graph, the performance of the controller can be analysed, with this simple combination of a feed-forward and a PID controller a clear improvement is achieved, concretely a reduction of the transient time and achieving the desired yaw rate at all the speeds at the grip limit of the vehicle.

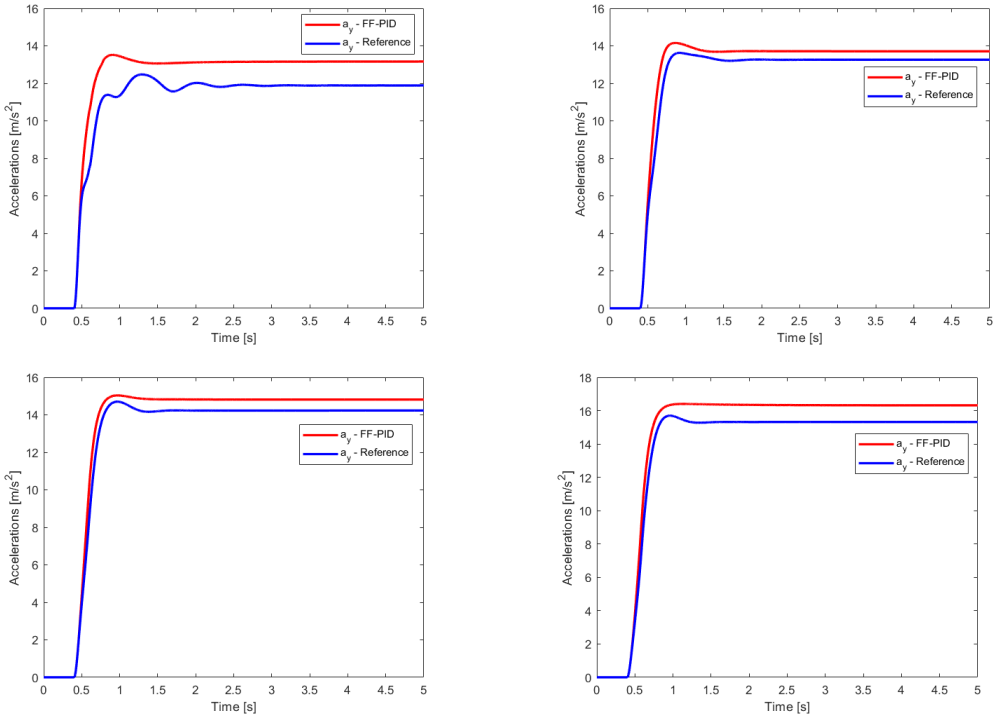

FIGURE 4.10: Step steer simulation case, lateral acceleration. Top left: speed of 7 m/s. Top right: speed of 10 m/s. Bottom left: speed of 15 m/s. Bottom right: speed of 20 m/s.

Similarly to the previous graph, this figures can be used to analyse the performance of the controller. Concretely it can be seen that a higher, faster and smoother lateral acceleration is achieved in all the simulation cases, confirming the performance of the controller.

Finally, a review of typical performance graphs and tables of the controller has been used, analysing the steering vs lateral acceleration linearity, and the Root Mean Squared Error (RMSE) and the Integral of the Absolut Control action normalized in time (cite).

$$\text{RMSE} = \sqrt{\frac{1}{t_f - t_i} \int_{t_i}^{t_f} \left(r_{obj}(t) - r(t)\right)^2 dt} \tag{4.8}$$

$$\text{IACA} = \sqrt{\frac{1}{t_f - t_i} \int_{t_i}^{t_f} \mid u_{YR}(t) \mid dt} \tag{4.9}$$

TABLE 4.5: Key Performance Indicators (KPI) of the yaw rate controller. Limit grip conditions.

V [m/s]	7	7	10	10	15	15	20	20
KPI	On	Off	On	Off	On	Off	On	Off
RMSE [rad/s]	0.0902	0.2436	0.0476	0.0946	0.0310	0.0633	0.0247	0.0630
IACA [Nm]	2.5373	-	1.4751	-	1.2991	-	1.4368	-

In the table 4.5 the performance of the controller is evaluated achieving an important reduction of the error (more than a half), while using less than 5 Nm of mean torque difference.

TABLE 4.6: Key Performance Indicators (KPI) of the yaw rate controller. V = 10 m/s at different steering angles.

δ [^{o}]	7	7	10	10	15	15	20	20
KPI	On	Off	On	Off	On	Off	On	Off
RMSE [rad/s]	0.0902	0.2436	0.0476	0.0946	0.0310	0.0633	0.0247	0.0630
IACA [Nm]	2.5373	-	1.4751	-	1.2991	-	1.4368	-

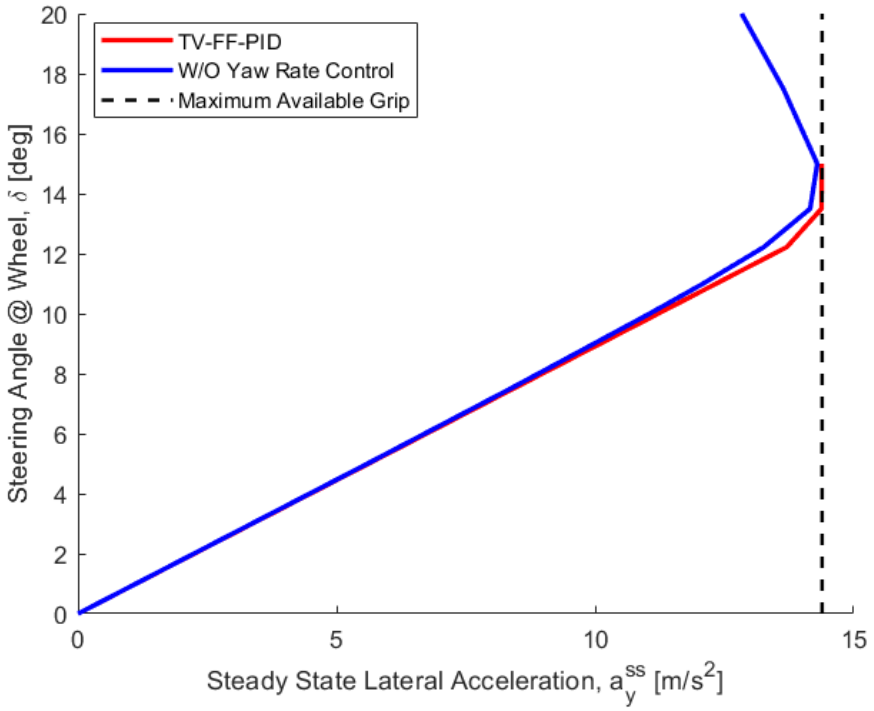

FIGURE 4.11: Steady state lateral acceleration versus the steering wheel angle at the wheel at a constant speed of $V = 10$ m/s.

It can be seen a clear improvement on the steering vs lateral acceleration linearity and at the same time the maximum grip condition is higher than without the controller. The main drawback is that after reaching the optimal steering angle the controller lose part of the stability of the system converting the previous stable point to a saddle point that slowly increase the yaw rate until exploding. In racing conditions this might not be any problem as the driver has some experience and it will have time to reduce the steering angle but if this controller is implemented in a passenger car could lead to some accidents, because of this two main actions have been considered, on one hand, reducing the grip condition to a 5% lower value that the expected one, obtaining a stable controller in a higher range (but it would have some problems if ice, rain or other grip destruction occurs). On the other hand, implementing the LQR controller that will maintain the slip angle in some bounded range increasing the stability and robustness when the vehicle is overdrived.

4.3.2 Pure acceleration

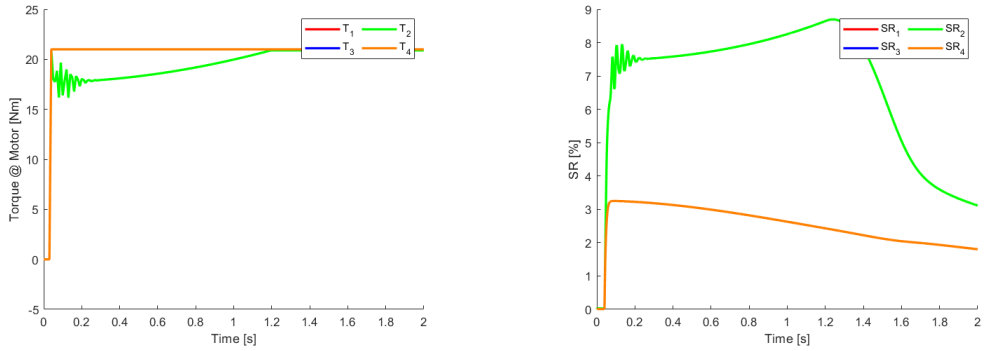

FIGURE 4.12: Pure acceleration simulation case. Left: Torque at each wheel. Right: Slip ratio at each wheel.

It can be seen that the traction control does only affect the front axle, it is important to consider that it is a formula student vehicle with very high mechanical grip. The target maximum slip ratio is considered to be 8% which is only reached by the front axle at the very beginning and at high speeds.

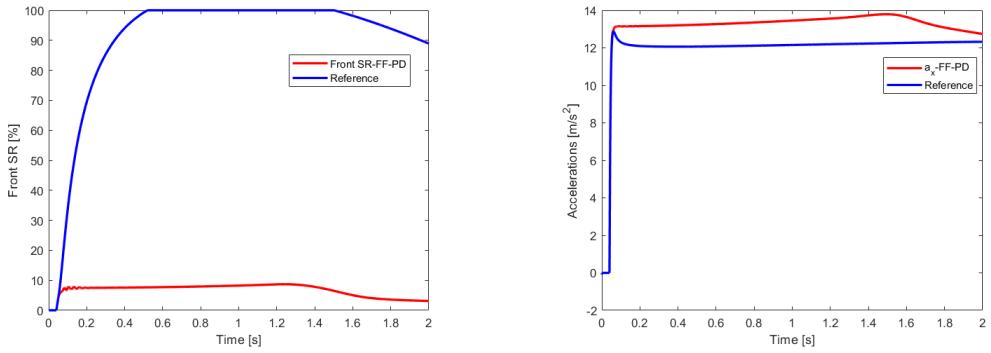

FIGURE 4.13: Pure acceleration comparison between active traction control and inactive (Reference). Left: Slip ratio at front axle. Right: Longitudinal acceleration.

In the left graph it can be seen that the traction control is necessary as if it is not connected the slip ratio increase uncontrollable up to the fully sliding condition $SR = 100$ %. This leads the uncontrolled longitudinal acceleration to a at least a 10% lower value which is very significant in terms of performance in racing conditions.

4.3.3 Pure braking

In this section the braking performance of the developed Anti-lock braking system is analysed and compared to the uncontrolled system.

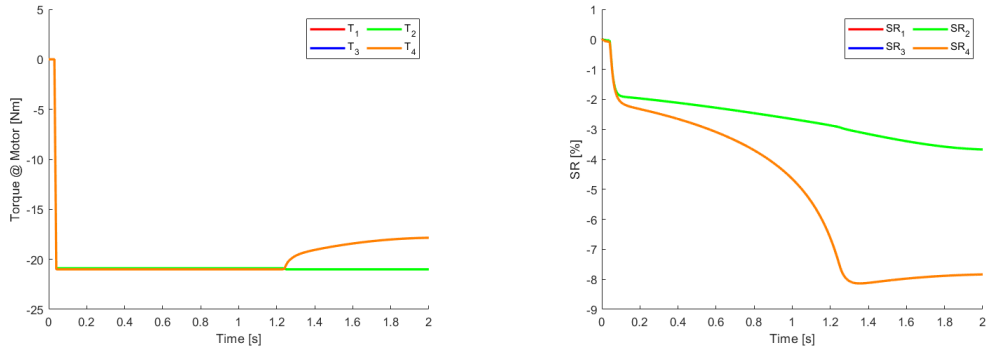

FIGURE 4.14: Pure braking simulation case. Left: Torque at each wheel. Right: Slip ratio at each wheel.

As it can be expected at high speeds the traction control does not interfere with the pedal torque demand. But at certain point when the downforce is reduced the rear slip ratio is increased significantly, it is at that point when the traction controller reduce the rear torque maintaining smoothly the torque near the desired maximum value -8 %.

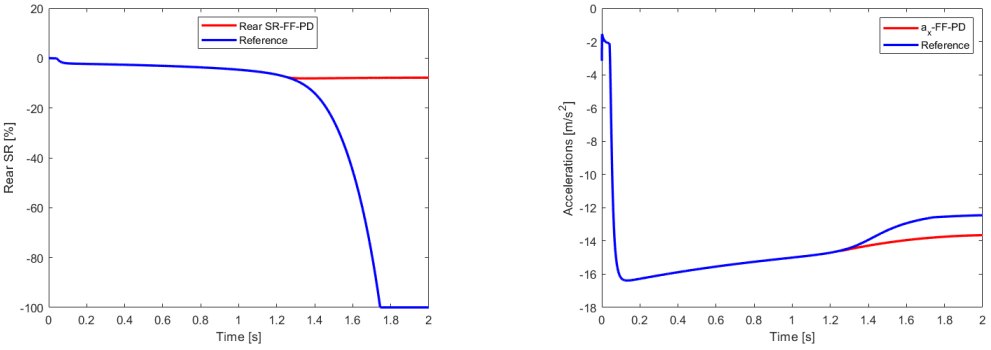

FIGURE 4.15: Pure braking comparison between active traction control and inactive (Reference), starting from $V_0 = 30$. Left: Slip ratio at front axle. Right: Longitudinal acceleration.

The rear axle slip ratio is reduced uncontrollably after surpassing the critical velocity (when the downforce is not sufficient to absorb all the motor torque), if the controller is disconnected. Also, it leads to a reduce of the performance of the braking acceleration.

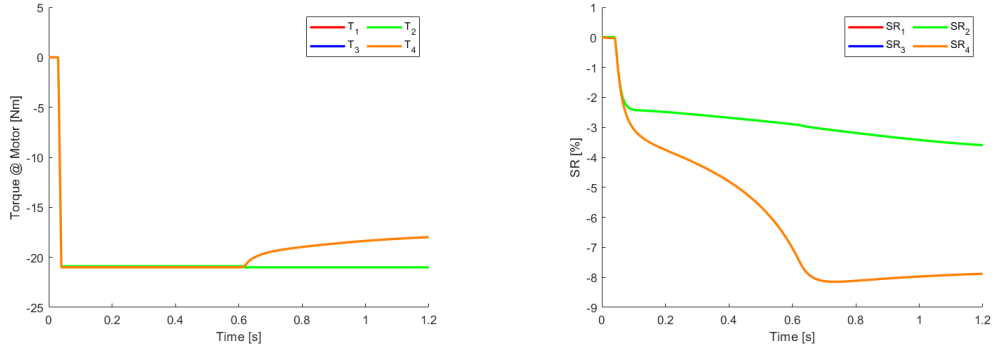

FIGURE 4.16: Pure braking simulation case starting from $V_0 = 20$. Left: Torque at each wheel. Right: Slip ratio at each wheel.

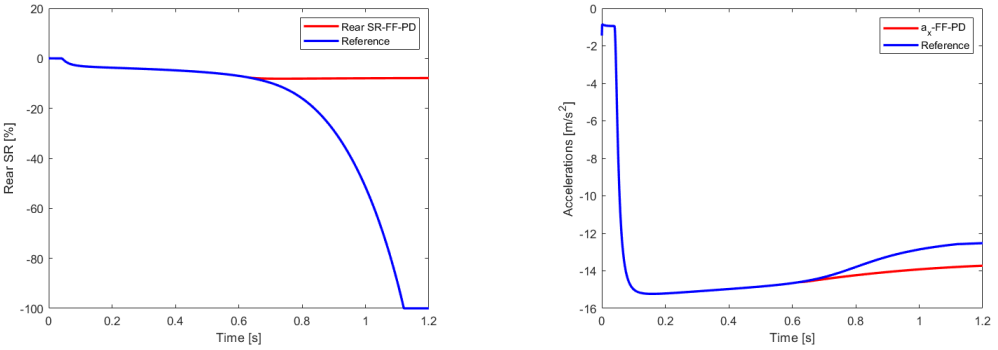

FIGURE 4.17: Pure braking comparison between active traction control and inactive (Reference), starting from $V_0 = 20$. Left: Slip ratio at front axle. Right: Longitudinal acceleration.

Similar graphs to the (figure 4.14 are obtained). The performance of the controller seems to be independent of the starting velocity.

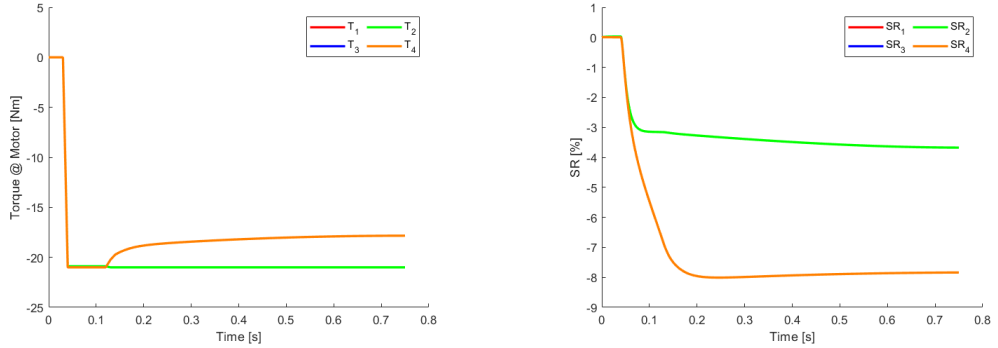

FIGURE 4.18: Pure braking simulation case starting from $V_0 = 10$. Left: Torque at each wheel. Right: Slip ratio at each wheel.

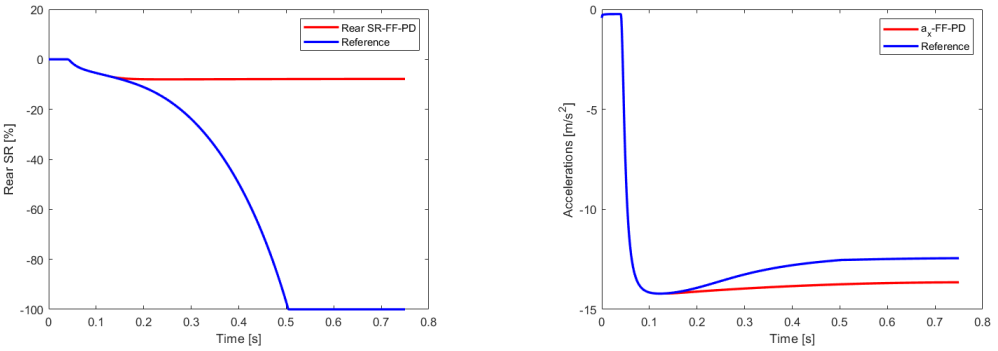

FIGURE 4.19: Pure braking simulation case starting from $V_0 = 10$. Left: Torque at each wheel. Right: Slip ratio at each wheel.

Similar graphs to the (figure 4.14 are obtained). The only difference is that the Slip ratio is increased from the very beginning of the braking condition, whereas in the previous cases it was stable due to the downforce.

4.3.4 Double lane change

It is a complex transient manoeuvre that is used to analyse the dynamic stability, performance and safety of passenger cars, although it is not applicable to a formula student race car a adaptation of this test (ISO-3888-1-2011 [30, 3]) has been used:

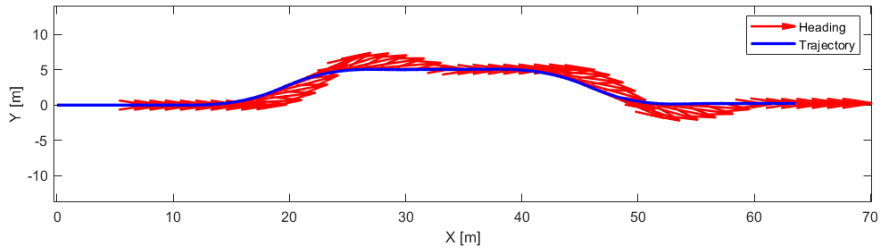

FIGURE 4.20: Double lane change simulation case, trajectory. (This trajectory is plotted from the bottom: $y > 0$ means right-hand side)

The obtained results of this manoeuvre are shown in the following figures.

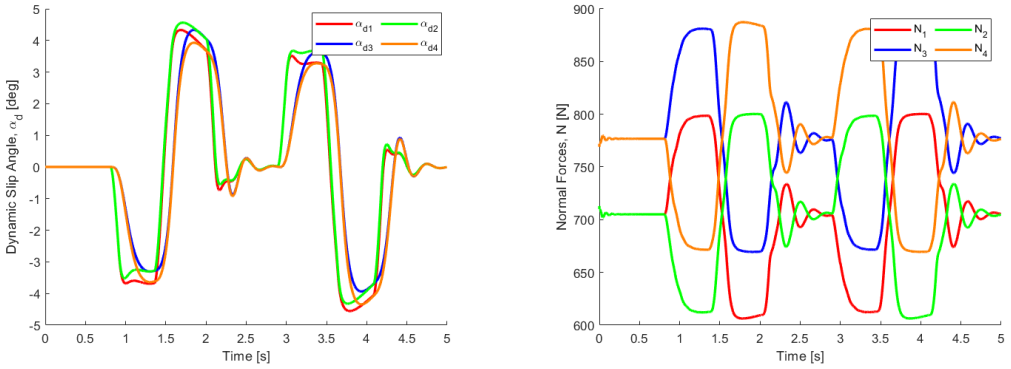

FIGURE 4.21: Double lane change simulation case. Top: dynamic slip angles. Bottom: normal forces.

It is possible to identify the different stages of this case, it start at constant speed, then there is a steering to the right, after half of a second the steer is turned left. Then, it is recovered to straight line position. Finally, the opposed manoeuvre is performed, first a rapid left steering is done and then a right steering, recovering the straight line trajectory.

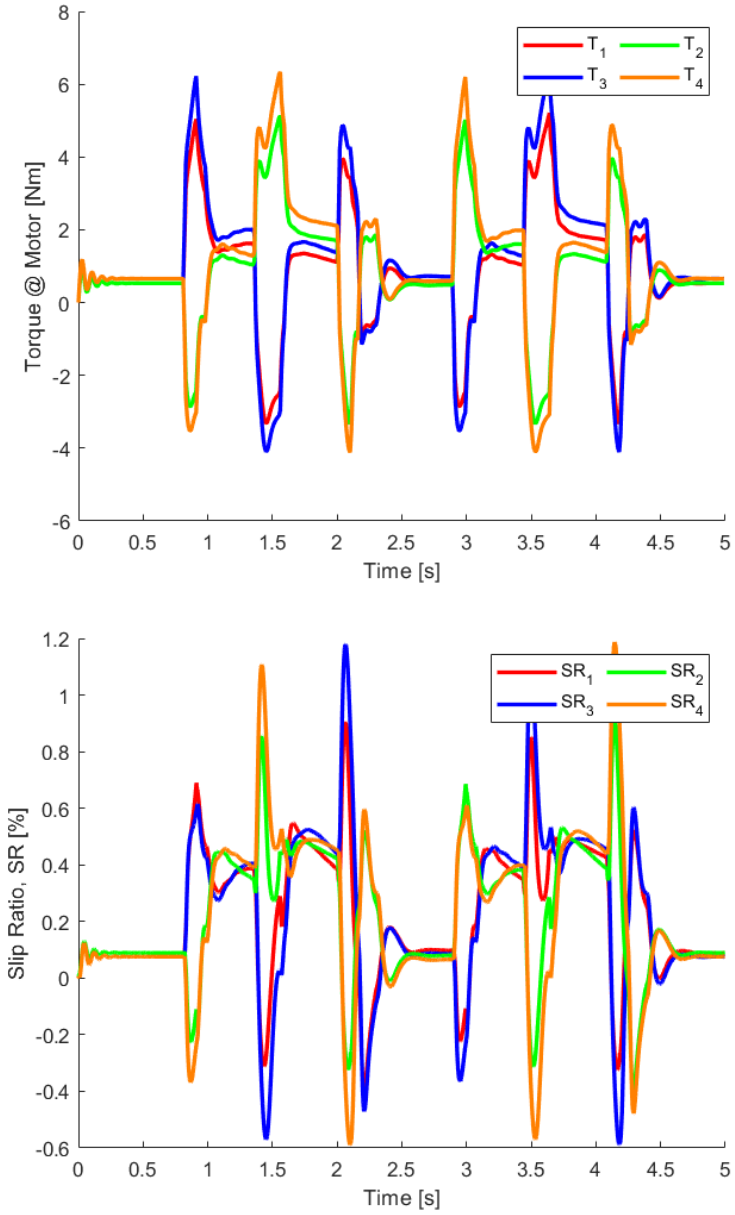

FIGURE 4.22: Double lane change simulation case. Top: motor torques at each wheel. Bottom: slip ratios at each wheel.

It can be seen that when the steering wheel is moved the right wheels are electrically braked and the left wheels are powered obtaining a net torque that helps the vehicle turning to the right, but in the meddle of the manoeuvre the torque difference is reduced and the right wheels slip ratio is increased to positive values. Then the same phenomenon is repeated but oppositely. to continue, the steering wheel is positioned in the straight line position obtaining a torque that damps the yaw rate speed to near 0 value. Then a very similar but opposite manoeuvre is performed starting from a quasi-steady-state position.

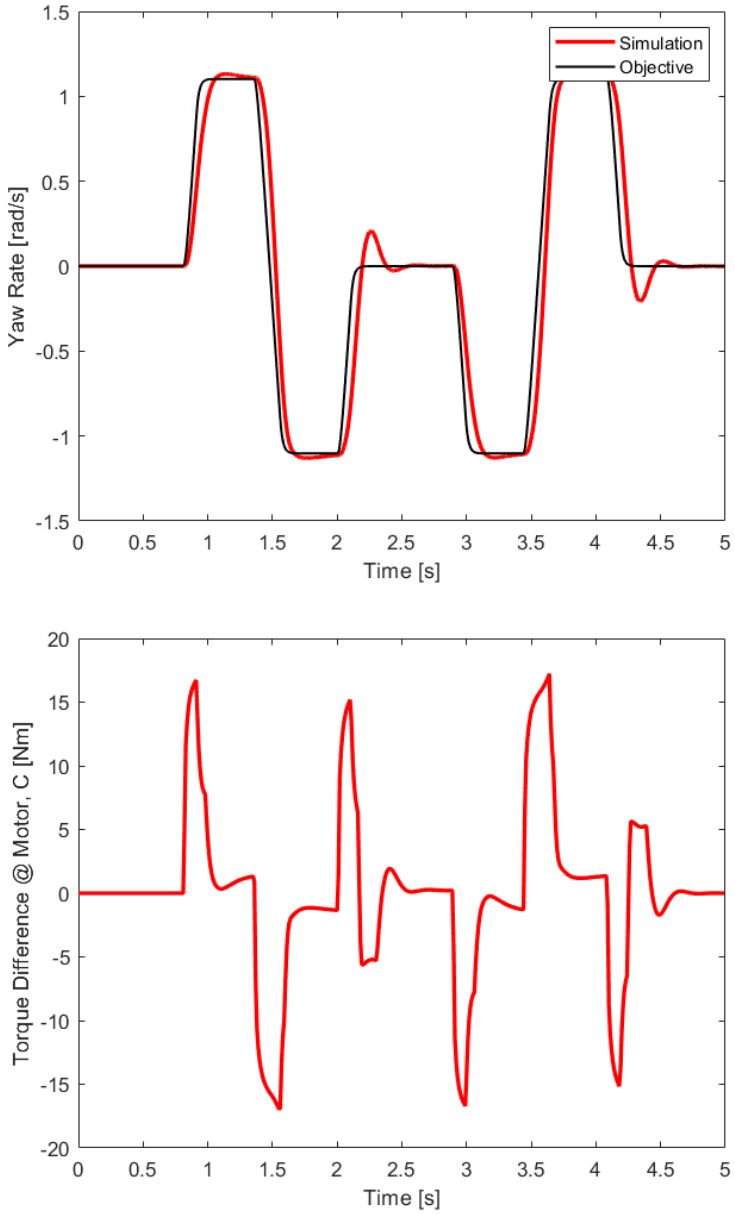

FIGURE 4.23: Double lane change simulation case. Top: yaw rate evolution. Bottom: Control action.

The controller dynamics are validated by achieving high level of performance when performing the double line change manoeuvre. The control has been effective and with high accuracy.

4.3.5 Combined case

In this case, the validation of the improvement of the new assembly system will be done by comparing with a fully independent yaw rate controller and traction controller and with a no-controlled system. The driver inputs of these case will simulate a high throttle corner exit.

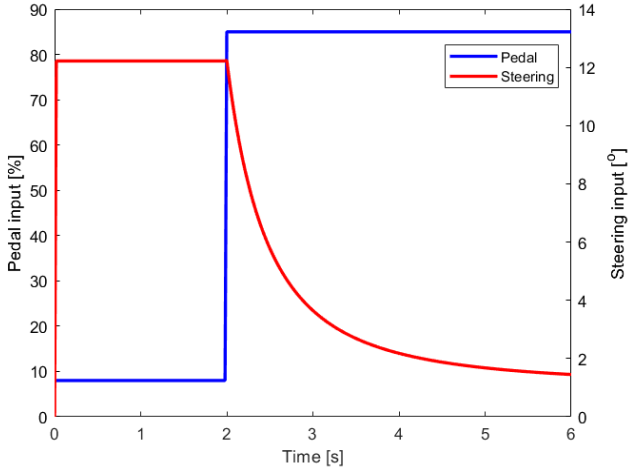

FIGURE 4.24: Combined case driver inputs. Left: Driver throttle. Right: driver steering wheel.

The obtained results are:

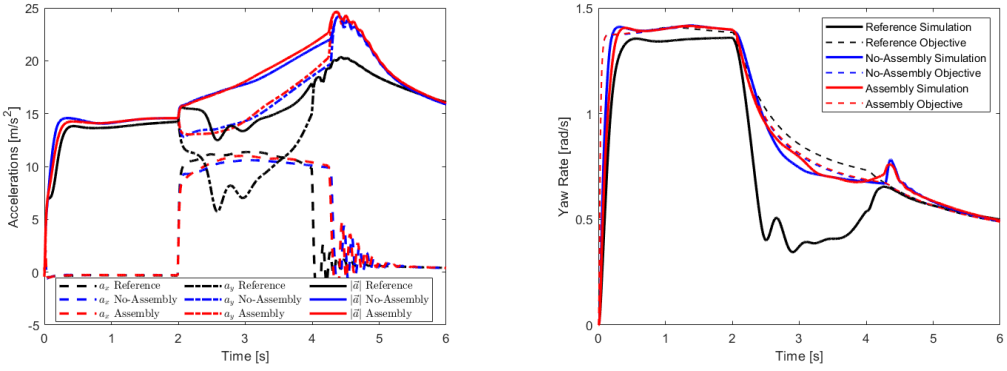

FIGURE 4.25: Performance of the new controller in a combined case. Left: Accelerations. Right: Yaw rate control.

It can be seen that there is a clear improvement in the lateral acceleration when both controllers are active. Also, an improvement in the longitudinal acceleration is seen when the new optimization assembly is performed, achieving a higher acceleration module. On the right, it can be seen that the yaw rate is better controlled with the new algorithm than with the two other simulation cases. Finally the trajectories are:

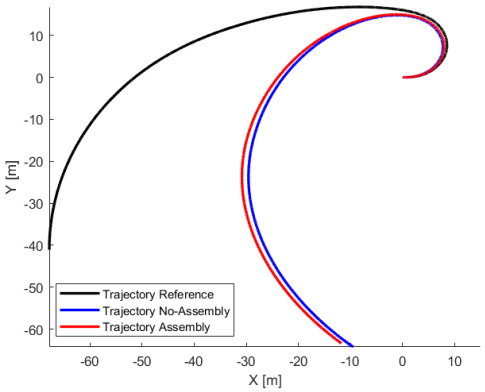

FIGURE 4.26: Combined case trajectories.

It can be seen that, when controlling the yaw rate the vehicle behaviour is less understeering than when it is not controlled, this is due to the slip ratio control of the front tires permitting a higher control.

Finally, a detailed view of the results of the new controller are shown bellow.

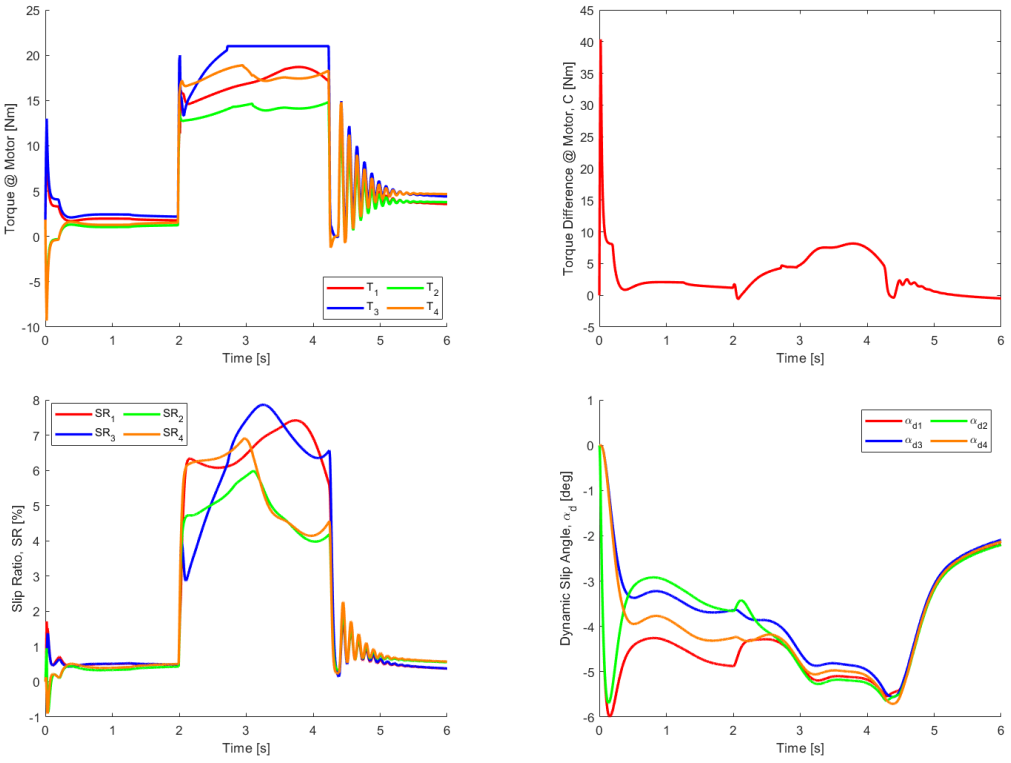

FIGURE 4.27: Performance of the new controller in a combined case.
Top left: Toruqe distribution. Top right: Yaw rate control.
Bottom left: Slip ratio control. Bottom right: Dynamic slip angles at each wheel.

4.4 Budget

In this section, the economical expenses which have been necessary to develop the project will be evaluated: the direct and indirect costs. The following criteria will be applied to distinguish the direct and indirect costs: the engineering process that must be made by a person is considered direct costs and the means to perform this engineering process are considered as indirect costs:

4.4.1 Direct Costs

At this point, and considering the standard salary of a aerospace engineer extracted from the [1] as 26323.57 €/*year* and with a total hours of 1792 h/*year* the direct costs estimated are:

TABLE 4.7: Direct Costs

Engineering			
Task	**Hours**	**€**/*h*	**€**
Research	100	14.69	1468.95
Software Development	200	14.69	2937.90
Report	100	14.69	1468.95
Total	**400**	**14.69**	**5875.80**

4.4.2 Indirect costs

The indirect costs including licensing, amortizations and electricity costs are described as:

TABLE 4.8: Indirect Costs

Software				
Program	**Years**		**€**/*Year*	**€**
MATLAB ©	0.5		1200	600
Facilities Amortization				
Computer	**Years**		**€**/(5 **Years**)	**€**
Mountain Iridium	0.5		2200	220
Energy Consumption				
Computer	**Hours**	**Consumption [W]**	**€**/*kWh* [9]	**€**
Mountain Iridium	500	60.00	0.13594	4.08
Total Indirect Costs				
Total			**1813.34 €**	

4.4.3 Total Costs

Obtaining a final cost of the study of:

TABLE 4.9: Total Expenses

	Amount [€]
Direct Costs	5875.80
Indirect Costs	1624.08
Total	**7499.88**

4.5 Environmental Study

The emitted CO_2 due to this study is considered to be only caused by the energy consumption due to the computers so using the relation between energy and kg_{CO_2} [27] the results are:

Mountain:

$$\frac{60.00W \cdot 500h}{1000} = 30kWh \tag{4.10}$$

Total CO_2 generated:

$$30kWh \cdot \frac{0.703kg_{CO_2}}{1kWh} = 21.09kg_{CO_2} \tag{4.11}$$

Chapter 5

Conclusions

5.1 Conclusion

This study was done with the intention of developing a control algorithm that improve the performance of a race car. Although the model is based in a Formula student type vehicle the same algorithm and development will be used to optimize any other electric 4 wheel drive racing vehicle.

This study has shown the capabilities of the electric vehicle as a race car, following the current trend in the motorsport industry in introducing the electric vehicles in new competitions. Showing the advantages of using reversible electric machines, permitting the use of the regenerative braking capabilities as a efficient way to increase the response and stability of the vehicle and at the same time reduce the braking distance by increasing the performance of the tire.

In addition, a review of the current technologies has been used to decide the most suitable application for the level of knowledge of the author and complexity of the system.

Finally, a combination of two independent controllers has been done by using a optimization function with restrictions that increase the performance when the available torque is limited while maintaining the simplicity of a PID or LQR controllers.

5.2 Comments and further development

As it have been said above, this software establishes the basis of a mathematical model of any kind of vehicle, but if more accuracy is needed some improvements to the model may be done:

1. Improving the dynamic model would be the first thing that is recommended to do in order to obtain better results and a better representation of the vehicle. Using real test data of the suspension movement as a model taking into account not only the springs stiffness but also the compliance and the no-linearities due to the fact that the small deformation are not fulfilled.
2. Improving the inertia of the car by testing the inertia factors and the CoG position.
3. Implementing other controllers as MPCs or robust controllers that may improve the performance.
4. Implement the code using data from different vehicles confirming the robustness of the developed methodology of calibrating the controller parameters.

5.2.1 Validation

The final step is validating the algorithm by testing the algorithm in a race car. This validations may be done testing the circuit and comparing the main variables with the extracted from the simulator. To do so, some devices must be mounted on the vehicle:

1. GPS: Extracting the position and the velocity direction of the car. Differential GPS System (DGPS) may be used for a better resolution and accuracy.
2. IMU: All the angular velocities and accelerations are the basic factors that have to be measured to be compared with the simulated ones.
3. Slip angle sensor: This sensor evaluated the real slip angle and velocity modulus of the car at each point.
4. 3 axis accelerometer or a second IMU: With them the location of the CoG can be estimated at any point of the circuit.
5. Steering angle sensor: Obtaining the angular position of the steering at each point.
6. Linear potentiometers: Measuring the springs deformation and then the applied forces at each moment.
7. ...

5.2.2 Validation Budget

Finally an estimation of the needed budged for the software validation is exposed at Table 5.1 Obtaining a total costs of about 30350€ without considering the necessity of mounting a differential GPS system.

TABLE 5.1: Software Validation Budget

Sensor type	**Company supplier**	**Device reference**	**Units**	**Price/Unit [€/u]**	**Total Price [€]**
GPS and IMU	XSENS	MTI-710-G-NGSS	1	4000	4000
DGPS	-	-	1	-	-
Slip Angle sensor	Kistler	Correvit S-350: 2-Axis Optical Sensors	1	25000	25000
IMU2	Continental	SC13S - 6DOF IMU 3-34543-256	1	150	150
Steering angle sensor	SKF	97203-BEP	1	200	200
Linear Potentiometers	TE Connectivity	MLP-75	4	250	1000
TOTAL				**30350 €**	

References

[1] BOE-A-2019-14977: XIX CONVENIO COLECTIVO NACIONAL DE EMPRESAS DE INGENIERÍA Y OFICINAS DE ESTUDIOS TÉCNICOS. *BOE*, Núm. 251 Sec. III:pag, 114772–114802, 2019-08-18.

[2] M. Ángel and G. Tierno. *Mecánica de vuelo*. Garceta, Madrid, 2 edition, 2012. ISBN 9788415452010.

[3] S. Angelis, M. Tidlund, A. Leledakis, M. Lidberg, M. Nybacka, and D. Katzourakis. Optimal steering for double-lane change entry speed maximization. 09 2014.

[4] J. Antunes, C. Cardeira, and P. Oliveira. Torque Vectoring for a Formula Student Prototype. In *Advances in Intelligent Systems and Computing*, volume 694, 2018. doi: 10.1007/978-3-319-70836-2_35.

[5] I. J. M. Besselink, A. J. C. Schmeitz, and H. B. Pacejka. An improved Magic Formula/Swift tyre model that can handle inflation pressure changes. In *Vehicle System Dynamics*, volume 48, pages 337–352, 2010. ISBN 0042-3114. doi: 10.1080/00423111003748088.

[6] C. G. Bobier-Tiu, C. E. Beal, J. C. Kegelman, R. Y. Hindiyeh, and J. C. Gerdes. Vehicle control synthesis using phase portraits of planar dynamics. *Vehicle System Dynamics*, 57(9):1318–1337, 2019. ISSN 17445159. doi: 10.1080/00423114.2018.1502456.

[7] L. Brown. *Torque Vectoring on on Electric All-Wheel-Drive Formula SAW Race Car*. Bachelor thesis, The university of western Australia, 35 Stirling Hwy, Crawley WA 6009, Australia, 2014.

[8] S. C. Chapra and R. P. Canale. *Métodos Matemáticos Para Ingenieros*. The McGraw-Hill, Mexico,D. F., 5 edition, 2006. ISBN 9789701061145.

[9] ENDESA. Precio de la electricidad en tiempo real, 2020. URL https://tarifaluzhora.es/?tarifa=normal{&}fecha=2021-01-05.

[10] J. He. Matlab Quick Reference, 2014. URL http://www.cs.cmu.edu/~tom/10601_fall2012/recitations/matlab_quickref.pdf.

[11] B. Huang, S. Wu, S. Huang, and X. Fu. Lateral Stability Control of Four-Wheel Independent Drive Electric Vehicles Based on Model Predictive Control. *Mathematical Problems in Engineering*, 2018, 2018. ISSN 15635147.

[12] M. D. Jahnke, F. Cosco, R. Novickis, J. P. Rastelli, and V. Gomez-Garay. Efficient neural network implementations on parallel embedded platforms applied to real-time torque-vectoring optimization using predictions for multi-motor electric vehicles. *Electronics (Switzerland)*, 8(2), 2019. ISSN 20799292. doi: 10.3390/electronics8020250.

[13] G. Kaiser. *Torque Vectoring Linear Parameter-Varying Control for an Electric Vehicle*. Phd's thesis, Hamburg University of Technology, Am Schwarzenberg-Campus 1, 21073 Hamburg, Germany, 2015.

[14] E. Kuiper and J. J. Van Oosten. The PAC2002 advanced handling tire model. *Vehicle System Dynamics*, 45(SUPPL. 1):153–167, 2007. ISSN 00423114. doi: 10.1080/00423110701773893.

[15] Z. Liang, J. Zhao, Z. Dong, Y. Wang, and Z. Ding. Torque Vectoring and Rear-Wheel-Steering Control for Vehicle's Uncertain Slips on Soft and Slope Terrain Using Sliding Mode Algorithm. *IEEE Transactions on Vehicular Technology*, 69 (4):3805–3815, 2020. ISSN 19399359. doi: 10.1109/TVT.2020.2974107.

[16] C. Lin and Z. Xu. Wheel torque distribution of four-wheel-drive electric vehicles based on multi-objective optimization. *Energies*, 8(5):3815–3831, 2015. ISSN 19961073. doi: 10.3390/en8053815.

[17] A. Lucchini, S. Formentin, M. Corno, D. Piga, and S. M. Savaresi. Torque Vectoring for High-Performance Electric Vehicles: An Efficient MPC Calibration. *IEEE Control Systems Letters*, 4(3):725–730, 2020. ISSN 24751456. doi: 10.1109/LCSYS.2020.2981895.

[18] Mathworks Inc. Matlab optimization toolbox. URL https://es.mathworks.com/store/link/products/student/new.

[19] E. Mikuláš, M. Gulan, and G. Takács. Model Predictive Torque Vectoring Control for a Formula Student Electric Racing Car. *2018 European Control Conference, ECC 2018*, pages 581–588, 2018. doi: 10.23919/ECC.2018.8550124.

[20] M. &. Milliken, W. F. Milliken, and D. L. Milliken. *Race Car Vehicle Dynamics*. SAE, Warrendale, Pennsilvania, 5 edition, 1995. ISBN 1560915269.

[21] H. B. Pacejka. *Tyre and vehicle dynamics*. SAE Technical Papers, 2005.

[22] S. Piche, J. Keeler, G. Martin, G. Boe, D. Johnson, and M. Gerules. Neural network based Model Predictive Control. *Advances in Neural Information Processing Systems*, pages 1029–1035, 2000. ISSN 10495258.

[23] D. Richeson. a-quick-guide-to-latex. 2018. URL https://www.overleaf.com/latex/templates/a-quick-guide-to-latex/fghqpfgnxggz.

[24] C. Rouelle. Advanced Vehicle Dynamics Applied to Race Car Design & Development. Terrassa, 2017. OptimumG.

[25] E. Siampis, E. Velenis, S. Gariuolo, and S. Longo. A real-time nonlinear model predictive control strategy for stabilization of an electric vehicle at the limits of handling. *IEEE Transactions on Control Systems Technology*, 26(6):1982–1994, 2018. ISSN 1558-0865. doi: 10.1109/TCST.2017.2753169.

[26] A. Stoop. *Design and Implementation of Torque Vectoring for the Forze Racing Car*. Master's thesis, Delft University of Technology, 2600 AA Delft, Netherlands, 2013.

[27] US Enviromental Protection Agency. Greenhouse Equivalencies Calculator, 2020.

[28] R. A. Villamar. Vibracions mecàniques. 2016.

[29] Z. Wang, U. Montanaro, S. Fallah, A. Sorniotti, and B. Lenzo. A gain scheduled robust linear quadratic regulator for vehicle direct yaw moment Control. *Mechatronics*, 51, 2018. ISSN 09574158. doi: 10.1016/j.mechatronics.2018.01.013.

[30] Z. Zainal, W. Rahiman, and M. N. Baharom. Yaw rate and sideslip control using PID controller for double lane changing. *Journal of Telecommunication, Electronic and Computer Engineering*, 9(3-7), 2017. ISSN 22898131.

[31] K. Zarkadis, E. Velenis, E. Siampis, and S. Longo. Predictive Torque Vectoring Control with Active Trail-Braking. In *2018 European Control Conference, ECC 2018*, 2018. ISBN 9783952426982. doi: 10.23919/ECC.2018.8550061.

Appendix A

Tire Model: Magic Formula 6.1

In this appendix, the equations and description of the Magic Formula 6.1 tire model will be performed.

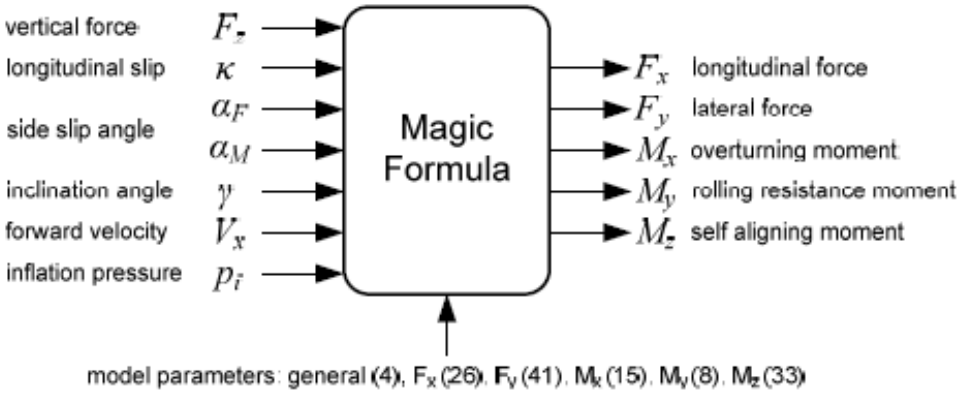

FIGURE A.1: Inputs and outputs of the Magic Formula. Source: [5], pag. 11

The first step is to dimensionless the vertical force and the pressure:

$$df_z = \frac{F_z - F_{z,0}}{F_{z,0}} \tag{A.1}$$

$$dP_i = \frac{P_i - P_{i,0}}{P_{i,0}} \tag{A.2}$$

A.1 Longitudinal force F_x

$$F_x = (D_x \sin [C_x \arctan\{B_x\kappa_x - E_x \arctan(B_x\kappa_x - \arctan(B_x\kappa_x))\}] + S_{V_x}) \cdot G_{x\alpha} \quad \text{(A.3)}$$

Pure slip:

$$\kappa_x = \kappa + S_{Hx} \quad \text{(A.4)}$$

$$C_x = P_{Cx1}\lambda_{Cx} \quad \text{(A.5)}$$

$$D_x = \mu_x F_z \quad \text{(A.6)}$$

$$\mu_x = (p_{Dx1} + p_{Dx2}df_z)(1 - p_{Dx3}\gamma^2)(1 + p_{px3}dp_i + p_{px4}dp_i^2)\lambda_{\mu x} \quad \text{(A.7)}$$

$$E_x = (p_{Ex1} + p_{Ex2}df_z + p_{Ex3}df_z^2)(1 - p_{Ex4}\mathrm{sgn}(\kappa_x))\lambda_{Ex} \quad \text{(A.8)}$$

$$K_{x\kappa} = (p_{Kx1} + p_{Kx2}df_z)\exp(p_{Kx3}df_z)(1 + p_{px1}dp_i + p_{px2}dp_i^2)F_z\lambda_{Kx\kappa} \quad \text{(A.9)}$$

$$B_x = \frac{K_{x\kappa}}{C_x D_x} \quad \text{(A.10)}$$

$$S_{Hx} = (p_{Hx1} + p_{Hx2}df_z)\lambda_{Hx} \quad \text{(A.11)}$$

$$S_{Vx} = (p_{Vx1} + p_{Vx2}df_z)F_z\lambda_{Vx}\lambda_{\mu x} \quad \text{(A.12)}$$

Combined longitudinal correction factor:

$$G_{x\alpha} = \frac{\cos[C_{x\alpha} \arctan\{B_{x\alpha}\alpha_s - E_{x_\alpha}(B_{x\alpha}\alpha_s - \arctan(B_{x\alpha}\alpha_s))\}]}{\cos[C_{x\alpha} \arctan\{B_{x\alpha}S_{Hx\alpha} - E_{x_\alpha}(B_{x\alpha}S_{Hx\alpha} - \arctan(B_{x\alpha}S_{Hx\alpha}))\}]} \quad \text{(A.13)}$$

$$\alpha_s = \alpha_F + S_{Hx\alpha} \quad \text{(A.14)}$$

$$B_{x\alpha} = (r_{Bx1} + r_{Bx3}\gamma^2)\cos(\arctan(r_{Bx2}\kappa))\lambda_{x\alpha} \quad \text{(A.15)}$$

$$C_{x\alpha} = r_{Cx1} \quad \text{(A.16)}$$

$$C_{x\alpha} = r_{Ex1} + r_{Ex2}df_z \quad \text{(A.17)}$$

$$S_{Hx\alpha} = r_{Hx1} \quad \text{(A.18)}$$

A.2 Overturning moment M_x

$$M_x = R_0 F_z \lambda_{Mx} \{ q_{sx1} \lambda_{vMx} - q_{sx2} \gamma (1 + P_{pMx1} dp_i) - q_{sx12} \gamma \mid \gamma \mid + q_{sx3} \frac{F_y}{F_{z0}} + q_{sx4} \cos \left[q_{sx4} \arctan \left(\left(q_{sx6} \frac{F_z}{F_{z0}} \right)^2 \right) \right] \cdot \sin \left[q_{sx7} \gamma + q_{sx8} \arctan \left(\left(q_{sx9} \frac{F_y}{F_{z0}} \right)^2 \right) \right] + q_{sx10} \arctan \left(q_{sx11} \frac{F_z}{F_{z0}} \right) \gamma \} + R_0 F_y \lambda_{Mx} \{ q_{sx13} + q_{sx13} \mid \gamma \mid \} \quad \text{(A.19)}$$

A.3 Rolling resistance moment M_y

$$M_y = -R_0 F_{z0} \lambda_{My} (q_{sy1} + q_{sy2} \frac{F_x}{F_{z0}} + q_{sy3} \left| \frac{V_x}{V_{ref}} \right| + q_{sy4} \left(\frac{V_x}{V_{ref}} \right)^4 + q_{sy5} \gamma^2 + q_{sy6} \frac{F_z}{F_{z0}} \gamma^2) \left(\frac{F_z}{F_{z0}} \right)^{q_{sy7}} \left(\frac{p}{p_0} \right)^{q_{sy8}} \quad \text{(A.20)}$$

A.4 Lateral force F_y

$$F_y = G_{y\kappa} F_{yp} + S_{V_{y\kappa}} \tag{A.21}$$

Pure slip:

$$F_{yp} = D_y \sin\left[C_y \arctan\{B_y\alpha_y - E_y(B_y\alpha_y - \arctan(B_y\alpha_y)\}\right] + S_{V_y} \tag{A.22}$$

$$\alpha_y = \alpha + S_{Hy} \tag{A.23}$$

$$C_y = P_{Cy1}\lambda_{Cy} \tag{A.24}$$

$$D_y = \mu_y F_z \tag{A.25}$$

$$\mu_y = (p_{Dy1} + p_{Dy2}df_z)(1 - p_{Dy3}\gamma^2)(1 + p_{py3}dp_i + p_{py4}dp_i^2)\lambda_{\mu y} \tag{A.26}$$

$$E_y = (p_{Ey1} + p_{Ey2}df_z)(1 + p_{Ey5}\gamma^2 - (p_{Ey3} + p_{Ey4}\gamma)\mathrm{sgn}(\alpha_y))\lambda_{Ey} \tag{A.27}$$

$$K_{y\alpha} = (p_{Ky1}F_{z0}(1 + p_{py1}dp_i)\sin\left[p_{Ky4}\arctan\left\{\frac{F_z}{(p_{Ky2} + p_{Ky5}\gamma^2)(1 + p_{py2}dp_i)F_{z0}}\right\}\right] (1 - p_{Ky3}|\gamma|)\lambda_{Ky\alpha} \tag{A.28}$$

$$K_{y\gamma} = (p_{Ky6} + p_{Ky7}df_z)(1 + p_{py5}dp_i)F_z\lambda_{Ky\gamma} \tag{A.29}$$

$$B_y = \frac{K_{y\alpha}}{C_y D_y} \tag{A.30}$$

$$S_{Hy} = S_{Hy0 + S_{Hy\gamma}} \tag{A.31}$$

$$S_{Hy0} = (p_{Hy1} + p_{Hy2}df_z)\lambda_{Hy} \tag{A.32}$$

$$S_{Hy\gamma} = \frac{K_{y\gamma}\gamma - S_{Vy\gamma}}{K_{y\alpha}} \tag{A.33}$$

$$S_{Vy} = S_{Vy0 + S_{Vy\gamma}} \tag{A.34}$$

$$S_{Vy0} = (p_{Vy1} + p_{Vy2}df_z)F_z\lambda_{Vy}\lambda_{\mu y} \tag{A.35}$$

$$S_{Vx} = (p_{Vy3} + p_{Vy4}df_z)F_z\gamma\lambda_{Ky\gamma}\lambda_{\mu y} \tag{A.36}$$

Combined lateral correction factor:

$$S_{Vy\kappa} = D_{Vy\kappa} \sin(r_{Vy5} \arctan(r_{Vy6}\kappa))\lambda_{Vy\kappa} \tag{A.37}$$

$$D_{Vy\kappa} = \mu_y F_z (r_{Vy1} + r_{Vy2} df_z + r_{Vy3}\gamma) \cos(\arctan(r_{Vy4}\alpha)) \tag{A.38}$$

$$G_{y\kappa} = \frac{\cos[C_{y\kappa} \arctan\{B_{y\kappa}\kappa_s - E_{y_\kappa}(B_{y\kappa}\kappa_s - \arctan(B_{y\kappa}\kappa_s))\}]}{\cos[C_{y\kappa} \arctan\{B_{y\kappa}S_{Hy\kappa} - E_{y_\kappa}(B_{y\kappa}S_{Hy\kappa} - \arctan(B_{y\kappa}S_{Hy\kappa}))\}]} \tag{A.39}$$

$$\kappa_s = \kappa + S_{Hy\kappa} \tag{A.40}$$

$$B_{y\kappa} = (r_{By1} + r_{By4}\gamma^2) \cos(\arctan(r_{By2}(\alpha - r_{By3})))\lambda_{y\kappa} \tag{A.41}$$

$$C_{y\kappa} = r_{Cy1} \tag{A.42}$$

$$C_{y\kappa} = r_{Ey1} + r_{Ey2} df_z \tag{A.43}$$

$$S_{Hy\kappa} = r_{Hy1} + r_{Hy2} df_z \tag{A.44}$$

A.5 Self-aligning moment M_z

$$M_z = -t \cdot F_{yp0} \cdot G_{y\kappa 0} + M_{zr} + s \cdot F_x \tag{A.45}$$

Where $F_{yp0} \cdot G_{y\kappa 0}$ is the combined slip side force with zero inclination angles $\gamma = 0$.

$$\alpha_t = \alpha + S_{Ht} \tag{A.46}$$

$$S_{Ht} = q_{Hz1} + q_{Hz2} df_z + (q_{Hz3} + q_{Hz4} df_z)\gamma \tag{A.47}$$

$$\alpha_r = \alpha + S_{Hy} + \frac{S_{Vy}}{K_{y\alpha}} \tag{A.48}$$

$$\alpha_{t,eq} = \arctan(\sqrt{\tan^2(\alpha_t) + \left(\frac{K_{x\kappa}}{K_{y\alpha}}\right)^2 \kappa^2} \mathrm{sgn}(\alpha_t)) \tag{A.49}$$

$$\alpha_{r,eq} = \arctan(\sqrt{\tan^2(\alpha_r) + \left(\frac{K_{x\kappa}}{K_{y\alpha}}\right)^2 \kappa^2} \mathrm{sgn}(\alpha_r)) \tag{A.50}$$

$$s = \left(s_{sz1} + s_{sz1}\left(\frac{F_y}{f_{z0}}\right) + (s_{sz1} + s_{sz1} df_z)\gamma\right) R_0 \lambda_s \tag{A.51}$$

Pneumatic trail t:

$$t = D_t \cos\left[C_t \arctan\{B_t\alpha_{t,eq} - E_t(B_t\alpha_{t,eq} - \arctan(B_t\alpha_{t,eq})\}\right] \cos(\alpha) \tag{A.52}$$

$$B_t = (q_{Bz1} + q_{Bz2} df_z + q_{Bz3} df_z^2)(1 + q_{Bz4} q_{Bz5} |\gamma|) \frac{\lambda_{Ky\alpha}}{\lambda_{\mu_y}} \tag{A.53}$$

$$C_t = q_{Cz1} \tag{A.54}$$

$$D_t = (q_{Dz1} + q_{Dz2}df_z)(1 - q_{Dz1}dp_i)(1 + q_{Dz3}\gamma + q_{Bz4}\gamma^2)F_z\frac{R_0}{F_{z0}}\lambda_t \tag{A.55}$$

$$E_t = (q_{Ez1} + q_{Ez2}df_z + q_{Ez3}df_z^2)\left(1 + (q_{Ez4}q_{Bz5}\gamma)\left(\frac{2}{\pi}\right)\arctan(B_tC_t\alpha_t)\right) \tag{A.56}$$

Residual moment M_{zr}:

$$M_{zr} = D_r\cos\left[\arctan\{B_r\alpha_{r,eq}\}\cos(\alpha)\right] \tag{A.57}$$

$$B_r = q_{Bz9}\frac{\lambda_{Ky\alpha}}{\lambda_{\mu y}} + q_{Bz10}B_yC_y \tag{A.58}$$

$$\begin{aligned} D_r = [(q_{Dz6} + (q_{Dz7}df_z)\lambda_r + ((q_{Dz8} + (q_{Dz9}df_z)(1 - p_{pz2}dp_i)\gamma\lambda_{Kz\gamma} \\ + (q_{Dz10} + (q_{Dz11}df_z)\gamma|\gamma|\lambda_{Kz\gamma}]F_zR_0\lambda_{\mu y} \end{aligned} \tag{A.59}$$

A.6 Tire model Matlab code

```
function [Fx,Fy,Mx,My,Mz,cx,cy,cz,Rl]=Evaluate_Tyre_Model(inputs,coefficients,
    scaling_factors,Tot)
%% Index
        %Adimensionalization
        %Fx calculation
        %Fy calculation
        %Mx calculation
        %My calculation
        %Mz calculation
        %Radius calculation (Cancelled)
        %Contact patch calculation (Cancelled)
        %Stiffness calculation
%% Bibliography
    % Using UPC ecoRacing Pacejka Model extracted from the paper:
        % [4] An improved Magic Formula/Swift tyre model that can handle in
    action pressure changes.
        % In Vehicle System Dynamics, volume 48, pages 337-352, 2010.
    %% Adimensionalization
    dFz=(inputs(1)-coefficients(1))/coefficients(1);
    dPi=(inputs(6)-coefficients(4))/coefficients(4);

    %% Fx calculation
    %Pure slip (34-42)
    Kxk=(coefficients(40)+coefficients(41)*dFz)*exp(coefficients(42)*dFz)*(1+
    coefficients(47)*dPi+coefficients(48)*dPi^2)*inputs(1)*scaling_factors(5);
    SHx=(coefficients(43)+coefficients(44)*dFz)*scaling_factors(11);
    SVx=(coefficients(45)+coefficients(46)*dFz)*inputs(1)*scaling_factors(2)*
    scaling_factors(13);
    kx=inputs(2)+SHx;
    Mux=(coefficients(33)+coefficients(34)*dFz)*(1-coefficients(35)*inputs(4)^2)
    *(1+coefficients(49)*dPi+coefficients(50)*dPi^2)*scaling_factors(2);
    Cx=coefficients(32)*scaling_factors(7);
    Dx=Mux*inputs(1);
    Ex=(coefficients(36)+coefficients(37)*dFz+coefficients(38)*dFz^2)*(1-
    coefficients(39)*sign(inputs(2)))*scaling_factors(9);
    Bx=Kxk/Cx/Dx;

    if Ex>1
        Error=['Error in the value of E: Ex=' Ex]; %#ok<NASGU>
        disp('Error')
        display(inputs)
        clear Error
    end

    %Combined slip (43-48)
    SHxa=coefficients(100);
    SAs=inputs(3)+SHxa;
    Bxa=(coefficients(96)+coefficients(98)*inputs(4)^2)*cos(atan(coefficients(97)
    *inputs(2)))*scaling_factors(19);
    Cxa=coefficients(99);
    Exa=coefficients(101)+coefficients(102)*dFz;

```

```
46      Gxa=cos(Cxa*atan(Bxa*SAs-Exa*(Bxa*SAs-atan(Bxa*SAs))))/cos(Cxa*atan(Bxa*SHxa-
        Exa*(Bxa*SHxa-atan(Bxa*SHxa))));
47
48      if Exa>1
49          Error=['Error in the value of E: Exa=' Exa]; %#ok<NASGU>
50          disp('Error')
51          display(inputs)
52          clear Error
53      end
54
55      %Pacejka formula (33)
56      Fx=(Dx*sin(Cx*atan(Bx*kx-Ex*(Bx*kx-atan(Bx*kx))))+SVx)*Gxa;
57      %% Fy calculation
58      %Pure slip (53-66)
59      Kya=coefficients(14)*coefficients(1)*(1+coefficients(27)*dPi)*sin(
        coefficients(17)*atan(inputs(1)/...
60          ((coefficients(15)+coefficients(18)*inputs(4)^2)*(1+coefficients(28)*dPi)
        *coefficients(1))))*(1-coefficients(16)*abs(inputs(4)))*scaling_factors(6);
61      Kyia=(coefficients(19)+coefficients(20)*dFz)*(1+coefficients(31)*dPi)*inputs
        (1)*scaling_factors(15);
62      SVy0=inputs(1)*(coefficients(23)+coefficients(24)*dFz)*scaling_factors(3)*
        scaling_factors(14);
63      SVyia=inputs(1)*(coefficients(25)+coefficients(26)*dFz)*inputs(4)*
        scaling_factors(3)*scaling_factors(15);
64      SHy0=(coefficients(21)+coefficients(22)*dFz)*scaling_factors(12);
65      SHyia=(Kyia*inputs(4)-SVyia)/Kya;
66      SHy=SHy0+SHyia;
67      SVy=SVy0+SVyia;
68      SAy=inputs(3)+SHy;
69      Muy=(coefficients(6)+coefficients(7)*dFz)*(1-coefficients(8)*inputs(4)^2)*(1+
        coefficients(29)*dPi+coefficients(30)*dPi^2)*scaling_factors(3);
70      Cy=coefficients(5)*scaling_factors(8);
71      Dy=Muy*inputs(1);
72      Ey=(coefficients(9)+coefficients(10)*dFz)*(1+coefficients(13)*inputs(4)^2-(
        coefficients(11)+coefficients(12)*inputs(4))*sign(SAy))*scaling_factors(10);
73      By=Kya/Cy/Dy;
74
75      if Ey>1
76          Error=['Error in the value of E: Ey=' Ey]; %#ok<NASGU>
77          disp('Error')
78          display(inputs)
79          clear Error
80      end
81
82      %Combined slip (67-74)
83      SHyk=coefficients(88)+coefficients(89)*dFz;
84      ks=inputs(2)+SHyk;
85      Byk=(coefficients(81)+coefficients(84)*inputs(4)^2)*cos(atan(coefficients(82)
        *(inputs(3)-coefficients(83))))*scaling_factors(20);
86      Cyk=coefficients(85);
87      Eyk=coefficients(86)+coefficients(87)*dFz;
88      DVyk=Muy*inputs(1)*(coefficients(90)+coefficients(91)*dFz+coefficients(92)*
        inputs(4))*cos(atan(coefficients(93)*inputs(3)));
89      SVyk=DVyk*sin(coefficients(94)*atan(coefficients(95)*inputs(2)))*
        scaling_factors(21);
```

```
90
91      Gyk=cos(Cyk*atan(Byk*ks-Eyk*(Byk*ks-atan(Byk*ks))))/cos(Cyk*atan(Byk*SHyk-Eyk
        *(Byk*SHyk-atan(Byk*SHyk))));
92
93      if Eyk>1
94          Error=['Error in the value of E: Eyk=' Eyk]; %#ok<NASGU>
95          disp('Error')
96          display(inputs)
97          clear Error
98      end
99
100     %Pacejka formula (51-52)
101     Fy=Gyk*(Dy*sin(Cy*atan(By*SAy-Ey*(By*SAy-atan(By*SAy))))+SVy)+SVyk;
102
103     %% Mx calculation (49)
104     Mx=coefficients(2)*inputs(1)*scaling_factors(24)*(coefficients(107)*
        scaling_factors(26)-coefficients(108)*inputs(4)*(1+coefficients(121)*dPi)...
105        -coefficients(118)*inputs(4)*abs(inputs(4))+coefficients(109)*Fy/
        coefficients(1)...
106        +coefficients(110)*cos(coefficients(111)*atan((coefficients(112)*inputs(1)
        /coefficients(1))^2))*sin(coefficients(113)*inputs(4)...
107        +coefficients(114)*atan(coefficients(115)*Fy/coefficients(1)))+
        coefficients(116)*atan(coefficients(117)*inputs(1)/coefficients(1))*inputs(4)
        )...
108        +coefficients(2)*Fy*scaling_factors(24)*(coefficients(119)+coefficients
        (120)*abs(inputs(4)));
109
110     %% My calculation (50)
111     My=-coefficients(2)*coefficients(1)*scaling_factors(25)*(coefficients(122)+
        coefficients(123)*Fx/coefficients(1)...
112         +coefficients(124)*abs(inputs(5)/coefficients(3))+coefficients(125)*(
        inputs(5)/coefficients(3))^4+coefficients(126)*inputs(4)^2 ...
113         +coefficients(127)*inputs(1)/coefficients(1)*inputs(4)^2)*(inputs(1)/
        coefficients(1))^coefficients(128)*(inputs(6)/coefficients(4))^coefficients
        (129);
114
115     %% Mz calculation
116     %Combined slip force with zero inclination angle Fy@IA=0
117     if inputs(4)==0
118         Fy0=Fy;
119     else
120         %Pure slip (53-66)
121         Kya=coefficients(14)*coefficients(1)*(1+coefficients(27)*dPi)*...
122             sin(coefficients(17)*atan(inputs(1)/(coefficients(15)*(1+coefficients
        (28)*dPi)*coefficients(1))))*scaling_factors(6);
123         SVy=inputs(1)*(coefficients(23)+coefficients(24)*dFz)*scaling_factors(3)*
        scaling_factors(14);
124         SHy=(coefficients(21)+coefficients(22)*dFz)*scaling_factors(12);
125         SAy=inputs(3)+SHy;
126         Muy=(coefficients(6)+coefficients(7)*dFz)*(1+coefficients(29)*dPi+
        coefficients(30)*dPi^2)*scaling_factors(3);
127         Cy=coefficients(5)*scaling_factors(8);
128         Dy=Muy*inputs(1);
129         Ey=(coefficients(9)+coefficients(10)*dFz)*(1-coefficients(11)*sign(SAy))*
        scaling_factors(10);
```

```
130         By=Kya/Cy/Dy;
131
132         if Ey>1
133             Error=['Error in the value of E: Ey=' Ey]; %#ok<NASGU>
134             disp('Error')
135             display(inputs)
136             clear Error
137         end
138
139         %Combined slip (67-74)
140         SHyk=coefficients(88)+coefficients(89)*dFz;
141         ks=inputs(2)+SHyk;
142         Byk=coefficients(81)*cos(atan(coefficients(82)*(inputs(3)-coefficients
    (83))))*scaling_factors(20);
143         Cyk=coefficients(85);
144         Eyk=coefficients(86)+coefficients(87)*dFz;
145         DVyk=Muy*inputs(1)*(coefficients(90)+coefficients(91)*dFz)*cos(atan(
    coefficients(93)*inputs(3)));
146         SVyk=DVyk*sin(coefficients(94)*atan(coefficients(95)*inputs(2)))*
    scaling_factors(21);
147
148         Gyk=cos(Cyk*atan(Byk*ks-Eyk*(Byk*ks-atan(Byk*ks))))/cos(Cyk*atan(Byk*SHyk
    -Eyk*(Byk*SHyk-atan(Byk*SHyk))));
149
150         if Eyk>1
151             Error=['Error in the value of E: Eyk0=' Eyk]; %#ok<NASGU>
152             disp('Error')
153             display(inputs)
154             clear Error
155         end
156
157         %Pacejka formula (51-52)
158         Fy0=Gyk*(Dy*sin(Cy*atan(By*SAy-Ey*(By*SAy-atan(By*SAy))))+SVy)+SVyk;
159     end
160
161     %Equivalent slip (76-81)
162     SHt=coefficients(75)+coefficients(76)*dFz+(coefficients(77)+coefficients(78)*
    dFz)*inputs(4);
163     SAt=inputs(3)+SHt;
164     SAr=inputs(3)+SHy+SVy/Kyia;
165     SAteq=atan(sqrt((tan(SAt))^2+(Kxk/Kya)^2*inputs(2)^2))*sign(SAt);
166     SAreq=atan(sqrt((tan(SAr))^2+(Kxk/Kya)^2*inputs(2)^2))*sign(SAr);
167
168     %Pneumatic scrub (82)
169     s=(coefficients(103)+coefficients(104)*(Fy/coefficients(1))+(coefficients
    (105)+coefficients(106)*dFz)*inputs(4))*coefficients(2)*scaling_factors(22);
170
171     %Pneumatic trail (83-87)
172     Bt=(coefficients(51)+coefficients(52)*dFz+coefficients(53)*dFz^2)*(1+
    coefficients(54)+coefficients(55)*abs(inputs(4)))*scaling_factors(15)/
    scaling_factors(3);
173     Ct=coefficients(59);
174     Dt=(coefficients(60)+coefficients(61)*dFz)*(1-coefficients(79)*dPi)*(1+
    coefficients(62)*inputs(4)+coefficients(63)*inputs(4)^2)*inputs(1)*
    coefficients(2)/...
```

```
175         coefficients(1)*scaling_factors(17);
176     Et=(coefficients(70)+coefficients(71)*dFz+coefficients(72)*dFz^2)*(1+(
        coefficients(73)+coefficients(74)*inputs(4))*2/pi*atan(Bt*Ct*SAt));
177     t=Dt*cos(Ct*atan(Bt*SAteq-Et*(Bt*SAteq-atan(Bt*SAteq))))*cos(inputs(3));
178
179     %Resudial moment (88-90)
180     Br=coefficients(57)*scaling_factors(15)/scaling_factors(3)+coefficients(58)*
        By*Cy;
181     Dr=((coefficients(64)+coefficients(65)*dFz)*scaling_factors(18)+(coefficients
        (66)+coefficients(67)*dFz)*(1-coefficients(80)*dPi)*inputs(4)...
182         *scaling_factors(16)+(coefficients(68)+coefficients(69)*dFz)*inputs(4)*
        abs(inputs(4))*scaling_factors(16))*inputs(1)*coefficients(2)*scaling_factors
        (3);
183     Mzr=Dr*cos(atan(Br*SAreq))*cos(inputs(3));
184
185     %Pacejka formula (75)
186     Mz=-t*Fy0+Mzr+s*Fx;
187     cx=0;
188     cy=0;
189     cz=0;
190     Rl=0;
191     if Tot==1
192         %% Radius calculation
193         c=coefficients(1)/coefficients(2)*sqrt(coefficients(133)^2+4*coefficients
        (134))*(1+coefficients(138)*dPi); %Vertical stiffness [N/m] used in (5)
194         w=(1+inputs(2))*inputs(5)/coefficients(2); %Initial point of angular
        speed [rad/s] (6) supposing Re=R0
195         for i=1:3 %Resolving of Rfr, Re and w
196             wo=w;
197             Rfr=coefficients(2)*(coefficients(130)+coefficients(131)*(wo*
        coefficients(2)/coefficients(3))^2); %Free tyre radius [m] (1)
198             Re=Rfr-coefficients(1)/c*(coefficients(141)*atan(coefficients(142)*
        inputs(1)/coefficients(1))+coefficients(143)*inputs(1)/coefficients(1));...
199                 %Effective radius [m] (7)
200             w=(1+inputs(2))*inputs(5)/Re; %Angular speed [rad/s] (6)
201             if abs(w-wo)<0.1
202                 break;
203             end
204         end
205         if abs(w-wo)>0.1
206             Error=['Error in the convergence of the agular velocity. Last
        iteration error of ',abs(w-wo),' rad/s.'];
207             disp(Error);
208             display(inputs);
209             clear Error
210         end
211
212         k3=(1+coefficients(132)*coefficients(2)/coefficients(3)*abs(w)-(
        coefficients(136)*Fx/coefficients(1))^2-(coefficients(137)*Fy/coefficients(1)
        )^2)...
213           *(1+coefficients(138)*dPi)*coefficients(1); %Terms part of (3)
214
215         deflection=(-coefficients(133)/coefficients(2)+sqrt(coefficients(133)^2/
        coefficients(2)^2+4*coefficients(134)/coefficients(2)^2*inputs(1)/k3))...
```

```
216                     /(2*coefficients(134)/coefficients(2)^2); %Deflection [m]
    resulting of solve (3)
217
218         Rl=min(Rfr,Rfr-deflection); %Loaded radius [m] (2)
219 %         %% Contact patch calculation
220 %          a=coefficients(2)*(coefficients(145)*inputs(1)/c/coefficients(2)+
    coefficients(144)*sqrt(inputs(1)/c/coefficients(2)));...
221 %           %Half of the contact patch length [m] (9)
222 %          b=coefficients(146)*(coefficients(148)*inputs(1)/c/coefficients(2)+
    coefficients(147)*(inputs(1)/c/coefficients(2))^(1/3));...
223 %           %Half of the contact patch width [m] (10)
224         %% Stiffness calculation
225         cx=coefficients(153)*(1+coefficients(154)*dFz+coefficients(155)*dFz^2)
    *(1+coefficients(156)*dPi);   %Longitudinal stiffness [N/m] (17)
226         cy=coefficients(149)*(1+coefficients(150)*dFz+coefficients(151)*dFz^2)
    *(1+coefficients(152)*dPi);   %Lateral      stiffness [N/m] (18)
227         cz=k3*(coefficients(133)/coefficients(2)+2*coefficients(134)/coefficients
    (2)^2*deflection);          %Vertical     stiffness [N/m] resulting of dFz/dRl
     (3)
228     end
229 end
```

Appendix B

Simulink vehicle model

In this appendix, Simulink vehicle model will be shown.Starting from the general overview of the Simulink blocks and, finally, entering in detail in each function of the model.

B.1 Simulink blocks and connections

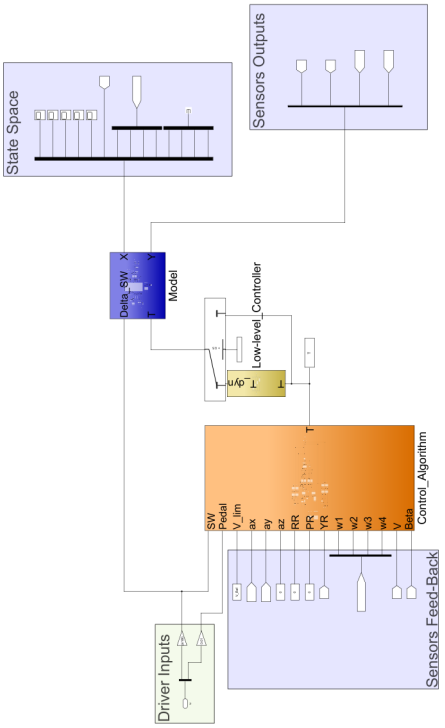

FIGURE B.1: Simulink model general overview.

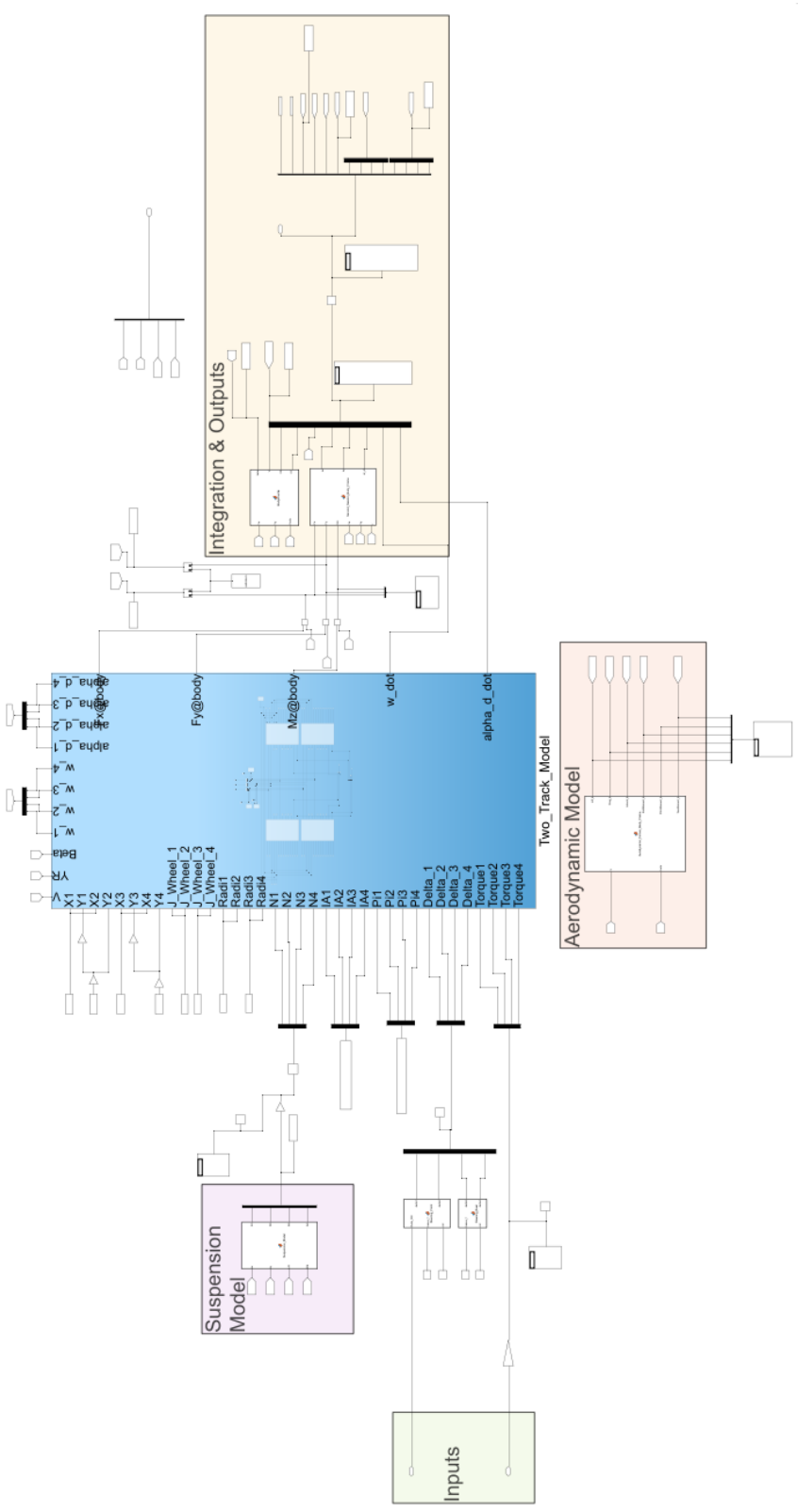

FIGURE B.2: Simulink vehicle physical model overview.

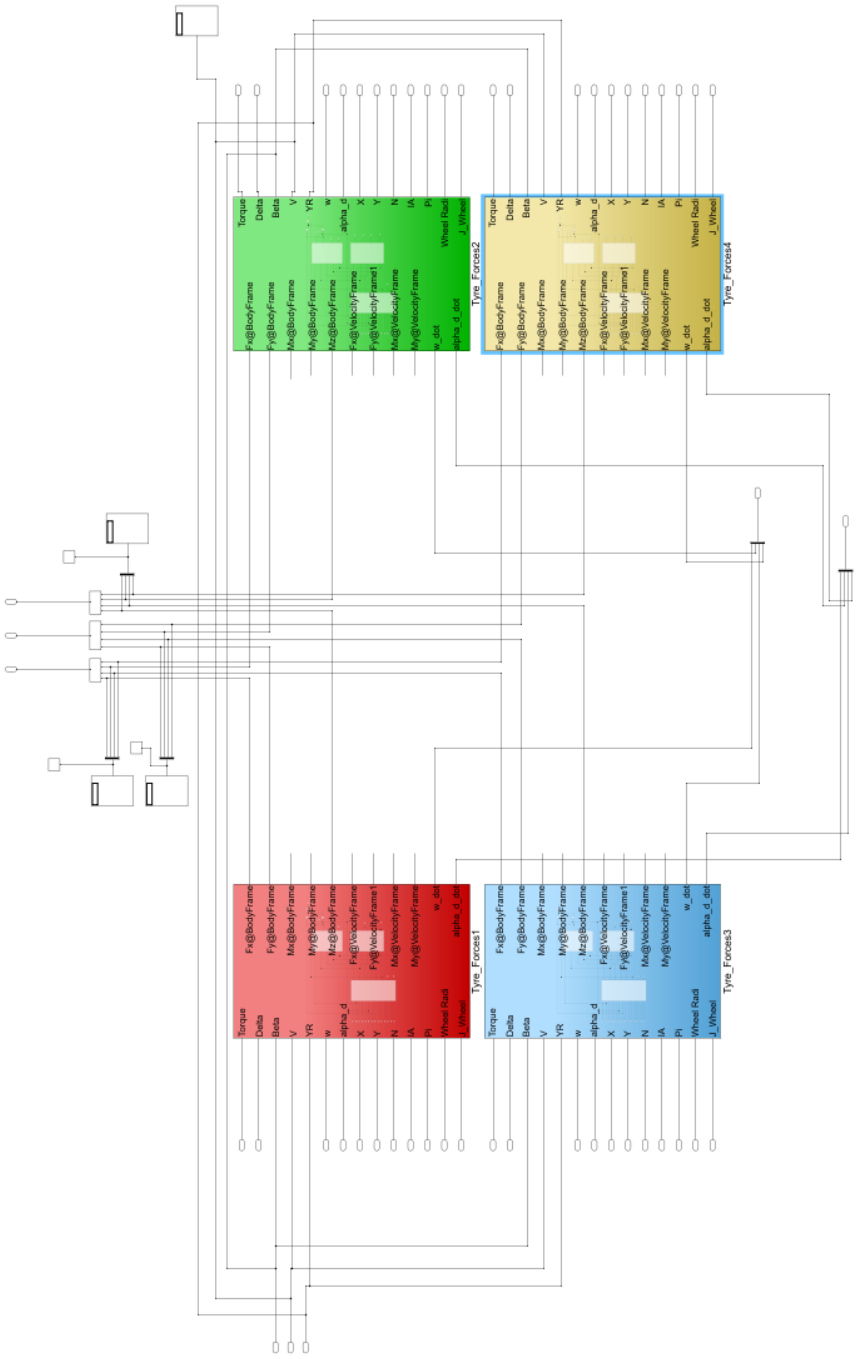

FIGURE B.3: Simulink two-track model overview.

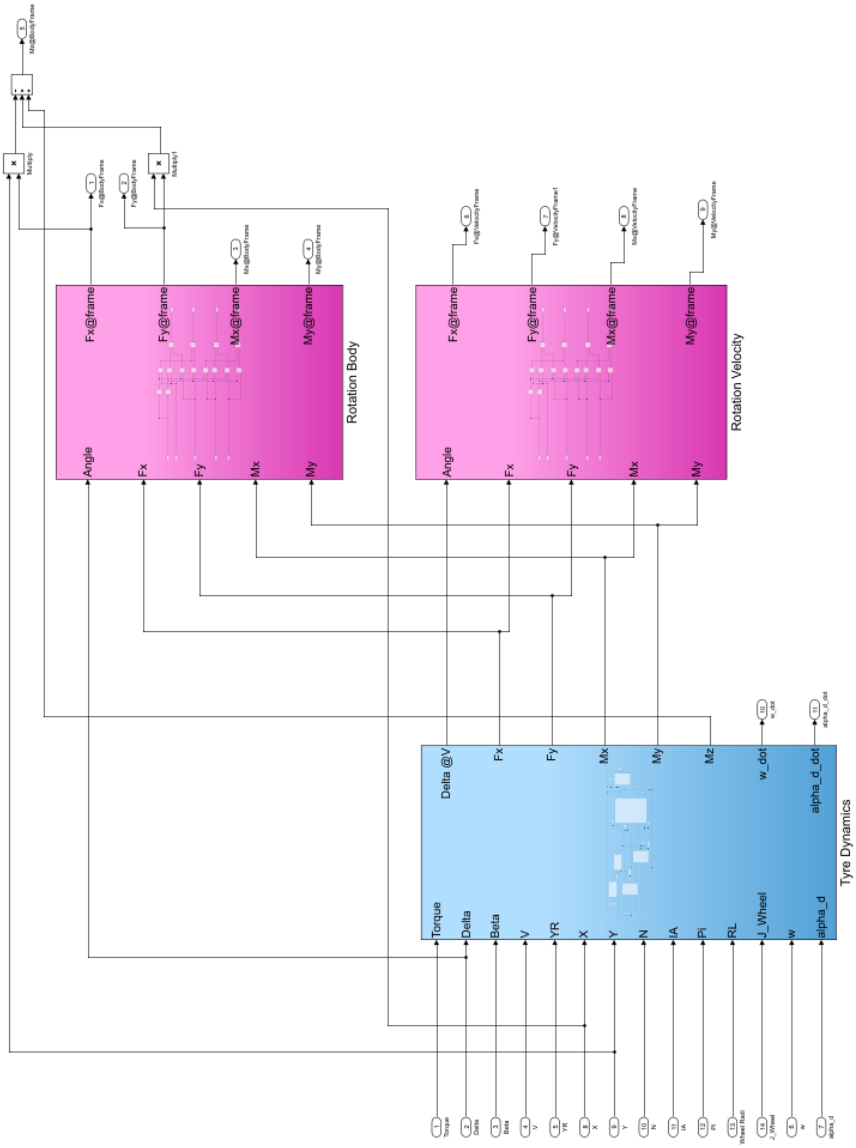

FIGURE B.4: Simulink tire dynamics and reference system projection.

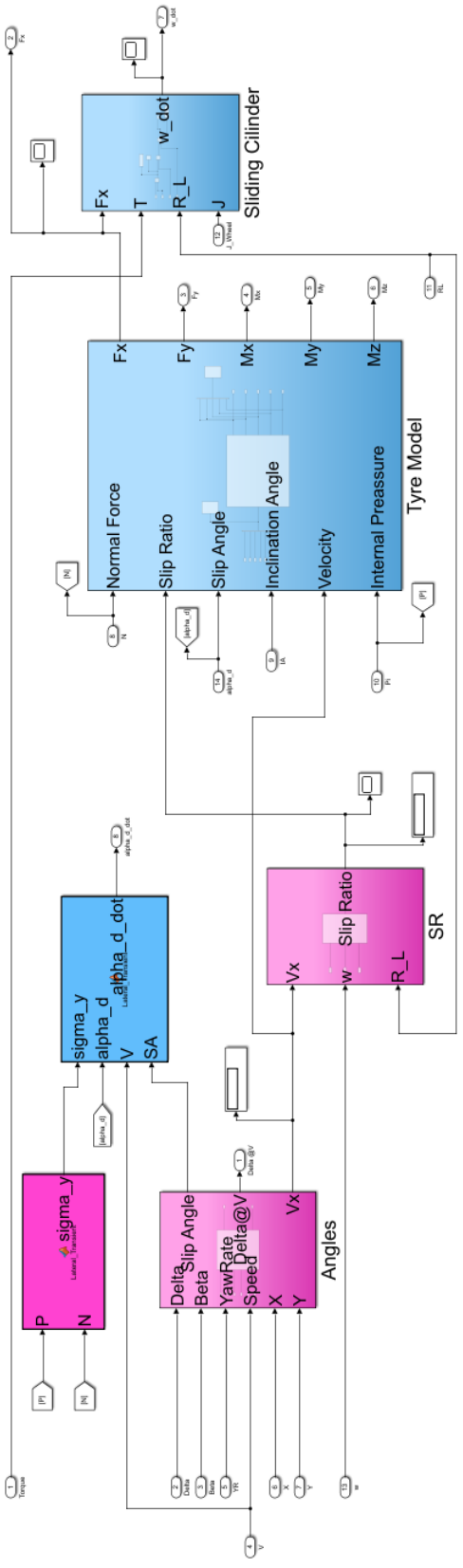

FIGURE B.5: Simulink tire dynamics and Magic Formula 6.1 tire model.

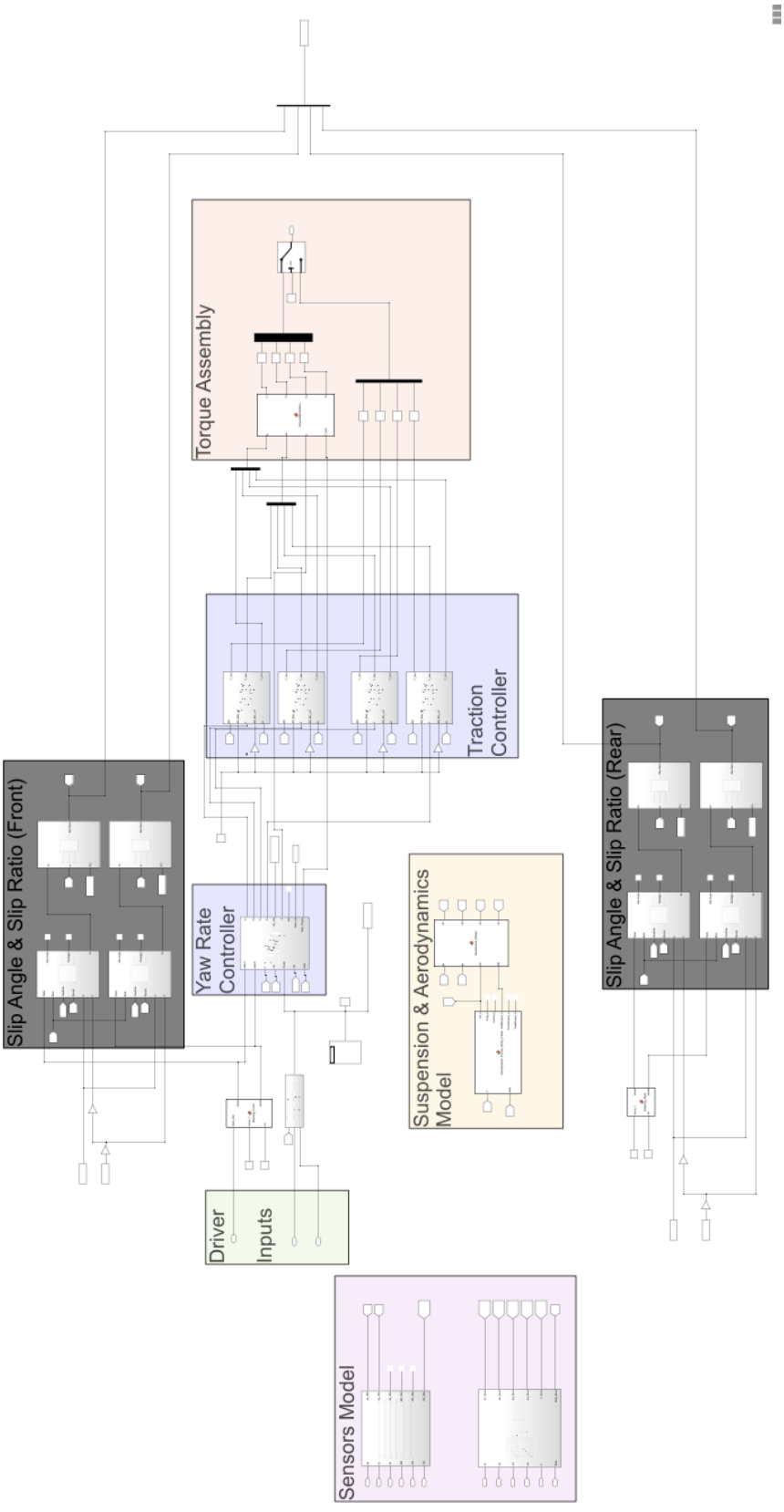

FIGURE B.6: Simulink control algorithm general overview.

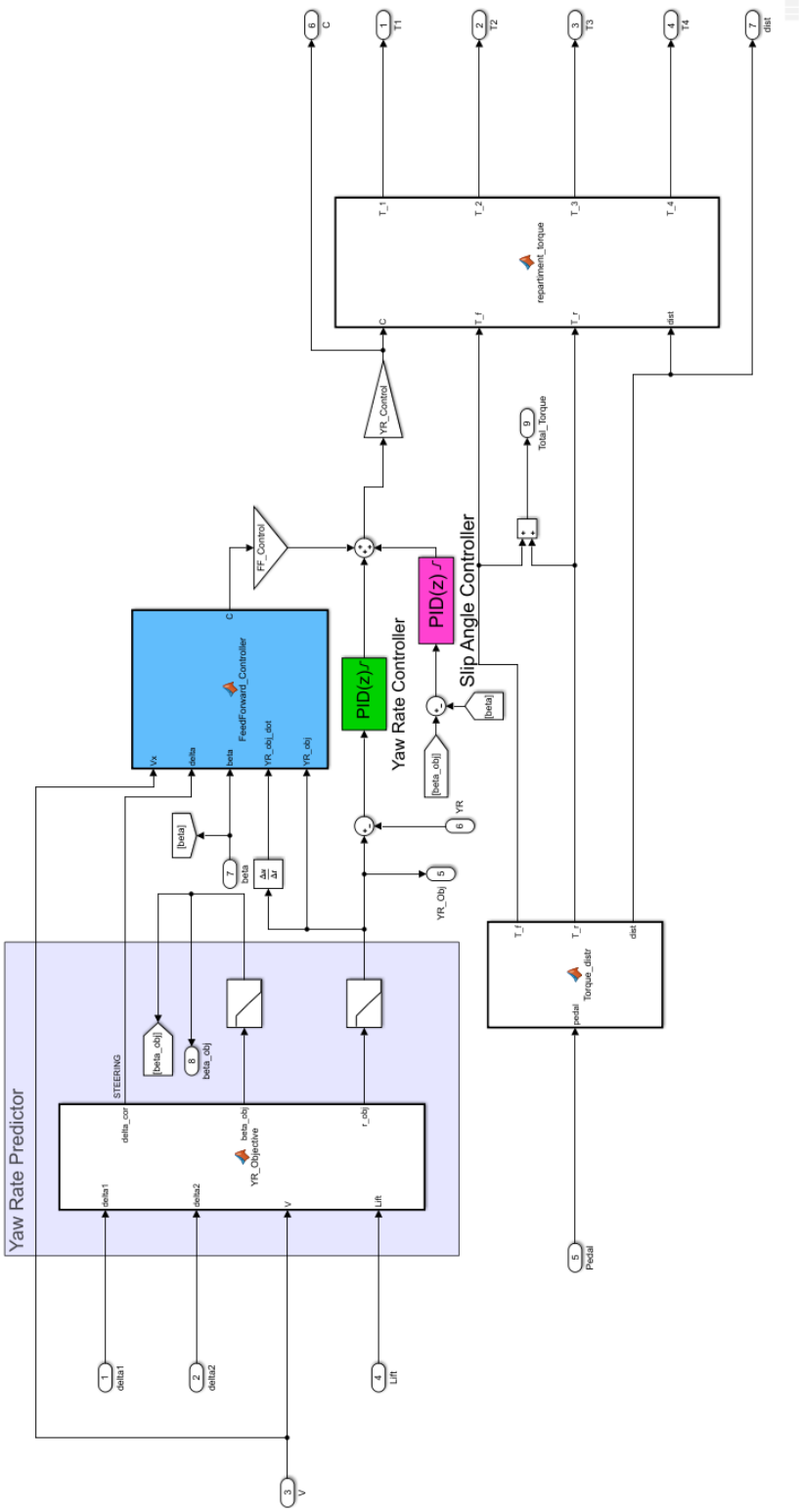

FIGURE B.7: Simulink yaw rate control algorithm general detailed.